Breaking of Waves over a Steep Bottom Slope

Jensen, Morten S.

Publication date:
2004

Document Version
Publisher's PDF, also known as Version of record

Breaking of Waves over a Steep Bottom Slope

Morten Sand Jensen

Hydraulics & Coastal Engineering Laboratory
Department of Civil Engineering
AALBORG UNIVERSITY

Hydraulics & Coastal Engineering Laboratory
Department of Civil Engineering
Aalborg University
Sohngaardsholmsvej 57
DK-9000 Aalborg, Denmark

ISSN 0909-4296
SERIES PAPER N0. 22

Breaking of Waves Over a Steep Bottom Slope

by

Morten Sand Jensen

Published by
Hydraulics & Coastal Engineering Laboratory
Aalborg University

Printed in Denmark, 2002
Reprinted in June 2004 with inclusion of Appendix H

ISSN 0909-4296
SERIES PAPER NO. 22

PREFACE

The present thesis is submitted as one of the requirements for the Danish Ph.D. degree according to the notice (no. 989) of December 1992 from the Danish Ministry of Education. The study was carried out at Aalborg University, Department of Civil Engineering with Prof., dr. techn. Hans Falk Burcharth as supervisor.

Besides the Ph.D. thesis the following report was prepared:

Jensen, M.S., (2001)
A Study of Coastal Zone Problems related to Coral-sand Beaches in East Africa – with special attention to Coastal Erosion. A report supported and published by DANIDA.

The above-mentioned report is the result of a 3-year study programme of the coastal zone problems along the East Africa Coast supported by the Danish International Development Assistance (DANIDA). The object was to investigate the experienced coastal zone problems. In this connection the author performed a series of field measurements in Tanzania during the period 1998-2001 reflecting the parameters important to understand the complicated near-shore coastal system. The project raised several questions on the wave energy dissipation of breaking waves propagating a steep bottom slope, which is the process focused upon in the present thesis.

I would like to thank the technicians at Aalborg Hydraulic Laboratory for their kind collaboration and help during the hydraulic tests. Furthermore, I would like to compliment my colleagues for fruitful discussions and a helpful attitude.

Copenhagen, December 2002

Morten Sand Jensen

DANISH RESUME

Denne Ph.D afhandling er rettet imod undersøgelsen af brydende bølgers passage over en stejl bundgradient. Dette kan være bølger, som bryder ved passage af et koralrev, men også eksempelvis en neddykket mole til sikring af kysten. Brydende bølger i kystnære områder er af interesse, da processen har indflydelse på påvirkningen af kysten med hensyn til transport af sediment og medfølgende erosion. Mængden af omsat energi ved brydningsprocessen og indflydelsen af relevante parametre er af interesse i denne afhandling. Formålet med undersøgelsen er at udvikle redskaber til at beskrive mængden af omsat energi i forbindelse med uregelmæssige, brydende bølger over en stejl bundgradient. Resultatet er blevet en samling af formler baseret på et teoretisk grundlag til beskrivelse af energi omsat ved brydende bølger over stejle hældninger. Endvidere er udviklet en numerisk model til simulering af bølgebrydningen. Begge redskaber viser god overensstemmelse med eksperimentelle data målt i hydraulisk laboratorium.

I afhandlingen er indledningsvis kort gennemgået de mest anvendte formler til beregning af den maksimale bølgehøjde før brydning samt en beskrivelse af anvendte metoder til at beskrive bølgetransformation af brydende bølger over en stejl bundgradient.

Et stort antal forsøg af regelmæssige og uregelmæssige bølger, brydende over en stejl bundhældning, er foretaget i et hydraulisk laboratorium. Forsøgene danner grundlag for en bestemmelse af kriteriet for bølgebrydning. Desuden er opnået et grundlag af data vedrørende information af energiomsætningen under bølgebrydning. Tre styrende parametre i bølgebrydningsprocessen er identificeret som værende; vanddybden på det lave koral plateau eller den neddykkede mole, den indkommende signifikante bølgehøjde og en karakteristisk periode af bølgen. Det undersøgte område af stejle bundhældningsgradienter viser ringe indflydelse på mængden af omsat energi.

Som indledningsvis beskrevet er en numerisk beregningsmodel udviklet og kalibreret på baggrund af de eksperimentelle test foretaget i det hydrauliske laboratorium. Metoden for udbredelse af bølgerne er baseret på en udvidet refraktions- og diffraktionsligning, som er en udvidelse af den klassiske Mild-Slope ligning. Udvidelsen består i muligheden for medtagelse af en hurtigt varierende bundhældning ved at inkludere henholdsvis bundgradienten samt bundens krumning. Tab af bølgeenergi hidrørende fra bundfriktion er modelleret på baggrund af et ofte anvendt udtryk for gennemsnitlig omsætning af energi i bølgen. En ”Periodic Bore” model danner baggrund for beskrivelsen af energitabet af brydende bølger.

Der er god overensstemmelse mellem numeriske resultater og eksperimentelle data baseret på en empirisk bestemt faktor, som bestemmer raten af omsat energi i de brydende bølger.

På baggrund af de eksperimentelle data er der desuden kalibreret og givet diverse praktiske formler til at beregne den transporterede energi.

SUMMARY

The present thesis yields a description regarding the wave breaking process of waves propagating over a steep submerged bottom slope. The steep bottom slope could be a coral reef or a submerged breakwater for protection of the coast. The amount of energy dissipated in the wave breaking process and the influence of various parameters is focused upon.

The transformation of waves propagating over a coral reef is of great importance regarding the coastal processes in the near shore area. This work will contribute with tools to predict the dissipated wave energy for irregular waves passing a steep submerged slope. A formulae and a numerical wave model are developed both capable of predicting the transmitted wave energy over steep slopes. The results from this study will be applicable in the design of coastal structures as submerged breakwaters or artificial reefs.

The first part of the thesis presents a review of breaker height formulae and a description of the energy dissipation process for waves propagating over a steep bottom slope.

An extensive number of tests using regular and irregular waves breaking over a simulated reef in the hydraulic laboratory have been performed. These tests yield knowledge of the initiation of wave breaking and the tests provide substantial data reflecting the wave energy dissipation along the reef-plateau. Three governing parameters in the wave breaking process are identified as being the water level on the reef-plateau, the incidentally significant wave height and the peak period of the waves. The range of reef-slopes tested shows no significant difference of the amount of dissipated energy in the wave breaking process.

As mentioned, a wave model is developed, which can simulate irregular waves propagating steep slopes and the related wave energy dissipation. The numerical model of the wave breaking process is calibrated based on before mentioned experimental tests in the hydraulic laboratory. The propagation of waves in the model is based on the extended refraction and diffraction equation. This formulation is able to account for rapidly varying bottom topography. Energy dissipation due to bottom friction is modelled by an acknowledged expression for the average rate of energy dissipation in waves. The breaking process has been parameterised using a modification of the Battjes and Janssen [1978] periodic bore approach. An empirical parameter related to the bore model is calibrated against the experimental data. The model is able to predict the experimental data very well.

Finally, based on the experimental data practical formulae are provided, which can predict the transmitted energy on the reef-plateau.

CONTENTS

CHAPTER 1 INTRODUCTION

The thesis is focused upon the wave transformation of waves propagating over steep bottom slopes. It is the objective to develop methods and formulae able to describe and quantify the energy dissipation related to the wave breaking process.

In the following, motivation and objective with present thesis is given. Attention is given to a research study, which the author conducted in parallel with the PhD project. Also, coral reef degradation in general is introduced.

1.1 Research project in Tanzania

The motivation to perform a detailed study of the wave breaking process and to establish a practical engineering method for evaluating the dissipation of wave energy of the incident waves is due to a field study project performed by the author in Tanzania, East Africa, during the years 1998-2001.

The East Coast of Africa bordering the Indian Ocean is subject to coastal erosion, which has escalated during the last decade. In recognition of the coastal zone problems along the East African Coast, the Danish International Development Assistance (DANIDA) sponsored a study with the object of investigating the experienced coastal zone problems. In this connection the author performed a series of field measurements in Tanzania in the period 1998-2001 to measure the parameters important for understanding the complicated near-shore coastal system.

Figure 1: *A picture showing coastal erosion. Taken in the field study area, Tanzania.*

The coastal system in these regions is quite different compared to the more investigated coastal systems in Europe. The coastal processes are mainly governed by the monsoon cycles and a significant tidal range system. The coastal nearshore area holds a complicated bathymetry combined with fringing reefs, small islands and river outlets, see Figure 2.

The objectives relevant to the research project supported by DANIDA was to

- improve present knowledge of coastal processes along the coast
- develop low-tech equipment for measuring coastal processes
- exchange knowledge and establish a collaboration between universities

The relevance of the research project in relation to present PhD thesis was to

- obtain practical knowledge of coastal near-shore processes
- focus the process of wave energy transmission of breaking waves

The parameters studied for a period of three years are currents, waves, beach profiles, sediment concentrations and sediment characteristics and nearshore bathymetry. Waves are breaking on shallow coral reefs. It is noted that wave measurements are taken behind the coral reefs and some on the coral reefs. Unfortunately, wave measurements are not taken offshore the reefs and therefore no data are obtained of wave energy dissipation due to breaking waves on the reefs.

Due to the research project several important coastal parameters have been subject to quantification and there was no doubt that severe coastal erosion is taking place and the coastal reefs were in a state of deterioration. Furthermore, there is an indication of a strong correlation between deteriorating coral reefs and coastal erosion.

The conclusions highlighted the need for a simple tool to predict the amount of wave energy transmitted over steep submerged bottom slopes, such as coral reefs, in order to evaluate the consequences of reef deterioration.

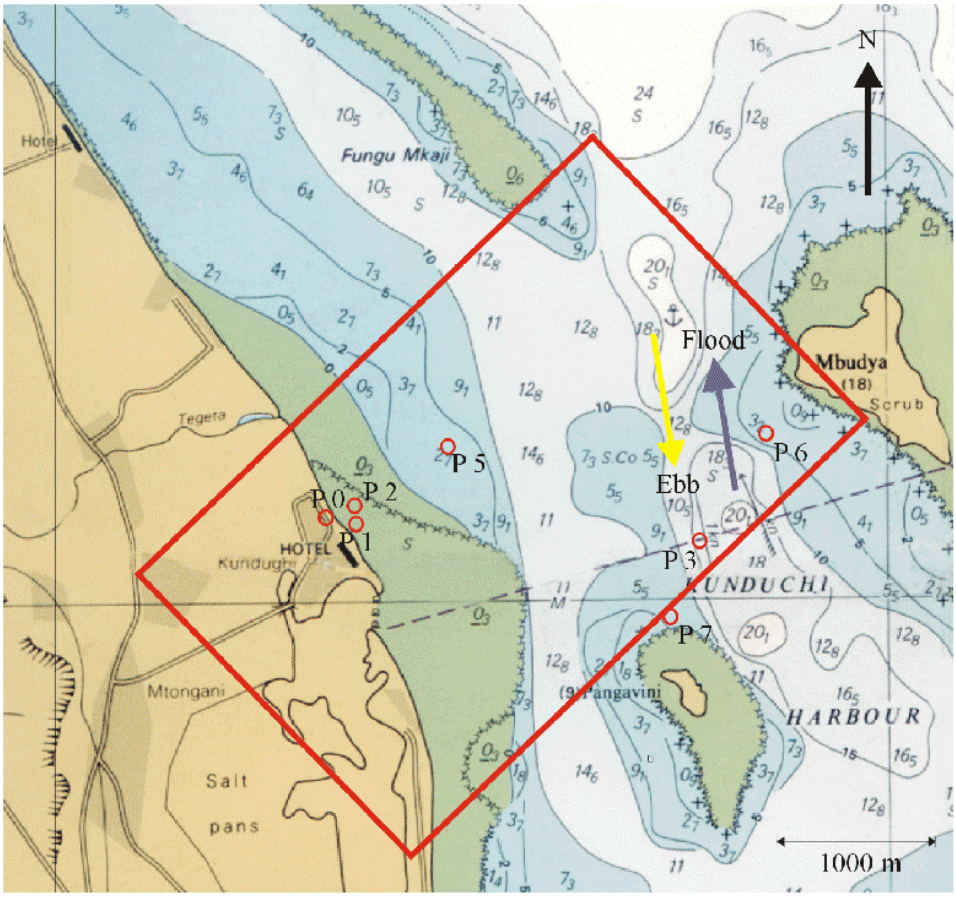

Figure 2: *Area for various measurements (reefs are indicated with curves lines).*

1.2 Coral reef degradation

Recently, numerous institutions and scientists have focused upon the shoreline retreat and beach erosion in the coral zone area. The coral reefs act as a natural protection of the coastline. The waves break offshore when they pass the submerged reefs, which cause a reduction of the wave energy flux reaching the coastline.

It is a recognised fact that the coral reef system worldwide is in a state of degradation. This vulnerable ecological biological system consists of a rich variation of plant and fish species, which only exist in this area.

A changed wave climate, a rising sea level or sinking of the land are possible causes for beach erosion. Still, the fact that the sea level rises in some areas has to be compared with the fact that healthy reefs grow faster than the slow process of rising

sea level and land sinking. Coral growth at optimal depths of living colonies is reported in Hawaii to be 8-10 mm/year [Article 1, 1999]. In areas where the coral reefs suffer from degradation, reef destruction will escalate the process of beach erosion. Finally, there are the man-made causes to erosion as extracting sand from out-let rivers or cutting down protective plantation.

Bleaching and subsequent mortality of corals as a result of increased sea temperatures is a relative recent phenomenon that has resulted in a dramatic decline in the number of healthy reefs around the world.

The state of the coral reefs has been intensively examined over the last decades. The official figures state that in some areas more than 30 % of the reefs have died in areas such as the Great Barrier Reef, Australia. The main factor has been identified as especially coral bleaching and the invasion of starfish. Coral bleaching is caused by a rise in seawater temperature of several degrees for longer periods. Along the East African coast the degradation of the coral reef system is furthermore caused by man due to violent fishing methods as using dynamite or the use of chemicals. The author has observed destructive fishing methods on several occasions. Among numerous articles on the subject the following is mentioned [Oceanspace Issue 165, 1999] by Professor Indur Fagoonee, Pro-vice Chancellor of the University of Mauritius:

During 1997/1998 coral reefs were subjected to the most severe and widespread bleaching and mortality observed. In particular, the coral reef bleaching in the Indian Ocean was more extensive and severe than observed ever before, with mortality recorded as high as 90 %. Warm waters moved from north causing extreme bleaching in Tanzania, Kenya, Madagascar, Reunion, Comoros, Seychelles, Socotra, Maldives and Sri Lanka.

Wilkinson [1993] stated that 10% of the world's reefs had already disappeared and predicted that within the next two decades additional 20% would disappear. Reefs in the Indian Ocean have already suffered major damage [Souther and Linden, 2000].

The problem of reefs degrading seems well established and recognised and is currently taken as a serious threat worldwide. The consequences of reef deterioration are fatal to the vulnerable ecological and biological systems and will cause enhanced coastal erosion.

CHAPTER 2 OBJECTIVE OF STUDY

The objective of the study is to establish a method to predict the wave energy dissipation for waves breaking on a steep submerged slope as a reef.

It is necessary to predict the wave energy dissipation for doing further investigations of the relation between coastal erosion and reduction in coral reef height. Also, a realistic model for prediction of the wave energy dissipation is an important tool in design of submerged breakwaters for protection of the coastline.

In order to illustrate the phases and methodology of the thesis the diagram in Figure 3 is shown. To summarize, a literature review aimed at existing models for wave transformation is undertaken. A numerical wave model is developed capable of can simulating the transformation process associated with waves breaking when they are propagating over a steep submerged bottom slope. Experimental tests of waves breaking over a steep slope are performed in order to create data for development of practical formulae. Based on the experimental data the numerical model can be calibrated. Understanding of the coral reef hydrodynamics is supported from the knowledge and experience obtained during the field studies in Tanzania. Hence, the outcome of the following study is to develop

- simple formulae for prediction of wave energy transmission
- a numerical wave propagation model for dissipating waves

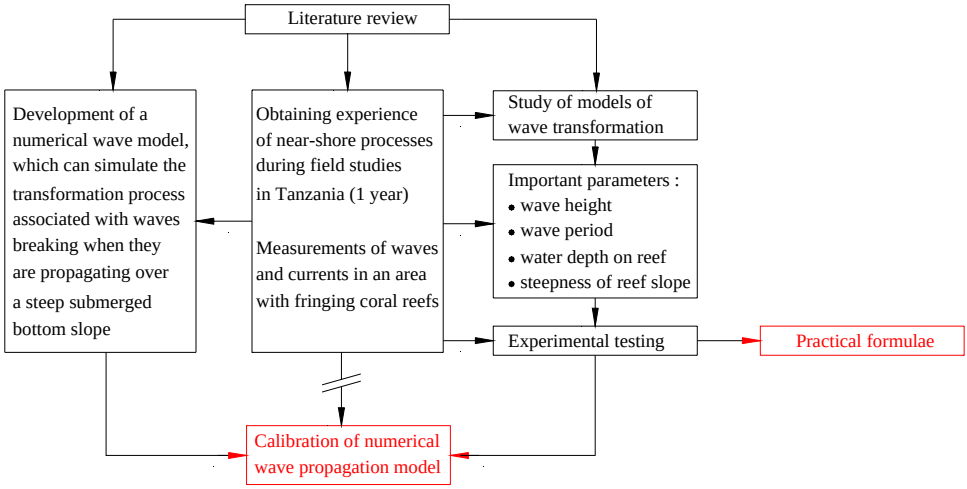

Figure 3: *Project phases.*

CHAPTER 3 WAVE TRANSFORMATION ON CORAL REEFS

The transformation of waves across coral reefs is a complex problem, including processes as refraction, shoaling, reflection and energy dissipation due to breaking waves and bottom friction. As waves pass from deep water over a steep reef-slope onto the flat reef-plateau, the wave transformation process becomes highly non-linear.

This chapter will present the state of knowledge of transformation of waves propagating over steep reefs regarding experimental observations. Furthermore, a brief characterisation of coral reefs is given.

3.1 Coral reef profiles

Gourlay [1996b] presented a useful characterisation of a general coral reef as given in Figure 4. These definitions will be used throughout the thesis. For further clarification of used symbols and definitions reference is made to Appendix A, where a collection of symbols is provided.

The geometry considered in later chapters describing the experimental and numerical layout is simplified and consists of a steep slope and a reef-crest followed by a longer shallow reef-plateau.

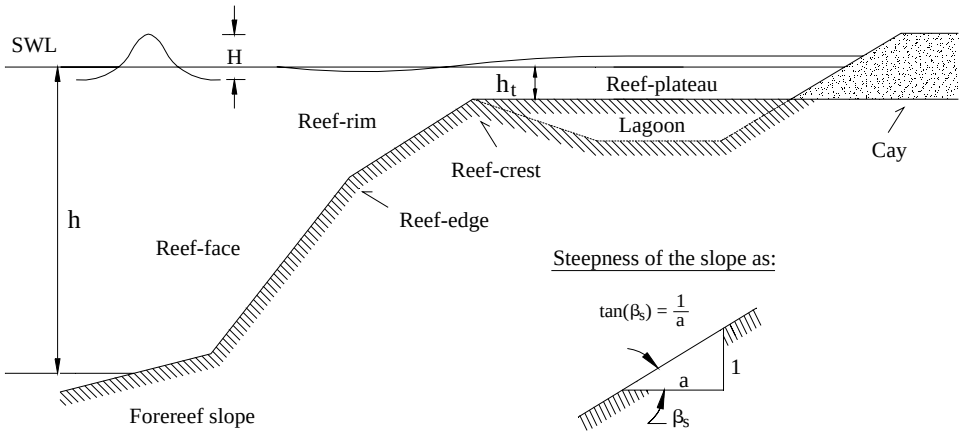

Figure 4: *Characterisation of a coral reef.*

Forereef-slope:	the relatively flat slope seaward of the reef-face
Reef-face:	the relatively steep seaward facing underwater slope of the reef
Reef-plateau:	the skyward facing surface of the reef, usually submerged except at low tides
Reef-rim:	the relatively flat seaward inclined surface between the reef-plateau and the reef-face
Reef-edge:	the intersection between the reef-face and the reef-rim
Reef-crest:	the highest part of the reef-rim or the intersection between the reef-rim and the reef-plateau
Lagoon:	a body of water ponded on or enclosed by a reef or by a reef and a continental land mass or island
Fringing reef:	a reef which fronts a continental land mass
Platform/island reef:	a reef surrounded by the sea
Cay:	a reef-plateau island formed from reef-derived sediments

Essentially, there are two kinds of reefs. Reef fronting a continental land mass are denoted fringing reefs, while reefs located in the open ocean are termed platform reefs. Coral reefs exist in the tropical regions of the Pacific, Indian and Atlantic Oceans in the form of fringing reefs and surrounding islands, barrier reefs or separate atolls and island reefs [Vernon 1986].

The form and the morphology of coral reefs vary depending on the local conditions. Especially, the wave climate is a factor shaping the reef. Roberts et al. [1975] found that there were significant differences between the physical and ecological profiles of the reefs depending upon whether they are located in high or low wave energy environments. If the offshore reef-face is subject to a condition of high-energy wave climate, then significant spur–and-groove features appears. This will influence the energy dissipation due to bottom friction. In locations with low energy conditions such features are missing and the slopes are generally flatter. In the present thesis the energy loss due to wave breaking is emphasised and spur-and-groove features are not considered. Only the effect of a uniform bottom friction is included.

Average slopes of the reef-face are about 1:2 [Hopley, 1982] but can be as flat as 1:5 or may also be vertical or even overhanging.

Recent field measurements of waves breaking on a reef are obtained by Lee and Black [1978], Roberts [1980], Gerritsen [1981], Young [1989], Hardy et al. [1990, 1996] and Massel and Brinkman [1998].

3.2 Wave transformation on a submerged steep reef

In the following, the transformation of waves propagating a steep reef is described. This section gives a short résumé of the most important findings and experience within this topic. Different scientists are mentioned for work relevant for the topic of this thesis. The main work presented consists of experiments in the laboratory. Field measurements are more rare. Such studies are quite expensive and also difficult to perform compared to laboratory model tests. It is noted that the literature on coral reef hydrodynamics is not numerous.

During the wave breaking process the wave energy is dissipated and the wave height distribution is changed due to breaking. Offshore, the wave heights in general have a Rayleigh distribution. The breaking waves change the wave height distribution, where the highest waves disappear in the distribution and then are redistributed to smaller waves. The resulting transformed wave energy spectrum becomes flatter [Young 1989, Hardy et al. 1990]. The wave energy dissipated within a few wavelengths is significant. Depending on the tide level and the characteristics of the incident wave field, wave breaking occurs close to the reef-crest. Evidently, this results in a water level set-up, which allows larger waves to propagate onto the top. Gourlay [1994] reported that up to 95 % of the offshore wave energy is dissipated when waves break at the reef-face. Moreover, it was noted by Nelson [1983] that the ratio of maximum wave height to mean water depth on the reef-plateau is as low as 0.55. This value is significantly lower than the general value of approximately 0.8 used in coastal engineering.

The first detailed study of waves in the vicinity of coral reefs was conducted at the Bikini Atoll by Munk and Sargent [1948]. From wave height observations over the Atoll they estimated that 95 % of the incident wave energy dissipated for waves breaking and travelling across the reef-plateau. More recent studies [e.g. Roberts et al. 1977; Suhayda and Roberts 1977; Roberts 1980; Roberts and Suhayda 1983; Lee and Black 1978; Kono and Tsukuyama 1980] found values of 75 % to 86 % wave energy reduction of the incident wave. The tests showed that the dissipation of wave energy is not uniform across the spectrum. Filtering of large wave heights is more effective than filtering of smaller ones. Ahrens [1987] found that wave transmission is a function of water depth at the crest, and the greater this depth, the greater the transmission of energy. In cases where the SWL in combination with the present wave set-up is in level with the reef-crest, the transmission will also consist of run-up or wave overtopping. In some cases transmission of wave energy can also occur through the reef. The difference in the level of dissipated wave energy is due to the variability of the studied reefs and the present wave climate.

Breaking waves induce a set-up of the water surface over the reef, and differences in breaking characteristic along the reef can cause variations in wave set-up, producing significant long-shore currents.

For waves breaking at a steep reef one could expect significant reflection of the energy. Although field data [Roberts et al. 1975, Young 1989] has shown the reflected wave height to be in the order of only 10 % of the incident height due to the porosity of the reef.

Energy losses due to bottom friction are usually negligible in wave transformation across sandy beach profiles, but at reef-slopes they may be an order of magnitude larger than for a sandy beach [Roberts et al. 1975, Gerritsen 1981]. Nelson [1996] shows field data results for irregular, non-breaking waves, where the bottom friction at the reef plateau is very similar to the bottom friction across sandy beach profiles. The wave energy dissipation factor f_r, which describes the intensity of wave energy dissipation due to bottom friction, is expected to be in the order of 0.1 [Nelson, 1994]. Energy dissipation due to bottom friction for plunging waves breaking over a steep slope cannot directly be compared with the wave energy dissipation process described by Nelson [1994], where waves are not breaking and propagating over a horizontal bed. It is therefore expected to find the wave energy dissipation factor in the area between 0.1-1.0 along the reef slope. When the waves are reformed a few wave lengths after the reef-edge, the factor is expected to be close to 0.1 referring to Nelson's conclusions.

Tait [1972] employed the method of Bowen et al. [1968] to quantify the set-up caused by waves breaking in front of a fringing reef. Since the incoming wave field was presumed to be narrow-banded, the derivation of the set-up was based on linear wave theory. By assuming that the wave height depends linearly on the mean water depth, the horizontal component of the depth-integrated momentum equation provides an expression for the reef-plateau wave set-up as a function of the still water depth at both the reef-plateau and the breaking point. In the case of a reef-plateau level coinciding with the still water level, a comparison was made with measurements by Bowen et al. [1968] showing that the analytical model was able to predict the wave set-up.

Gerritsen [1981] developed a semi-empirical model for the variation of the wave height and the wave induced set-up of waves propagating onto a shallow coastal reef. By employment of time series of the surface elevation measured offshore, the model was used to compute the set-up and the root-mean-square wave height at the reef. The results compared reasonably with experiments.
Laboratory measurements of both regular and irregular waves breaking at the face of a fringing reef located on the coast of Guam were conducted by Seelig [1983]. The bed profile considered incorporated a relatively steep reef-face and an adjacent reef-crest submerged below the still water level. Various incident wave conditions were

considered and the maximum wave induced set-up was measured in a closed lagoon inshore the reef-crest.

In a closed flume Nelson and Lesleigher [1985] studied the transformation of waves breaking at the crest of a submerged coral reef. The bathymetry of the reef resembled a vertical step with the reef-plateau located in shallow water. The wave periods under consideration gave rise to a substantial amount of undesired reflections and therefore the incident wave field was generated in short bursts, implying that a stationary situation was not reached. The test showed that approximately 25% of the incident wave energy dissipated within the first wavelength after the reef edge. Furthermore, it appeared that the broken waves reformed into oscillatory waves a distance of four to seven water wavelengths from the reef-edge.

Gourlay [1994] studied wave transformation and set-up on a model of a fringing reef at Hayman Island. The purpose was to obtain design data for a proposed reef-top bund wall. A semi-empirical model was developed.

Massel [1993] extended the classical Mild-Slope equation valid for regular waves of small amplitude propagating over varying bottom topography. Based on the Galerkin Eigenfunction method, an extended refraction-diffraction equation was derived which incorporated the effect of a seabed consisting of substantial variations in the water depth within one wavelength. In addition to the freely propagating waves, the resulting equation involved the non-propagating (evanescent) modes. The extended equation was used to study the wave height variation of regular non-breaking waves of initially small amplitude as they propagated across a submerged coral reef consisting of rapid bed variations.

One important feature of the extended Mild-Slope equation [Massel 1993, Massel and Gourley 2000] is missing. It is known, that in this model the velocity potential dependence on the vertical co-ordinate is prescribed in a form of a hyperbolic function. It is clear that this function does not satisfy the condition at the sloping bottom, namely vanishing of the velocity normal to the bottom. Recently, the problem of correct formulation of the bottom condition was addressed in a few papers of Athanassoulis and Belibassakis [1999].

Based on the momentum equation and the extended refraction-diffraction equation, Massel and Gourlay [2000] studied the variation of the root-mean-square wave height and the wave set-up of a narrow-banded irregular wave field breaking on a steep reef-slope. The energy dissipation caused by wave breaking was modelled by employment of the Rayleigh distribution and the expression for the energy loss in a hydraulic jump. Similarly, the energy dissipation caused by the bed friction was described in terms of the friction factor f_r, and the horizontal velocity amplitude at the bed. The momentum equation and the extended refraction-diffraction equation were solved simultaneously yielding the root-mean-square wave height and the wave-induced set-

up at each water depth. The model was used to study the transformation of an irregular wave field propagating a steep reef-face. The predicted set-up and computed wave height variation are compared with experimental data, and showed a reasonable agreement.

CHAPTER 4 PREDICTION OF MAXIMUM STABLE WAVE HEIGHT

Wave breaking is one of the most important processes to coastal engineers because it influences both the behaviour of sediments on beaches and induced forces on coastal structures.

The present knowledge of the wave breaking mechanism is still incomplete. At present, few properties of breaking waves can be predicted with reasonable accuracy.

In order to predict the wave height transformation, it is necessary to define the initiation of wave breaking and the wave height at the breaking point. In the following chapter a review of formulae predicting the breaker height is briefly presented. The aim is to identify all parameters and their relations regarding the wave breaking process at steep slopes.

4.1 Estimation of maximum breaker height

The breaking of waves is in general experienced in two cases. In open seas the wind energy flow from the wind will be transferred to the waves. The waves grow larger and when the energy content is sufficiently intensive, the waves lose their stability and break. This process is also referred to as “whitecaps”. Breaking is a local and a non-stationary phenomenon. The second mode of wave breaking is due to shoaling waves and in the extreme case where waves break propagating steep bottom slopes at small water depths.

The wave breaking mechanism is complex and most predictions of the breaker height are based on empirical or semi-empirical formulae calibrated from laboratory tests. Many breaker height formulae have been suggested during the last century. More than 150 years ago Stokes [1847, 1880] established several criteria of the breaking of regular waves. The breaking criteria of Miche [1944] (later modified by Battjes and Janssen [1978]), and Goda [1970] seem to be widely used. However, a majority of the formulae are developed with limited laboratory tests and their validity may be limited according to the range of experimental conditions employed. Especially, the bottom slopes tested seem to include only gentler slopes. Other problems often addressed in the literature are connected to the wave flume tests where various techniques yield limitations. Especially, the generation of waves and how to deal with the re-reflected waves have been a problem in the past. Much emphasis is given to the wave generation technique regarding the experimental model tests performed and presented later in this thesis, where an active absorbing system is applied.

In Table 1 a summary of laboratory data used to validate the most recognised breaker formulae is given [Rattanapitikon et al. 2000]. Notation given in the text and in Table 1 can also be found in Appendix A, where a summation of the used notation is given.

Source / Scientist	No. of cases	Bottom slope	Max bottom slope	Offshore wave steepness
		$\tan(\beta_s)$	1:a	H_0/L_0
Galvin [1969]*	19	0.05 – 0.20	1:5	0.001 – 0.051
Hansen and Svendsen [1979]	17	0.03	1:33	0.002 – 0.069
Hattori and Aono [1985]	3	0.00	-	0.006 – 0.021
Horikawa and Kuo [1966]	158	0.00 – 0.05	1:20	0.006 – 0.100
Hwung et al. [1992]	2	0.07	1:14	0.026 – 0.048
Iversen [1952]*	63	0.02 – 0.10	1:10	0.003 – 0.080
Iwagaki et al. [1974]	39	0.03 – 0.10	1:10	0.005 – 0.074
Maruyama et al. [1983]*	1	0.03	1:33	0.091
Mizuguchi [1980]*	1	0.10	1:10	0.045
Nadaoka et al. [1982]	12	0.05	1:20	0.013 – 0.080
Nagayama [1983]	12	0.00 - 0.05	1:20	0.025 – 0.055
Okayasu et al. [1986, 1988]	12	0.03 - 0.05	1:20	0.009 – 0.054
Ozaki et al. [1977]	20	0.10	1:10	0.005 – 0.060
Saeki and Sasaki [1973]*	2	0.02	1:50	0.005 – 0.039
Sato et al. [1988, 1989, 1990]	12	0.03 - 0.05	1:20	0.003 – 0.073
Singamsetti and Wind [1980]*	95	0.03 – 0.20	1:5	0.018 – 0.079
Smith and Kraus [1990]*	80	0.03 – 0.44	1:2	0.008 – 0.096
Stive [1984]	2	0.03	1:33	0.010 – 0.032
Ting and Kirby [1994]	2	0.03	1:33	0.002 – 0.020
Visser [1982]*	7	0.05 – 0.10	1:10	0.014 – 0.079
Walker [1974]*	15	0.03	1:33	0.001 – 0.037
Total	574	0.00 – 0.44	1:2	0.001 – 0.100

Table 1: *Summary of laboratory tests used to validate the breaker height formulae (*Data from Smith and Kraus [1990]).*

Angle of the slope steepness is denoted β_s. The range of bottom slope used, $\tan(\beta_s)$, is 0.00–0.44, i.e. from a horizontal seabed to a slope of 1:2. The slope steepness will in the following also be denoted by a, see Figure 4 in Section 3.1. All 574 cases are performed during regular wave conditions. The tests are performed in small-scale wave flumes with exception of the experiments by Maruyama et al. [1983]. These tests were conducted in a large-scale wave flume.

The existing formulae presented in the following describe a relationship between the breaking wave height, H_b, and the variables at the breaking point or the deepwater conditions. The notation is: water depth at breaking, h_b, wavelength at breaking, L_b, deep water wavelength, L_0, bottom slope, $\tan(\beta_s)$ and deep water regular wave height, H_0. The deep-water wavelength is defined as $L_0 = (gT^2)/2\pi$, where T is the wave period.

The most used formulae are briefly described to clarify the parameters used in the accepted formulae:

- McCowan [1894] derived a limit of breaking wave height in water of constant depth based on a solitary wave theory and proposed that the breaking will occur when

$$H_b = 0.78 \cdot h_b \tag{1}$$

- Miche [1944] developed the semi-theoretical breaking criterion for periodic waves in finite water depth and proposed the limiting wave steepness as a function of h_b / L_b

$$H_b = 0.142 \cdot L_b \cdot \tanh\left(\frac{2\pi h_b}{L_b}\right) \tag{2}$$

When the formula is used with a horizontal seabed Danel [1952] suggested changing the coefficient from 0.142 to 0.12

- Goda [1974] analysed several sets of laboratory data of breaking waves on slopes obtained by several researchers [Iversen, 1952; Mitsuyasu, 1962; and Goda, 1964] and proposed a diagram presenting a criterion for predicting the breaking wave height. Later Goda [1974] gave an approximate expression for the diagram as

$$H_b = 0.17 \cdot L_0 \left\{1 - \exp\left[-1.5\frac{\pi h_b}{L_0}(1 + 15\tan(\beta_s)^{4/3})\right]\right\} \tag{3}$$

- Battjes and Janssen [1978] modified Miche's [1944] formula by including the term of $\gamma/0.88$ into the formula so that the formula is reduced to $H_b = \gamma h$ in shallow water condition, where γ is an adjustable coefficient. This parameter is often referred to as the breaker index. The calibration of the formula indicated that $\gamma = 0.8$ gave the best prediction.

$$H_b = 0.142 \cdot L_b \cdot \tanh\left(\frac{0.8}{0.88}\frac{2\pi h_b}{L_b}\right) \tag{4}$$

- Ostendorf and Madsen [1979] modified the formula of Miche [1944] by including the bottom slope into the formula. After comparison with the laboratory data, the formula by Miche [1944] was modified to be

$$H_b = 0.14 \cdot L_b \cdot \tanh\left[\left(0.8 + 5\tan(\beta_s)\right) \frac{2\pi h_b}{L_b} \right] \qquad for\ \beta_s \le 0.1$$

$$H_b = 0.14 \cdot L_b \cdot \tanh\left[\left(0.8 + 5(0.1)\right) \frac{2\pi h_b}{L_b} \right] \qquad for\ \beta_s > 0.1 \tag{5}$$

The angle β_S shall be given in radians.

- Singamsetti and Wind [1980] conducted laboratory tests and proposed two empirical formulae based on their own data. The experiments covered a range of 0.025 < tan (β_s) < 0.2 and 0.02 < H_0/L_0 < 0.065.

$$H_b = 0.575 \cdot H_0 \cdot \left(\tan(\beta_s)\right)^{0.031} \cdot \left(\frac{H_0}{L_0}\right)^{-0.254}$$

$$H_b = 0.937 \cdot h_b \cdot \left(\tan(\beta_s)\right)^{0.155} \cdot \left(\frac{H_0}{L_0}\right)^{-0.13} \tag{6}$$

- The only formula referenced to take into consideration irregular wave breaking is the formula provided by Kamphuis [1991]. The formula was based on a modified Miche [1944] formula by introducing the exponential form of the bottom slope into the formula. After calibrating to irregular breaking wave data, the formula for the significant wave height H_s of the irregular wave breaking was given by Eq.(7). For irregular waves the wavelength, L_p, was calculated after the peak period in the wave frequency spectrum.

$$(H_s)_b = 0.095 \cdot \exp\left(4\tan(\beta_s)\right) \cdot L_p \tanh\left(\frac{2\pi h_b}{L_b}\right) \quad (irregular\ waves)$$

$$H_b = 0.127 \cdot \exp\left(4\tan(\beta_s)\right) \cdot L_b \tanh\left(\frac{2\pi h_b}{L_b}\right) \quad (regular\ waves) \tag{7}$$

According to Kamphuis [1991] the breaking significant wave height was only 75 % of the singular breaking wave height.

- Nelson [1993] demonstrated that Eq.(8) defines the largest wave height to water depth ratio possible for stable, transitional and shallow waves propagating in water of constant depth, i.e. a horizontal bed, and that this value is applicable to the individual waves of a naturally occurring random wave train. The formula is based on field measurements. The parameter F_c relates to the type of waves being deep, transitional or shallow water waves and referenced as the non-linearity parameter after Swart and Loubster [1978]. The non-linearity parameter is described in greater detail later in the present thesis. The wave period T refers to the individual wave with the wave height H.

$$\frac{H_b}{h_b} = \frac{F_c}{22 + 1.82\,F_c}, \qquad F_c = \frac{g^{1.25} H^{0.50} T^{2.50}}{h_b^{1.75}} \tag{8}$$

  Values greater than $F_c > 500$ indicate shallow water waves and the largest wave height to water depth ratio approaches a value of 0.55.

By considering the formulae presented in the above, it is assumed that the parameters influencing the breaking process is the water depth at breaking, the wave height, the wave period and the bottom slope.

Rattanapitikon et al. [2000] performed a review of a large range of breaker height formulae including the formulae mentioned above and concluded that the existing formulae make good predictions for breaking of regular waves on gentle slopes in the range $0.00 < \tan(\beta_s) < 0.07$, but predict only fair predictions for the breaking waves on a steeper slope, $0.10 < \tan(\beta_s) < 0.44$. By including a dependence of the slope in several of the formulae, the predictions seem to improve according to Rattanapitikon.

CHAPTER 5 PRESENTATION OF WAVE MODEL

The aim of the present thesis is to give guidance on the evaluation of the wave energy dissipation for waves propagating steep slopes as coral reefs or artificial submerged reefs. The approach is to establish relevant data from small-scale tests and further to establish a simple numerical wave model, which can simulate irregular waves propagating steep slopes and the related wave energy dissipation. With such a model it is possible to simulate various wave climates, and thereby obtain a tool to evaluate the transmitted and dissipated energy of waves breaking over steep slopes. Such models have already been established as also briefly described in Section 3.2, but there is still some uncertainty connected to these models regarding how to describe the wave breaking process, especially when waves breaking over steep slopes are involved. Existing wave breaking models are based on various models of wave propagation and different wave breaking models. Still, all the models are using empirical coefficients to describe the wave energy dissipation. In order to establish these parameters, experimental tests often have to be performed.

As mentioned, a simple model will be developed describing propagating waves and the two significant wave energy dissipation processes being breaking waves and wave energy dissipation due to bottom friction. The dissipation processes will be based on various empirical coefficients, which shall be possible to estimate based on characteristic data often available.

The model actual consists of several models: a model able to propagate water waves and models to describe relevant energy dissipation processes. For simplification and in order to avoid confusions these models will in the following be referred to as “the wave model”.

5.1 Choice of the wave model - the Mild-Slope equation

In front of the submerged reef, the wave field consists of incident and reflected waves. When the waves propagate over the reef the water depth varies substantially and refraction and diffraction effects cannot be neglected. A simple and suitable formulation of the waves progressing over a steep slope will be the extended refraction-diffraction equation provided by Massel [1993] and Massel and Gourlay [2000], which takes into account steep, non-uniform slopes to comply with the geometry of reef structures. Furthermore, Massel suggested a method to include the two dominating energy dissipation processes being breaking of waves and bottom friction.

By tradition, two types of wave equations are used for describing the propagation and behaviour of waves, the Boussinesq equation and the Mild-Slope equation. In general, the Mild-Slope equation is used describing linear waves and the Boussinesq equations are used regarding non-linear shallow water waves. For some applications the Boussinesq equation is preferable, as determining the short-wave disturbance in

harbours. However, for other applications such as harbour resonance studies or wave-induced currents in the surf zone, the Mild-Slope equation proves preferable because of the reduction in the computational effort involved.

The Boussinesq equation is a more comprehensive approach and in general more difficult to implement and solve in a numerical model. The equation includes non-linearity as well as frequency dispersion. Basically, the frequency dispersion is introduced in the flow equations by taking into account the effect on the pressure distribution due to the vertical water flow acceleration. The major restriction of the classical Boussinesq equation is the water depth limitations, which to some extent has been solved in recent formulations.

Instinctively, a model based on the Boussinesq equations would be preferable because the wave breaking process on the steep reef slope and later on the shallow reef-plateau is highly non-linear. Still, it has been chosen to employ the approach by Massel and Gourlay [2000], because they presented promising results with their wave model based on the extended Mild-Slope equation. As mentioned in Section 3.2 the Extended Mild-Slope equation as proposed Massel and Gourlay [2000] does not satisfy the condition at the sloping bottom. A correct formulation of the bottom condition was addressed in a few papers of Athanassoulis and Belibassakis [1999]. It is chosen not to include Athanassoulis and Belibassakis correction and it is later seen that the original formulation by Massel still yields impressive results in several test calculations. In the following an introduction of the Mild-Slope equation is given.

Berkhoff [1972] derived the refraction-diffraction equation, which is also known as the classical Mild-Slope equation. The equation combines for the first time refraction, diffraction and shoaling into one consistent model. The equation is today widely used in order to predict wave properties in coastal regions. The equation can deal with complex wave fields with satisfactory accuracy. The theory is restricted to irrotational linear harmonic waves, and loss of energy due to friction or breaking is not taken into account. As indicated, the name Mild-Slope refers to the basic assumption that the bed is mildly sloping. Booij [1983] reported favourably on its applicability for slopes in the order of 1:3.

In a linear dispersive system, the combined effect of water wave transformation such as refraction, diffraction, shoaling, and reflection can be predicted by the Mild-Slope equation. This wave equation is useful in modelling surface wave propagation in a wide variety of situations in both deep and shallow water. Examples include wave propagation in the vicinity of islands, harbour resonance and especially wave fields in smaller coastal areas, where diffraction and wave breaking is important.

Berkhoff's equation is applied as a starting point for developing a suitable numerical model. For simulation of waves passing coral reef structures, important processes being wave breaking and energy dissipation due to bottom friction along the rough

coral-surface have to be included as previously mentioned. Furthermore, it is necessary to include higher-order terms of the seabed slope because of the relatively high steepness of the reefs.

The Mild-Slope equation developed by Berkhoff may be written as

$$\nabla \cdot (CC_g \nabla \varphi) + k^2 CC_g \varphi = 0 \tag{9}$$

where ∇ is the horizontal gradient operator. The velocity potential at the mean water level is denoted φ. C and C_g are the phase speed and group velocity, respectively, of a wave with the angular frequency, ω, and wave number, k. Berkhoff's assumption of a mild slope can be expressed as $\nabla h / kh << 1$.

Eq.(9) is the elliptic version of the Mild-Slope equation. Several numerical models are currently available, which solves the elliptic form of the Mild-Slope equation by a finite element technique or a finite difference technique. A discretisation of the governing partial differential equation using finite elements is flexible in terms of size and distribution of grid elements and therefore allows more detailed solutions to be obtained for particular areas of interest. However, a finite difference discretisation is generally simpler to implement and involves fewer equations to be solved, i.e. compared with the finite element method.

In order to overcome the computational efforts associated with solving the elliptic formulation of the Mild-Slope equation for large problem domains, several authors have proposed models based on the hyperbolic formulation. Radder and Dingemans [1985], provided a form of the time-dependent Mild-Slope equation based on the Hamiltonian theory of surface waves. Copeland [1985] also derived similar time-dependent equations using the characteristics of linear waves and the definition of a volume flux.

Another approach and a more economical method are based on the parabolic approximation. The disadvantage of such a formulation concerns the inadequate description of the underlying physics because wave reflection and diffraction effects in the direction of wave propagation are neglected. Only diffraction effects along the wave front are taken into account, and the mean direction of wave propagation has to be maintained. It is noted that such constraints cannot be neglected in harbour studies, thus limiting the applicability of the model in such circumstances.

5.2 The time-dependent extended refraction-diffraction equation

Berkhoff's assumption of a mild slope neglected the higher-order bottom terms $O((\nabla h)^2)$ and $O(\nabla^2 h)$. In order to account for rapidly varying topography and steep slopes Massel [1993; 1996a] developed the extended refraction-diffraction equation by using the Galerkin-Eigenfunction method. The equation includes the higher-order

bottom effect terms proportional to the square of bottom slope, $(\nabla h)^2$, and to the bottom curvature, $(\nabla^2 h)$. Furthermore, his derivation included the evanescent modes, i.e. the non-propagating modes.

In the following a derivation of the time-dependent wave equation is presented. The derivation is based on Green's formula method as also shown by Suh et al. [1997].

The three-dimensional velocity potential $\varphi(x, y, z, t)$ is governed by

$$\varphi_{xx} + \varphi_{yy} + \varphi_{zz} = \nabla^2 \varphi + \varphi_{zz} = 0 \quad (-h \le z \le 0) \tag{10}$$

where *x*, *y* are the horizontal coordinates. The vertical coordinate *z* is measured vertically upwards from still water level. The time is denoted *t*. The notation of the derivative is represented as a subscript, i.e., $\varphi_{zz} = \frac{\partial^2 \varphi}{\partial z^2}$.
The linearised free surface conditions for harmonic waves yield

$$\eta = -\frac{1}{g}\varphi_t \quad , z = 0 \quad (\textit{dynamic condition}) \tag{11}$$

$$\eta_t = \varphi_z \quad , z = 0 \quad (\textit{kinematic condition}) \tag{12}$$

the surface is denoted η. A combined free-surface condition can be obtained from Eqs.(11) and (12) as

$$\varphi_z = -\frac{1}{g}\varphi_{tt} \quad (z = 0) \tag{13}$$

The bottom condition yields

$$\varphi_z = -\nabla h \cdot \nabla \varphi \quad \{z = -h(x, y)\} \tag{14}$$

The solution to Eqs.(10), (13) and (14) can be expressed as

$$\varphi(x, y, z, t) = \tilde{f}(x, y, z) \cdot \tilde{\varphi}(x, y, t) + \sum \textit{evanescent modes} \tag{15}$$

where the function $\tilde{f} = \cosh(kh + kz)/\cosh(kh)$ is a slowly varying function in the horizontal plane. $\tilde{\varphi}(x, y, z)$ is the depth-averaged velocity potential. The wave

number, $k(x, y)$, must satisfy the linear dispersion relation, which relates k to the wave angular frequency, ω, and the water depth, $h(x, y)$, by

$$\omega^2 = gk \tanh(kh) \tag{16}$$

The propagating component of φ can be extracted applying Green's second identity to $\tilde{f}$ and φ by

$$\int_{-h}^{0} (\tilde{f}\varphi_{zz} - \varphi \tilde{f}_{zz}) dz = \left[\tilde{f}\varphi_z - \varphi \tilde{f}_z\right]_{-h}^{0} \tag{17}$$

Neglecting the evanescent modes and using Eqs.(10), (13), (14) and (15) the integrals can be reduced to

$$\tilde{\varphi}_{tt} - \nabla(CC_g \nabla\tilde{\varphi}) + (\omega^2 - k^2 CC_g)\tilde{\varphi} - g\left(\nabla h \cdot \left[\tilde{f}\,\nabla\tilde{f}\right]_{z=-h} + \int_{-h}^{0} \tilde{f}\,\nabla^2 \tilde{f}\, dz\right)\tilde{\varphi} = 0 \tag{18}$$

The terms describing a rapidly varying topography, $O((\nabla h)^2)$ and $O(\nabla^2 h)$, can be deducted by using the following relationships

$$\nabla\tilde{f} = \left(\frac{\partial\tilde{f}}{\partial h} + \frac{\partial\tilde{f}}{\partial k}\frac{\partial k}{\partial h}\right)\nabla h \tag{19}$$

$$\nabla^2 \tilde{f} = \frac{\partial}{\partial x}\left(\frac{\partial\tilde{f}}{\partial h}\frac{\partial h}{\partial x} + \frac{\partial\tilde{f}}{\partial k}\frac{\partial k}{\partial h}\frac{\partial h}{\partial x}\right) + \frac{\partial}{\partial y}\left(\frac{\partial\tilde{f}}{\partial h}\frac{\partial h}{\partial y} + \frac{\partial\tilde{f}}{\partial k}\frac{\partial k}{\partial h}\frac{\partial h}{\partial y}\right) \tag{20}$$

After a lengthy algebraic manipulation Eq.(18) becomes the time-dependent extended refraction-diffraction equation

$$\varphi_{tt} - \nabla\cdot(CC_g\nabla\varphi) + (\omega^2 - k^2 CC_g)\varphi + \omega^2\left\{R_1(\nabla h)^2 + R_2\nabla^2 h\right\}\varphi = 0 \tag{21}$$

For simplicity in notation the velocity potential will in the following be denoted without a sign above the symbol.

The parameters R_1 and R_2, determining the higher-order bottom effects, are given by

$$R_1 = \frac{1}{\cosh^2 kh}\left(W_1 I_1 + W_2 I_2 + W_3 I_3 + W_4 I_4 + W_5 I_5 + W_6\right) \tag{22}$$

$$R_2 = \frac{1}{\cosh^2 kh}\left(U_1 I_1 + U_2 I_2 + U_3 I_3\right) \tag{23}$$

The complicated expressions of *W*, *I* and *U* are given by Massel [1993]. Small errors in W_1 and W_2 are found in Massel's expressions and later provided by Suh et al. [1997], see Appendix B.

For a monochromatic wave Eq.(21) reduces to

$$\nabla \cdot (CC_g \nabla \varphi) + k^2 CC_g \varphi - \omega^2 \left\{ R_1 (\nabla h)^2 + R_2 \nabla^2 h \right\} \varphi = 0 \tag{24}$$

which is similar to the propagating time-invariant wave model developed by Massel [1993]. Neglecting the higher-order bottom terms, Eq.(24) reduces to the original Berkhoff Mild-Slope equation shown as Eq.(9).

5.3 Energy dissipation to be included into the time-dependent extended refraction-diffraction equation

The wave model described in Section 5.2 does not take into account any wave energy dissipation. For waves propagating over steep slopes in shallow waters the wave breaking yields the primary loss of energy, where a minor contribution is expected from wave energy dissipation due to bottom friction.

Massel [1996a] advised an introduction of the energy dissipation due to wave breaking and bed friction into the non-time-dependent extended refraction-diffraction equation. Such a representation was also suggested by Booij [1981], where the representation was based on the classical Mild-Slope equation. Booij took into account the wave energy dissipation due to bed friction but not wave breaking.

As shown by Dingemans [1997] the Mild-Slope equation can be written as a wave energy transport equation. The dissipation is included in the time-dependent extended Mild-Slope equation, Eq.(21), as

$$\varphi_{tt} - \nabla \cdot (CC_g \nabla \varphi) + (\omega^2 - k^2 CC_g)\varphi + \omega^2 \left\{ R_1 (\nabla h)^2 + R_2 \nabla^2 h \right\} \varphi + W \varphi_t = 0 \qquad (25)$$

where

$$W = \varepsilon / E \qquad (26)$$

W is the damping term and ε is the total rate of energy dissipation. E is the total energy of the waves. The total energy contained at a given location with irregular waves is given by

$$E = \frac{1}{8} \rho_w \, g \, H_{rms}^{\ 2} \qquad (27)$$

The total rate of damping due to the process of wave breaking and bed friction along the surf zone on the shallow reef-plateau consists of the two contributions as

$$W_f + W_b = \frac{\varepsilon_f + \varepsilon_b}{E} \qquad (28)$$

5.3.1 Wave energy dissipation due to wave breaking

There exists a wide range of literature aimed at parameterisation of the breaking process to provide an approximate energy dissipation rate during wave breaking, but mostly regarding gentle or mild bottom slopes. The most referenced studies are those of Battjes and Janssen [1978]; Thornton and Guza [1983]; Dally et al., [1985] and Lippmann et al. [1996]. The models are in general based on the assumption that the bottom profile and some offshore wave parameters are known. The breaking process is still poorly understood and the models require the specification of free unstrained coefficients. For steep slopes the knowledge of the process is even less compared to the breaking process at gentler bottom slopes. Some experimental studies of the breaking process at steep slopes were carried out by Gerritsen [1981]; Gourlay [1994] and Hardy et al. [1996].

The periodic bore model approach for description of the energy dissipated during the wave breaking is selected for later implementation in the wave model described in Section 5.2.

The energy, *D*, per unit span dissipated in a bore is [Massel and Belberova, 1990; Lamb, 1932]

$$D = \frac{1}{4}\rho_w g\,(Y_2 - Y_1)^3 \left\{ \frac{g(Y_1 + Y_2)}{2Y_1 Y_2} \right\}^{½} \tag{29}$$

The depths Y_1 and Y_2 are depicted in Figure 5. h is the local water depth and H is the wave height **before** wave breaking. The gravity is given by g and ρ_w is the density of seawater. The following relations of the geometry can be deduced

$$\begin{aligned} Y_2 - Y_1 &= \alpha H \\ Y_1 &= h - (1-\beta)\alpha H \\ Y_2 &= h + \alpha\beta H \end{aligned} \tag{30}$$

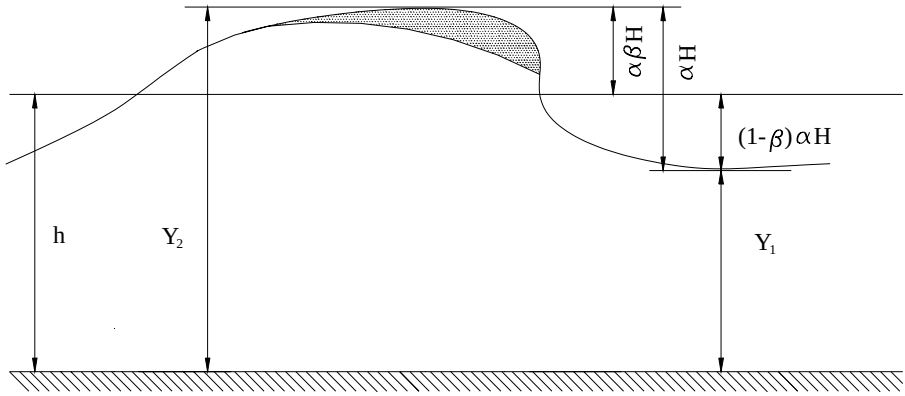

Figure 5: *Definitions related to the periodic bore model.*

The coefficient α is in the order of 1 and expresses the influence of turbulence in the breaking wave. The coefficient $\beta\,(0.5<\beta<1.0)$ is related to the steepness and the peakedness of the crest and flatness of the wave trough. According to first order wave theory then $\beta = 0.5$. The coefficient α can only be found from experiments.

An approximation of Eq.(29) using Eq.(30), where $\beta \approx 0.5$ and α being in the order of 1, yields

$$D = \frac{\alpha^3}{4}\rho_w g H^3 \sqrt{g/h\left[1-\frac{1}{4}\left(\frac{H}{h}\right)^2\right]} \tag{31}$$

For waves with the angular frequency, ω, the energy dissipated per unit area, ε_b, can be expressed as

$$\varepsilon_b = \frac{D}{L} = \frac{\omega}{2\pi C} D \tag{32}$$

where C is the wave celerity. This yields the expression

$$\varepsilon_b = \frac{\alpha_0\ \rho_w\ g\ \omega}{8\pi}\frac{H^3}{h}\left(\frac{\sqrt{gh}}{C}\right)\Psi \tag{33}$$

where

$$\Psi = \left[1 - \frac{1}{4} \left(\frac{H}{h} \right)^2 \right]^{-½} \tag{34}$$

For simplicity of notation, $\alpha_0 = \alpha^3$. The non-dimensional wave height, *H/h*, is less than 1 in the surf zone yielding $\Psi \approx 1$ and Eq.(33) becomes

$$\varepsilon_b = \frac{\alpha_0 \ \rho_w \ g \ \omega}{8\pi} \frac{H^3}{h} \left(\frac{\sqrt{gh}}{C} \right) \tag{35}$$

It is seen that the influence of the wave energy dissipation term α_0 is correlated with the dissipation. Stive [1984] showed that the classical bore model ($\Psi \approx 1$) underestimates the wave energy dissipation in breaking waves. The inclusion of α_0 is to compensate for this underestimate. Although, it is expected that α_0 is in the order of 1. A higher value will indicate the influence of the actual underestimation.

The estimation of α_0 and *H* will be discussed later. Eq.(35) relates to the expression given by Battjes and Janssen [1978].

5.3.2 Wave energy dissipation due to bottom friction

Wave energy dissipation due to bottom friction is the loss of wave energy due to the interaction between two boundary layers, i.e. the moving water particles and the bottom boundary layer. In the bottom boundary layer, within centimetres, the flow is strongly turbulent and associated with significant wave energy dissipation. In the following this process is denoted wave energy dissipation due to bottom friction.

It is not the scope of the present thesis to go into detailed studies of the hydraulic roughness of coral reef platforms or rock reefs. The primarily aim is to describe the wave breaking process, which is the main contributor to the dissipation of wave energy regarding waves breaking. Still, it is necessary to give a brief introduction of the subject in order to explain how wave energy dissipation due to bottom friction is adopted in the wave model.

For all prototype wave conditions of significance, the oscillatory flow at the bed is a fully developed rough turbulent flow as described by Jonsson [1963, 1966]. In rough turbulent conditions the friction factors, which normally have been associated with boundary layer theory, are independent of Reynolds number, and are only a function of the relative roughness at the seabed. The relative roughness is defined as the relationship between the hydraulic roughness and the amplitude of the oscillatory wave motion at the seabed. The amplitude of the wave motion is usually estimated

from the linear wave theory. Coral reefs or steep rocks slopes are fixed beds and only the amplitude of the water particle movement is a variable in the roughness ratio. It gets even more complicated when the bed is moving.

There are already some extensive laboratory studies available on the hydraulic roughness and associated friction factors for fixed beds, reference is made to Jonsson [1963, 1966] but also to the work by Kamphuis [1975]. Field measurements of the hydraulic roughness of fixed beds for irregular waves are rare, but Nelson [1996] performed such measurements under conditions ideal for extracting the influence of wave energy dissipation due to the bed friction. The measurements were carried out on a shallow coral reef plateau with constant depth for irregular waves propagating without breaking. The studies and conclusion by Nelson is of importance to this study because it is verified that the roughness of coral reefs is not much rougher in hydraulic terms than sandy beds. Furthermore, estimates of applicable frictions factors are given. It is however noted that Nelson did not study the wave energy dissipation due to bottom friction for waves breaking over a steep coral reef, but stable wave propagation on the shallow reef-plateau.

There exist mainly two wave related friction factors. The wave friction factor denoted f_w and the wave energy dissipation factor, f_r.

The wave friction factor, f_w, is defined as

$$\tau_{\max} = \frac{1}{2}\rho_w \ f_w U^2 \tag{36}$$

where τ_{max} is the maximal bed shear stress due to the horizontal oscillatory water particles at the seabed and ρ_ω is the water density.

The wave energy dissipation factor, f_r is defined in terms of the time-averaged rate of wave energy dissipation, ε_f, due to bed friction. The expression is acknowledged and first given by Gerritsen [1981], see also Nelson [1996]

$$\varepsilon_f = \frac{1}{T}\sum_{t=0}^{t=T} \tau \, u_b \Delta t = \frac{2}{3\pi}\rho_w \ f_r \left| U \right|^3 \tag{37}$$

where τ is the instantaneous bed shear stress, u_b is the instantaneous bed velocity and U is the amplitude of the bed velocity variation in the wave with the period T. Linear wave theory predicts the amplitude of the bed velocity variation for a regular wave with the wave period, T, and wave height, H, as

$$U = \frac{\pi H}{T} \frac{\cosh k(z+h)}{\sinh kh}, \quad (bottom\ z = -h) \tag{38}$$

The wave friction factor, f_w, requires direct or indirect measurements of the bed shear, while the determination of the wave energy dissipation factor, $f_{r,}$ requires the measurement of the loss of wave energy over a known distance. Such knowledge yields the rate of energy dissipation, and combined with measurements of the amplitude of the bed velocity variation, the wave energy dissipation factor can be found directly from Eq.(37).

Based on spectral estimates of the significant wave height and the peak period Nelson [1996] found f_r to be between 0.1 and 0.2 and furthermore showed that the wave friction factor and the wave energy dissipation factor are almost similar for fully developed rough turbulent flow. It is moreover found that the wave energy dissipation factor for the fixed reef surface equals the wave energy dissipation factor for a moveable bed when the moveable bed consisted of a bed particle size equal to 0.6 mm. This indicates that rough reefs/rock berms in hydraulic terms are equal to the hydraulic roughness of many sandy beds.

Later in present thesis a numerical model is presented, which is capable of simulating the wave energy dissipation processes. Experimental small-scale tests are performed in order to obtain essential data. The experimental data are also used to calibrate the numerical wave-breaking model. To reflect the conditions in the small-scale model the wave energy dissipation factor to be used in the numerical model is f_r = 0.01. This value is believed to be realistic for a smooth concrete surface.

For irregular waves the choice of the amplitude of the bed velocity, U, is not straightforward. Nelson [1996] calculated the wave energy dissipation values based on spectral estimates of the wave height and wave period. It has therefore been chosen to evaluate the bed velocity amplitude due to a characteristic wave height and period. This choice is discussed in later sections.

5.4 Wave set-up due to breaking waves

Wave breaking always induces denivelation of the mean water level. Massel and Gourlay [2000] showed that the extended Mild-Slope equation and set-up equation (momentum equation) have to be solved simultaneously yielding the root-mean-square wave height and the wave-induced set-up at each water depth. It is chosen not to simulate the wave setup in the numerical model to be developed. In the experimental model, which is described later, it was not possible to measure the induced wave set-up with the wave gauges used. Obvious, the wave-induced water level set-up is small during the experimental tests. It must be noted that a special draining system, used to avoid water being stored behind the slope, could have influenced the wave-induced set-up.

5.5 Energy dissipation in the case of breaking irregular waves

In order to relate the dissipation rate given by Eq.(35) to the process of the random waves breaking, Battjes and Janssen [1978] proposed the following procedure by introducing the factor Q_b, which is an estimate of the fraction of the waves breaking at a given location.

By assuming that the waves will break if they exceed a maximum wave height H_{max}, and that the wave heights before breaking follow a Rayleigh distribution [Massel, 1996a], the probability density function can be written as

$$f\,H = \begin{cases} \dfrac{H}{\hat{H}^2}\exp\left[-\dfrac{1}{2}\left(\dfrac{H}{\hat{H}}\right)^2\right] & for \quad 0 \le H \le H_{\max} \\ \dfrac{Q_b}{H_{\max}}\delta\left(\dfrac{H}{H_{\max}}-1\right) & for \quad H > H_{\max} \end{cases} \tag{39}$$

$\hat{H}$ is a modal value and is so far an unknown value. $\delta()$ is a delta function. The fraction of wave breaking can be expressed as

$$Q_b = prob.\,(H > H_{\max}) = \exp\left[-\frac{1}{2}\left(\frac{H_{\max}}{\hat{H}}\right)^2\right] \tag{40}$$

In a system with no loss of energy, $\hat{H} = 1/\sqrt{2}\cdot H_{rms}$, $H_{\max} \to \infty$ and the Rayleigh distribution is obtained. In Appendix G a brief description of the statistics of waves are given, and the Rayleigh distribution is introduced.

Expressing the wave statistics in terms of the root-mean-square wave height, H_{rms}, and $\hat{H}$ the following relation can be written

$$H_{rms}^2 = \int_0^\infty H^2 f(H) dH = \frac{1}{\hat{H}^2} \int_0^{H_{\max}} H^3 \exp\left[-\frac{1}{2}\left(\frac{H}{\hat{H}}\right)^2\right] dH + \frac{Q_b}{H_{\max}} \int_{H_{\max}}^\infty H^2 \delta\left(\frac{H}{H_{\max}} - 1\right) dH \tag{41}$$

and

$$H_{rms}^2 = 2\left\{1 - \exp\left[-\frac{1}{2}\left(\frac{H_{\max}}{\hat{H}}\right)^2\right]\right\}\hat{H}^2 \tag{42}$$

or

$$H_{rms}^2 = 2\left(1 - Q_b\right)\hat{H}^2 \tag{43}$$

It is more convenient to express the fraction Q_b in terms of H_{rms} and H_{max}. Eliminating $\hat{H}$ from Eq.(40) and Eq.(43) yields

$$\frac{1 - Q_b}{\ln(Q_b)} = -\left(\frac{H_{rms}}{H_{\max}}\right)^2 \tag{44}$$

or

$$Q_b = \exp\left(-\frac{(1 - Q_b)}{b^2}\right) \tag{45}$$

where $b = \dfrac{H_{rms}}{H_{\max}}$.

If the wave heights follow a Rayleigh distribution then H_{rms} is estimated as

$$H_{rms}^{\ 2} = 8\, m_0 = 8\, \sigma_\eta^{\ 2} \quad (m_0 = \sigma_\eta^{\ 2}) \tag{46}$$

where m_0 is the variance of the elevation of the non-breaking waves and more correctly defined as $m_0 = \int_0^\infty S(\omega)\, d\omega$, where $S(\omega)$ is the frequency spectrum.

When b increases, the fraction of broken waves, Q_b, also increases. In shallow water, where $H_{rms} \to H_{\max}$, all waves will break, i.e. $Q_b \to 1$.

The expected average energy dissipation per unit area according to Eq.(35) is estimated as

$$\varepsilon_b = \frac{\alpha_0\ \rho_w\ g\ \overline{\omega}}{8\pi} \left(\frac{H_{\max}^{\ 3}}{h} \right) \left(\frac{\sqrt{gh}}{\overline{C}} \right) Q_b \tag{47}$$

where $\overline{\omega}$ is taken as a characteristic value in the wave spectrum. This frequency is called the carrier frequency, which in the following is denoted with an overbar. The calculation of $\overline{C}$ is based on the carrier frequency. The use of such a frequency simplifies the numerical model and is justified when the spectrum is narrow. The choice of the wave carrier frequency is later discussed in detail.

The energy dissipation rate due to bed friction is given by Eq.(37)

$$\varepsilon_f = \frac{2}{3\pi} \rho_w\ f_r \left| U \right|^3 \tag{48}$$

where the size of U in the case of irregular waves shall be estimated as:

$$U = \frac{\pi\, H_{mean}}{T_P} \frac{\cosh k(z+h)}{\sinh kh}, \quad (bottom\ z = -h) \tag{49}$$

The choice of using H_{mean} is discussed later.

Finally, the total damping term W in Eq.(25) can be given accordingly to Eqs.(47), (48) and (28), as

$$W = W_f + W_b = \frac{\varepsilon_b + \varepsilon_f}{E} = \frac{\alpha_0 \overline{\omega}}{\pi h}\left(\frac{H_{\max}^3}{H_{rms}^2}\right)\left(\frac{\sqrt{gh}}{\overline{C}}\right) Q_b + \frac{16 f_r}{3\pi}\frac{|U|^3}{gH_{mean}^2} \tag{50}$$

yielding the equation governing the propagation of irregular waves over a rapidly varying slope including energy dissipation as

$$\varphi_{tt} - \nabla\cdot(\overline{C}\overline{C}_g\nabla\varphi) + (\overline{\omega}^2 - \overline{k}^2\overline{C}\overline{C}_g)\varphi + \overline{\omega}^2\left\{R_1(\nabla h)^2 + R_2\nabla^2 h\right\}\varphi + \left\{\frac{\alpha_0 \overline{\omega}}{\pi h}\left(\frac{H_{\max}^3}{H_{rms}^2}\right)\left(\frac{\sqrt{gh}}{\overline{C}}\right) Q_b + \frac{16 f_r}{3\pi}\frac{|U|^3}{gH_{mean}^2}\right\}\varphi_t = 0 \tag{51}$$

The initiation of energy dissipation due to wave breaking or the extent of the surf zone, in which Eq.(51) shall be used, is controlled by the maximum allowable wave height. Experimental tests are performed to establish the breaking criterion, which is discussed later. It is noted that Battjes and Janssen [1978] used the Miche type expression given by Eq.(4) as the maximum allowable wave height.

5.5.1 Estimation of wave energy dissipation term α_0

The value of the wave energy dissipation term α_0 is unknown for steep slopes. It has been shown that the coefficient should be in the order of *0*(1) [Battjes and Janssen, 1978, Thornton and Guza, 1983, Massel, 1996a].

Massel and Gourlay [2000] correlated the coefficient α_0 with a Swart and Loubser's [Swart and Loubser, 1978] type parameter F_{c0}:

$$F_{c0} = \left(\frac{H_0}{h_t}\right)^{1/2}\left(T\sqrt{\frac{g}{h_t}}\right)^{5/2} \tag{52}$$

where h_t is the still water depth at breaking and the deep-water wave height is denoted H_0. Originally, Nelson [1994] proposed this parameter in connection with wave breaking, as also described in Section 4.1. Although, Nelson used the local wave height and water depth to estimate the parameter. Gourlay [1994] argued that F_{c0}, based on the deep-water wave height, H_0, and a representative depth over the reef, h_t, are a suitable parameter for classifying wave transformation on a coral reef. It is known that values less than 10 indicate deep-water waves and values between 10-500 characterise transitional waves. Values above 500 indicate shallow water waves. It is noted by Massel and Gourlay [2000] that the extended refraction diffraction is not applicable for wave conditions yielding values of F_{c0} above 1000, i.e. if water depth on the reef-plateau is very shallow with waves being highly non-linear.

The parameter F_{c0} does not contain any information of the reef-face slope β_s. To take into account the dependence of the reef bottom slope Massel and Gourlay [2000] assumed a relationship between α_0 and reef geometry and incident wave parameters in a more general form as

$$\alpha_0 = f\left(F_{c0}, \beta_s\right) \tag{53}$$

in which β_s represents the slope of the reef-face. Tests by Massel and Gourlay [2000] showed that the following form of relationship is useful

$$\begin{aligned} &\alpha_0 = 0 \;\; if \, F_{c0} \le F_{c0}^{(\lim)} \\ &\alpha_0 = a\left(F_{c0} - F_{c0}^{(\lim)}\right)^b \;\; if \;\; F_{c0} > F_{c0}^{(\lim)} \end{aligned} \tag{54}$$

where a and b are fitted parameters and $F_{c0}^{(\lim)}$ is a threshold value of the parameter F_{c0}, where the observed or calculated value of energy dissipation and wave set-up are negligibly small [Massel and Gourlay, 2000]. This threshold value was found to be close to $F_{c0}^{(\lim)}$ =100. Based on test results obtained in the hydraulic laboratory of the dissipated wave energy, the coefficient α_0 will be further evaluated and new fitted values of a and b as introduced in Eq.(54), are presented for waves breaking at steep slopes.

CHAPTER 6 NUMERICAL DESCRIPTION OF THE WAVE MODEL

In order to develop the wave model based on the theory presented, it is necessary to convert the mathematical formulations into numerical schemes. A numerical formulation of the extended refraction-diffraction equation is described in the following. A formulation of Radder and Dingemans [1985] extended to include wave energy dissipation is chosen. This model is in the following referred to as the modified Radder and Dingemans model. Prior to this formulation, the Copeland formulation [Copeland, 1985] is tested in a numerical model to verify whether the approach using the extended Mild-Slope is a feasible approach to model the wave propagation over a rapidly varying bottom slope. The formulation provided by Copeland is easily implemented into a numerical model. Furthermore, the results using the Copeland approach are used to check the later implemented modified formulation by Radder and Dingemans. The Copeland formulation is only valid when generating regular waves. The formulation provided by Copeland, extended to include a rapidly varying sea bottom, is described in Appendix C.

6.1 Modified formulation based on Radder and Dingemans' equations

Using Copeland's formulation the group behaviour of irregular waves is not treated correctly. Based on Radder and Dingemans' formulation [Radder and Dingemans, 1985] irregular waves with a narrow frequency band can be simulated.

The original equations of Radder and Dingemans [1985] are given by

$$\eta_t = -\nabla \cdot \left(\frac{\overline{C}\,\overline{C}_g \nabla \varphi}{g} \right) + \left(\frac{\overline{\omega}^2 - \overline{k}^2 \overline{C}\,\overline{C}_g}{g} \right) \varphi = F(\varphi) \tag{55}$$

and

$$\varphi_t = -g\eta = G(\eta) \tag{56}$$

where Eq.(55) is equivalent to Eq.(21) neglecting the higher-order bottom terms and utilising the relation of the linearised free surface boundary condition given by Eq.(56). The overbar indicates that these parameters shall be calculated using a dominant frequency in the wave spectrum such as the spectral peak period.

Radder and Dingemans' [1985] original equations neglected the higher bottom terms and dissipations terms. Introducing these contributions Eq.(57) appears as

$$\eta_t = -\nabla\cdot\left(\frac{\overline{C}\overline{C}_g\nabla\varphi}{g}\right)+\left(\frac{\overline{\omega}^2-\overline{k}^2\overline{C}\overline{C}_g}{g}\right)\varphi+\frac{\overline{\omega}^2}{g}\left(R_1(\nabla h)^2+R_2\nabla^2 h\right)\varphi- \left\{\frac{\alpha_0\,\overline{\omega}}{\pi\,h}\left(\frac{H_{\max}^3}{H_{rms}^2}\right)\left(\frac{\sqrt{gh}}{\overline{C}}\right)Q_b+\frac{16\,f_r}{3\pi}\frac{|U|^3}{gH_{rms}^2}\right\}\eta = F(\varphi,\eta) \tag{57}$$

See also Eq.(51), which can be rewritten as Eq.(57) by use of the surface boundary condition Eq.(56).

Eqs.(56) and (57) constitute time-dependent wave equations including higher order terms according to a rapidly varying bottom and dissipation terms due to wave breaking and bottom friction.

6.2 Internal generation of waves

Wave generation in numerical models is relatively well documented in the literature. Waves can be generated by specifying the relevant values of water surface elevation, particle velocity or volume flux at each time step along the border of the model. Another method and the one chosen in the present numerical wave model is to generate waves by adding the values with desired wave energy to be computed at a wave generation line inside the boundary at each time step. When the former method is used, problems may occur because the waves passing the wave generation line from the inside of the computational domain will be trapped and cause unwanted addition of wave energy and distortion of the wave phase inside the domain. However, the latter method, internal generation of waves, does not give rise to such problems, because the method permits the waves to pass freely across the wave generation line while desired wave energy is generated at the line.

Internal generation of waves has been used by several researches (Larsen and Dancy [1983] regarding the Boussinesq equation of Peregrine [1967]; Madsen and Larsen [1987] regarding the Copeland equation).

The time-dependent wave equations predict the propagation of wave energy as well as the change of wave phase. The approach is to add the water surface elevation of the incident waves to the computed surface elevation at each time step. This is only done at the wave generation line. This results in a propagation of wave energy as well as a change in wave phase. The propagation of wave energy can be predicted by the transport equation for wave energy. That is, the velocity of disturbances caused by the incident wave is the energy velocity C_e and the value η^* added to the surface elevation at each time step at the wave generation line.

$$\eta^* = 2\eta \frac{\overline{C}_e \Delta t}{\Delta x} \tag{58}$$

Δx is the uniform grid spacing and Δt is the respective time step.

Lee and Suh [1997] showed by using the geometric approach that the energy velocity is given by

$$C_e = \overline{C}_g \frac{\overline{\omega}}{\omega} \sqrt{1 + \frac{\overline{C}}{\overline{C}_g} \left[\left(\frac{\omega}{\overline{\omega}} \right)^2 - 1 \right]} \tag{59}$$

where ω represents the individual frequencies in the spectrum, i.e. the value added to the surface elevation at each time step at the wave generation point is given by

$$\begin{aligned} \eta^* &= 2 \tanh(t/T_p) \cdot \sum_j \frac{C_{ej} \Delta t}{\Delta x} A_j \cos(\omega_j - \varepsilon_j) \\ &= 2 \tanh(t/T_p) \cdot \frac{\overline{C}_g \Delta t}{\Delta x} \sum_j \tilde{A}_j \cos(\omega_j - \varepsilon_j) \end{aligned} \tag{60}$$

where

$$\tilde{A}_j = A_j \frac{\overline{\omega}}{\omega_j} \sqrt{1 + \frac{\overline{C}}{\overline{C}_g} \left[\left(\frac{\omega_j}{\overline{\omega}} \right)^2 - 1 \right]} \tag{61}$$

A_j is the amplitude of incident waves with the angular frequency, ω_j, and ε_j is a random phase. The term tanh (t/T_p) is added for a slow start of the wave generation.

6.3 Sponge layers for minimising boundary wave reflection

Sponge layers are placed at the outside boundaries for minimising wave reflection from the boundaries by dissipating wave energy inside the sponge layers. Taking into account the sponge layer in the modified Radder and Dingemans approach, Eq.(56) is modified as

$$\varphi_t = -g\eta - D_s\varphi = G(\varphi,\eta) \tag{62}$$

The damping coefficient, D_s, is given by

$$D_s = \begin{cases} 0, & \textit{outside sponge layer} \\ \overline{\omega}_{\max}\left(\dfrac{e^{d/S}-1}{e-1}\right), & \textit{inside sponge layer} \end{cases} \tag{63}$$

where d is the distance from the starting point of the sponge layer and S is the thickness of the sponge layer. The damping increases exponentially through the sponge layer, with maximal damping, $\overline{\omega}_{\max}$, at the outer boundary. The circular wave frequency, $\overline{\omega}_{\max}$, is the maximal frequency used in the wave generation.

6.4 Discretisation of the modified Radder and Dingemans equations

Radder and Dingemans' modified formulations, Eq.(57) and Eq.(62), are discretised by a fourth-order Adams-Bashforth-Moulton scheme, which is referenced as having good stability properties [Kirby et al., 1992]. This is a so-called predictor-corrector method in time and by a three-point symmetrical formula in space. The Adams-Bashforth part is the predictor step and yields

$$\begin{aligned} \eta^{n+1} &= \eta^n + \frac{\Delta t}{24}\left(55F^n - 59F^{n-1} + 37F^{n-2} - 9F^{n-3}\right) \\ \varphi^{n+1} &= \varphi^n + \frac{\Delta t}{24}\left(55G^n - 59G^{n-1} + 37G^{n-2} - 9G^{n-3}\right) \end{aligned} \tag{64}$$

and the corrector step related to Moulton yields

$$\begin{aligned} \eta^{n+1} &= \eta^n + \frac{\Delta t}{24}\left(9F^{n+1} + 19F^n - 5F^{n-1} + F^{n-2}\right) \\ \varphi^{n+1} &= \varphi^n + \frac{\Delta t}{24}\left(9G^{n+1} + 19G^n - 5G^{n-1} - G^{n-2}\right) \end{aligned} \tag{65}$$

where the superscript *n [0…, N]* denotes the value in the *n*'th time step. $F(\varphi,\eta)$ and $G(\varphi,\eta)$ are the right-hand sides of Eqs.(57) and (62), respectively.

It is noted that the term $\nabla(\overline{C}\overline{C_g})$ in Eq.(57) is expressed

$$\frac{\nabla(\overline{C}\overline{C_g})}{\overline{C}\overline{C_g}} = \frac{\hat{G}(\bar{k}h)}{h}\nabla h \tag{66}$$

where

$$\hat{G}(\bar{k}h) = \frac{\bar{k}h}{\hat{T} + \bar{k}h(1-\hat{T}^2)}\left[1 - 3\hat{T}^2 + \frac{2\hat{T}}{\hat{T} + \bar{k}h(1-\hat{T}^2)}\right] \tag{67}$$

and

$$\hat{T} = \tanh(\bar{k}h) \tag{68}$$

For the slow start of wave generation, the left hand side of Eq.(58) is multiplied by the term $\tanh(t/T)$, where T is a characteristic wave period representing the assumed narrow wave spectrum. At outside boundaries, total reflection is assumed, but the reflected wave becomes negligible inside the domain because the sponge layer significantly reduces the incoming wave energy.

It is noted that doing several corrector steps does not improve the solution significantly. The step is accurate only to the finite order of the corrector term. This error term is of the same order as the correction the iteration is supposed to cure. An improvement is not worth an effort. An extra effort would be better spent in performing a smaller time step.

The Courant number is an often used stability parameter related to numerical schemes. The Courant number used and referenced in the present thesis is based on the group velocity as

$$C_r = \overline{C}_g \, \Delta t / \Delta x \tag{69}$$

The time step using the Adams-Bashforth-Moulton scheme is chosen so the maximum Courant number is less than 0.2 to ensure a stable solution.

It is possible to use other numerical schemes, which are faster and just as stable [Brorsen et al. 1998] but the focus has not been to optimise the numerical procedures. The chosen numerical scheme is stable and is well documented in the literature. The speed of calculation is relatively fast in the present one-dimensional model.

In Appendix E the numerical unit solving the modified Radder and Dingemans equations is provided in detail as written in the numerical language Delphi.

CHAPTER 7 VERIFICATION OF THE WAVE MODEL

The performance of the developed numerical model simulating propagation of time-dependent waves over a rapidly varying topography with the inclusion of energy dissipation due to bottom friction and wave breaking is verified by several examples.

7.1 Multi-directional monochromatic waves

Testing the internal generation of waves, multi-directional monochromatic waves are generated in a two-dimensional layout. The Radder and Dingemans' modified approach is used for this verification, but using the formulation provided by Copeland yields similar results. The modified approach by Radder and Dingemans is reduced to the classical model because the water depth is constant. No energy dissipation is introduced.

It is shown by the following example that a two-dimensional wave scenario can be simulated. It is noted that Lee and Suh [1998] verified that the Mild-Slope model based on Radder and Dingemans' approach is capable of generating not only monochromatic waves but also directional waves propagating over a rapidly varying bottom. This knowledge verifies a basis for the possibility to develop a model capable of generating irregular, directional waves propagating over a rapidly varying bottom.

Figure 6 shows the definition sketch of the area of calculation.

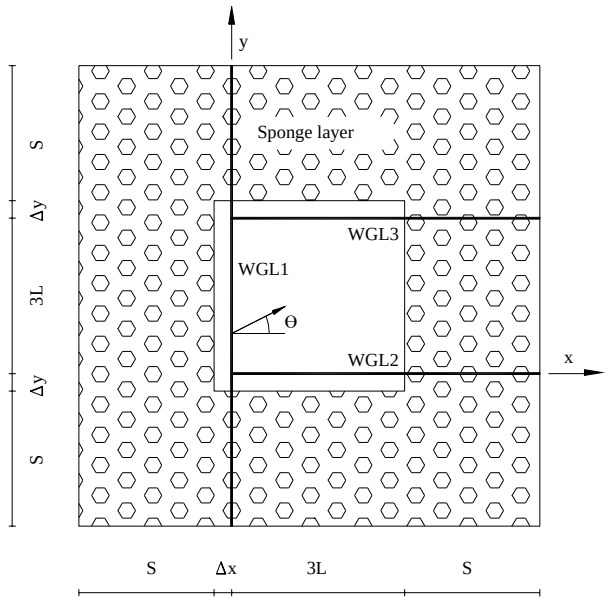

Figure 6: *Layout and definitions of the computational domain for generating multi-directional monochromatic waves.*

Three lines for wave generation are used to simulate multi-directional waves in a two-dimensional domain. WGL1 is the generation line situated along the y-direction and two lines, WGL2 and WGL3 along the x-direction. The computational domain consists of an inner domain being $3L \times 3L$ and sponge layers with a thickness of $S = 2.5 \times L$, L being the wavelength. WGL2 and WGL3 start at a distance of Δx away from the up-wave sponge layer and end at the down-wave boundary. In the case of normal incident waves (θ = 0°), WGL1 operates and is placed from the right-wave boundary to the left-wave boundary. In the case of a positive wave direction (θ >0°), WGL1 and WGL2 operate and WGL1 is placed from the starting point of WGL2 to the left-wave boundary. In the case of negative wave direction (θ <0°), WGL1 and WGL3 operate and WGL1 is placed from the right-wave boundary to the starting point of WGL3. The wave generation lines WGL1 and WGL3 operate simultaneously at each time step in order to get efficient computational time. The value η^* added to the water surface elevations at WGL1 at each time step is given by the following general description as

$$\eta^* = \sum_i \sum_j 2A_{i,j} \cos\left(k_i\, x \cos\theta_j + k_i y \sin\theta_j - \omega_i t + \varepsilon_{i,j}\right) \frac{C_{ei}\Delta t}{\Delta x} \cos\theta_j \qquad (70)$$

Overbars are omitted because the test involves monochromatic waves. The value, η^*, added to the water surface elevations at WGL2 and WGL3 at each time step is given by following general description

$$\eta^* = \sum_i \sum_j 2A_{i,j} \cos\left(k_i\, x \cos\theta_j + k_i y \sin\theta_j - \omega_i t + \varepsilon_{i,j}\right) \frac{C_{ei}\Delta t}{\Delta y} \sin\left|\theta_j\right| \qquad (71)$$

The subscripts *i* and *j* denote the components of different frequency and direction, respectively. $A_{i,j}$ is the amplitude of each wave component and $\varepsilon_{i,j}$ is the phase angle, which for random waves is randomly but uniformly distributed between 0 and 2π.

The case presented in Figure 7 considers two monochromatic waves propagating in different directions with the same frequency and amplitude. In case of constant depth the analytic solution reduces to the Helmoltz equation.

The conditions of the incident waves in the test are T = 10 sec, h = 35 m, $A_1 = A_2$ = 3.5 m, $\varepsilon_1 = \varepsilon_2$ = 0°, θ_1 = 60°, θ_2 = -30°. The grid size is $\Delta x = \Delta$ y = 14.25 m. The time step is taken as Δt = 0.15 sec, which yields a Courant number of $C_r = \overline{C}_g \Delta t / \Delta x = 0.1$.

It is seen in Figure 7 that the solution shown as the left graph compares well with the analytical solution. This confirms the wave generation utility in the model and the

numerical description of the refraction-diffraction equation for monochromatic waves propagating in a constant water depth.

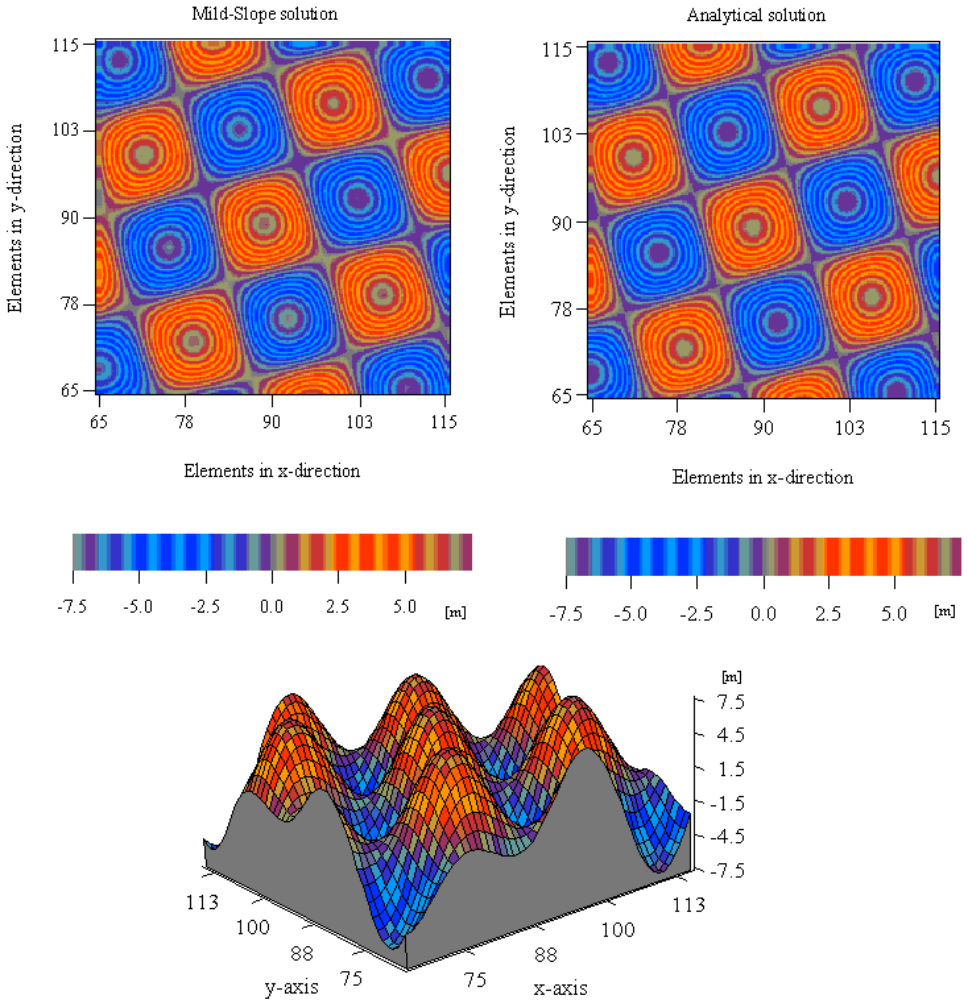

Figure 7: *Analytical (Helmholtz) and numerical simulations of 2D-monochrome waves.*

The influence of the thickness of the sponge layers is presented graphically in Figure 8, where the wave elevation is shown along two sections of two monochromatic waves travelling in different directions. A layer thickness of $S = 2.5 \times L$ corresponds to 25 elements. The element numbers referred to in Figure 8 are equivalent with the numbering and layout shown in Figure 7.

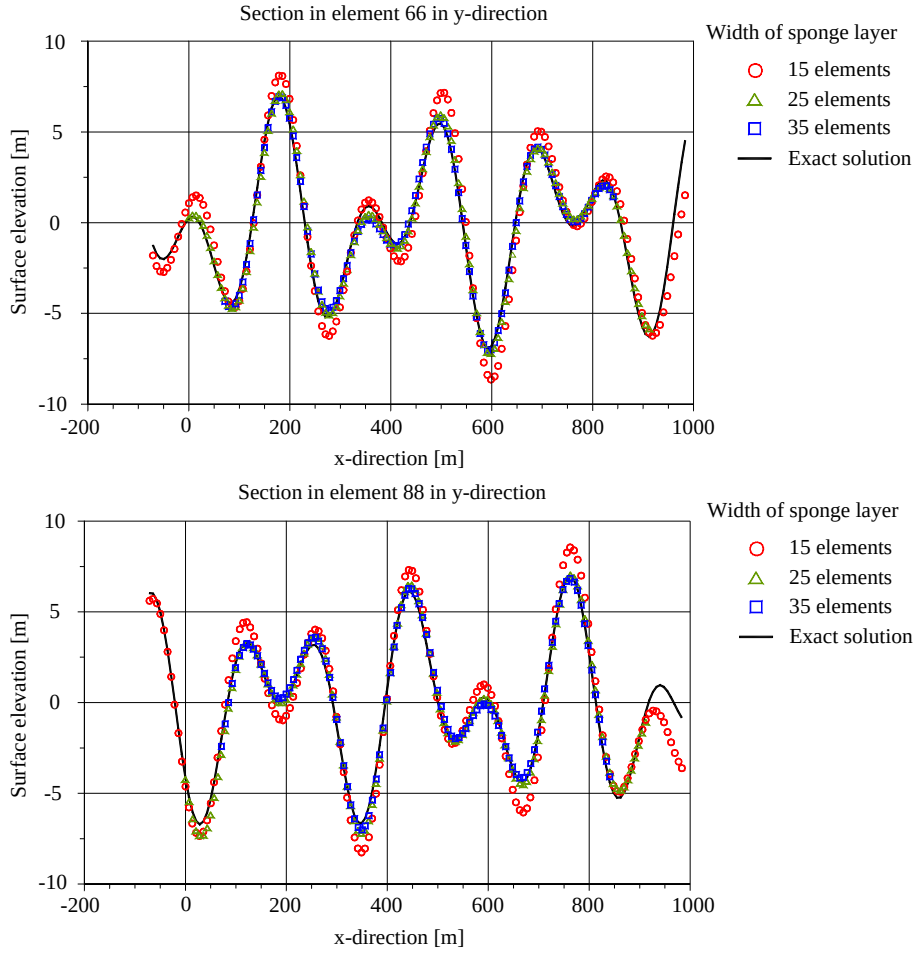

Figure 8: *Propagation of waves in a two-dimensional model using different length of the sponge layer.*

A thickness of 2.5 times the local wavelength yields a satisfactory solution. Using only 15 elements, i.e. 1.5 times the local wavelength the sponge layer yields some reflection inside the computational domain. This is indicated in Figure 8 because the elevations using 15 elements are larger than the exact solution. The generation of waves inside the region and the propagation of waves yield satisfactory results.

A two-dimensional example is hereby introduced. In the following only the one-dimensional model is considered. Still, it is important to emphasise that this method can be used in a two-dimensional layout.

7.2 Waves propagating over a plane slope

The importance of the higher-order bottom effects as introduced by Massel [1993] is illustrated in the following numerical tests, where the wave propagation over a plane slope is simulated.

7.2.1 Wave reflection from a plane slope

The following test has also been made by Lee et al. [1998] based on a modified formulation of Copeland. The formulation of the modified formulation of Radder and Dingemans and the formulation of Copeland are used in present test. It is noted that the original formulation by Copeland did not include the higher-order bottom terms, but has been modified to include these terms, see Appendix C. Only regular waves are simulated, but the test is later extended in Section 7.3 to simulate propagation of irregular waves, which is simulated using the modified approach by Radder and Dingemans. As mentioned, the aim is to verify the inclusion of the higher-order bottom effects of the seabed, which is of importance when simulating wave propagation along a rapidly varying bathymetry.

Figure 9 shows the computational domain for wave reflection from a plane slope.

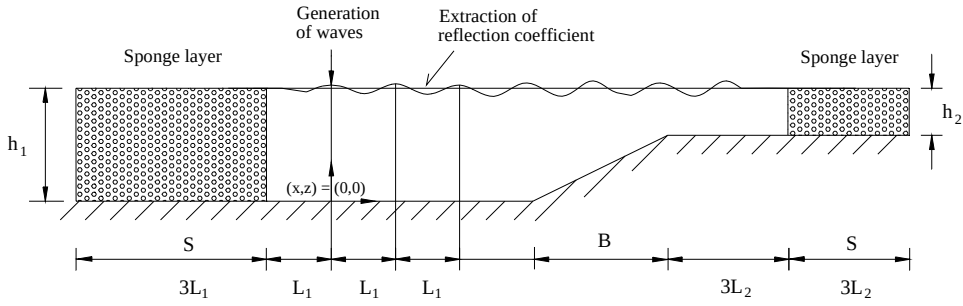

Figure 9: *Computational layout of wave reflection from a plane slope.*

Waves are propagating over a plane slope. The water depth on the up-wave and down-wave sides of the slope are h_1 = 0.6 m and h_2 = 0.2 m, respectively. The width of the slope, B, is varied so that the steepness of the slope varies. The wave period is T = 2 sec. The sponge layer thickness is three times the local wavelength to ensure that there is not created any substantial unwanted wave reflection from the boundaries. Waves are generated one wavelength from the up-wave sponge layer. After a start-up simulation period of $25 \times T$, wave amplitudes in the region between $x = L_1$ and $x = 2 \times L_1$ are found, where L_1 is the wavelength at depth h_1 and likewise is L_2 the wavelength at the water depth h_2. The grid spacing and the time step are constant in the test.

The reflection coefficient, K_r, is measured one wavelength from generation of the regular waves and is defined as the ratio between the reflected wave height and the incident wave height. Based on the linear theory the reflection coefficient is found as

$$K_r = \frac{H_{\max} - H_{\min}}{H_{\max} + H_{\min}} \tag{72}$$

where H_{max} is the highest wave height along one wavelength, i.e. between one wavelength and two wavelengths from the point of wave generation. H_{min} is the smallest wave height measured.

Figure 10 shows the performance of the numerical model and reflects the importance of the influence of the curvature term and the slope square term in the test.

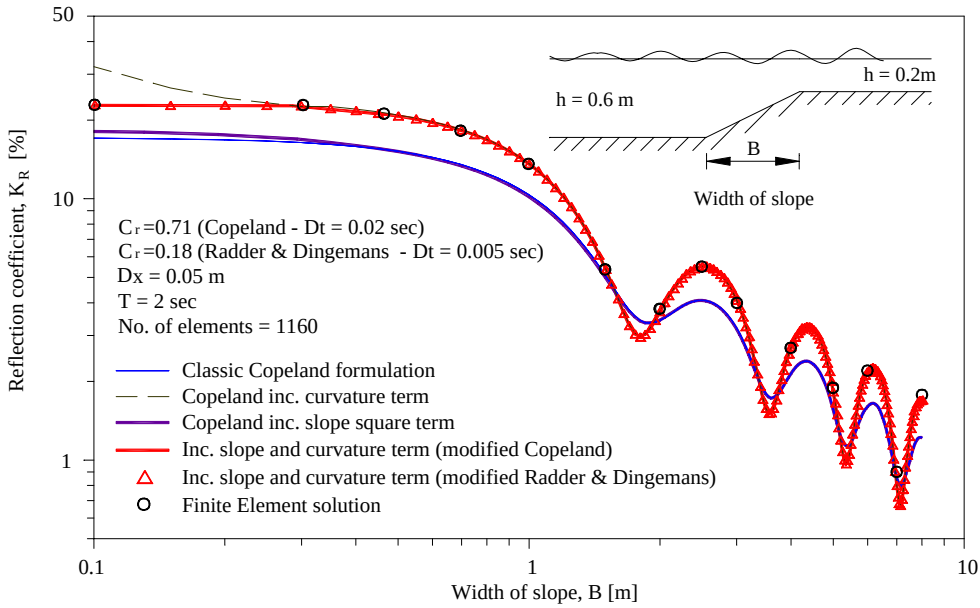

Figure 10: *The wave reflection versus the width of a plane slope and the included terms.*

Suh et al. [1997] calculated the reflection coefficients using a Finite Element model for this layout. Results from the Finite Element model are believed to be accurate. Results from this model are depicted in Figure 10.

The present model with inclusion of the slope square term and the curvature term, predicts results similar to the finite element solution and the reflection coefficient becomes stable even for very steep slopes.

Additional calculations are performed by including only the slope square term or the bottom curvature term. The inclusion of the bottom slope square term yields only some difference for very steep slopes, but the effect is minor. Instinctively, the term related to the curvature term is not expected to have impact on the solution because the slope is plane, but it is seen that this term affects the solution and improves the model significantly. Including the two slope discontinuity points in the transition between the plane bottom and the slope causes the improvement.

Applying central differencing in the numerical calculation scheme, that is, $\partial^2 h/\partial x^2 \approx \left[h(x+\Delta x) - 2h(x) + h(x-\Delta x)\right]/(\Delta x)^2$, the curvature terms are non-zero at the discontinuity points and by including those in the calculation, an accurate solution is obtained. In the case where only the curvature term is included, it is seen that for steep slopes there appears a deviation from the correct solution. This deviation will be reduced if the grid spacing is decreased but depends also on the missing contribution from the square slope term.

In the present case the inclusion of the curvature term seems to be more important than the square slope term. In fact, the contribution depends on the depth of water and the wave period. The terms R_1 and R_2 are controlling the influence of the square slope term and the bottom curvature term, respectively. These terms are functions varying with kh. Calculation of R_1 and R_2 are given in Appendix B.

The Mild-Slope formulation underestimates in general the reflection coefficient of waves propagation a steep slope. The model does not take into account the discontinuity points. Porter and Staziker [1995] also tested the Mild-Slope equation and the extended refraction-diffraction equation. The conclusion was that the Mild-Slope equation does not ensure continuity of mass flow at locations where the bed slope is discontinuous.

The results of the present model coincide with the finite element model for also very mild slopes. Suh et al. [1997] and Lee et al. [1998] performed the same tests as presented above and yielded approximately the same results. They found minor differences in the results from the finite element model for very mild slopes, i.e. b being larger than 5 m in Figure 10. Their numerical model included both bottom high-order terms and could be compared with the results presented here.

By comparing the results derived from the Mild-Slope equation and the results from a finite element model for the aforementioned problem, Booij [1983] concluded that the Mild-Slope equation is sufficiently accurate up to bottom slopes of 1:3 without providing the finite element results for the milder slopes. This conclusion is questioned by Suh et al. [1997]. Booij did the test in intermediate water depth and did not cover the entire range of water depth from deep to shallow water. The accuracy of the Mild-Slope equation will vary with not only the bottom slope, but also with the water depth. To investigate this further two scenarios are simulated by performing an

additional case with a water depth of h_1 = 0.8 m, i.e. a relative small increase in the seaward water depth. The results of the numerical simulation are shown in Figure 11. All other parameters are unchanged from the presented example described above.

Figure 11 shows the influence of the depth of water. The Radder and Dingemans formulation including the two higher-order bottom terms is compared with the classic Mild-Slope formulation, which is obtained using Radder and Dingemans' formulation without the second order bottom terms. The results are depicted after the steepness of the slope in the top graph and the width of the slope in the bottom graph. Choosing the approach where the results are depicted after the steepness of the slope it is easy to identify the slope of 1:3, which is the slope steepness referenced by Booij to yield satisfactorily results using the classic Mild-Slope formulation. The solution between the present model, which is shown to be precise, and the classical model for h_1 = 0.6 m (illustrated with thick lines) differs from a slope of 1:4 to 1:3. It can be discussed where the limit should be but if the difference for the milder slopes can be accepted a slope of 1:3 seem reasonable. Observing the results for h_1 = 0.8 m (illustrated with the thinner lines) it is seen that the limit of 1:3 changes to 1:2 but the differences between the solutions become even bigger than in the former case with h_1 = 0.6 m. An increase in the seaward water depth changes the limit where the use of the classical Mild-Slope equation is acceptable. Using a smaller seaward water depth the limit will be larger than 1:3, i.e. milder slopes are acceptable. To summarise, the accuracy of the solution of the classical Mild-Slope depends on the water depth, but in general the classical Mild-Slope equation does not provide accurate results.

Including the higher-order terms in the classical Mild-Slope formulation improves significantly the solution and it is shown that the extended Mild-Slope formulation yields a solution very close to the exact solution. Furthermore, the numerical model is capable of simulating the wave transformation on a steep reef. Still, the model will have to be provided with the utility of handling irregular waves and also to include wave energy dissipation.

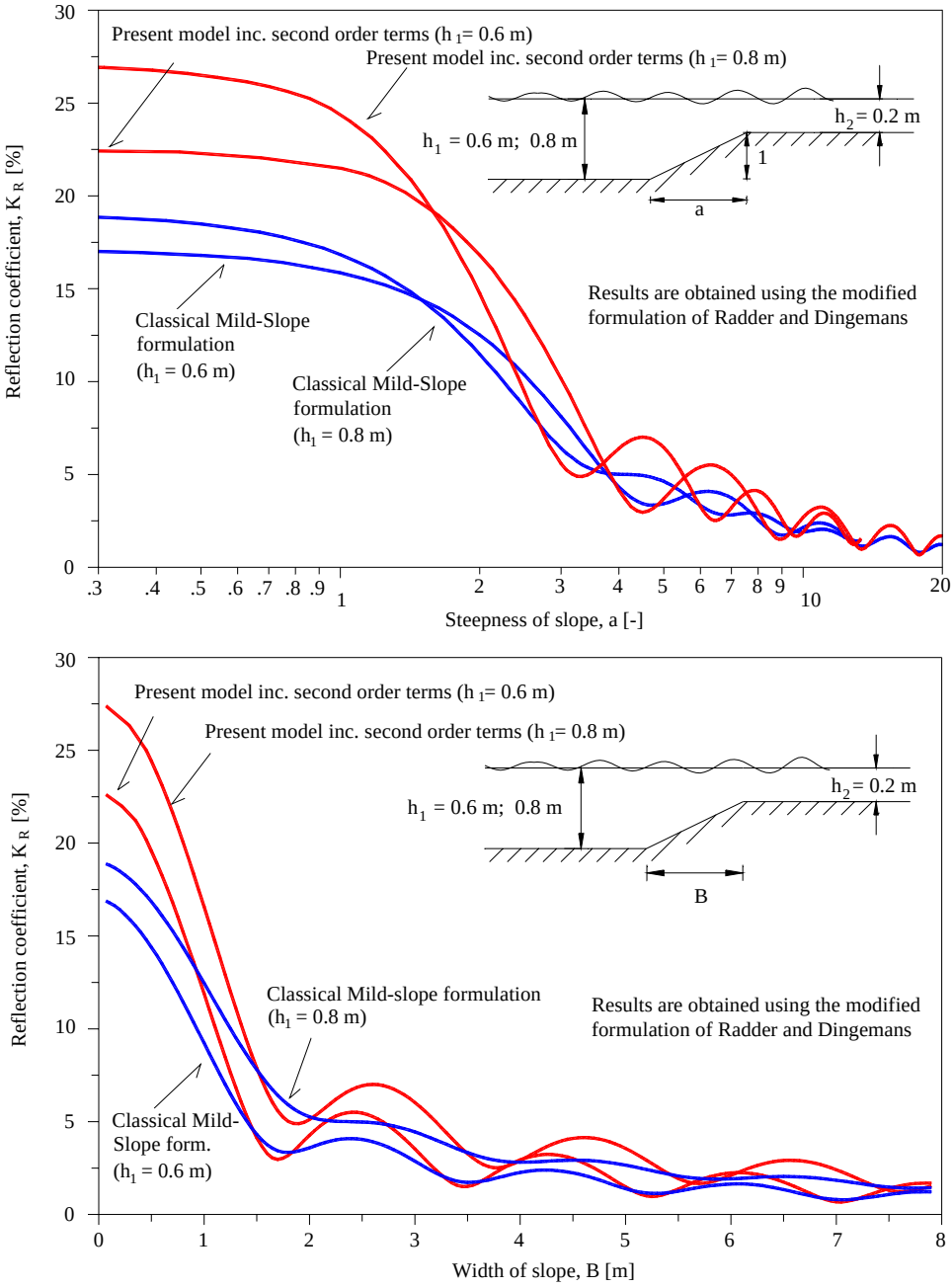

Figure 11: *Dependence of the reflection coefficient on the water depth and slope width.*

7.2.2 Restrictions on grid spacing

There are restrictions regarding the grid spacing. In Figure 12 different resolutions of the grid are shown for the solution of the reflection from a plane slope. The layout and parameters used is similar to the test described in Section 6.2.1. The solution is based on the modified Radder and Dingemans equations using the fourth-order Adams-Bashforth-Moulton scheme. The time step is varied to maintain a constant Courant number of C_r = 0.18.

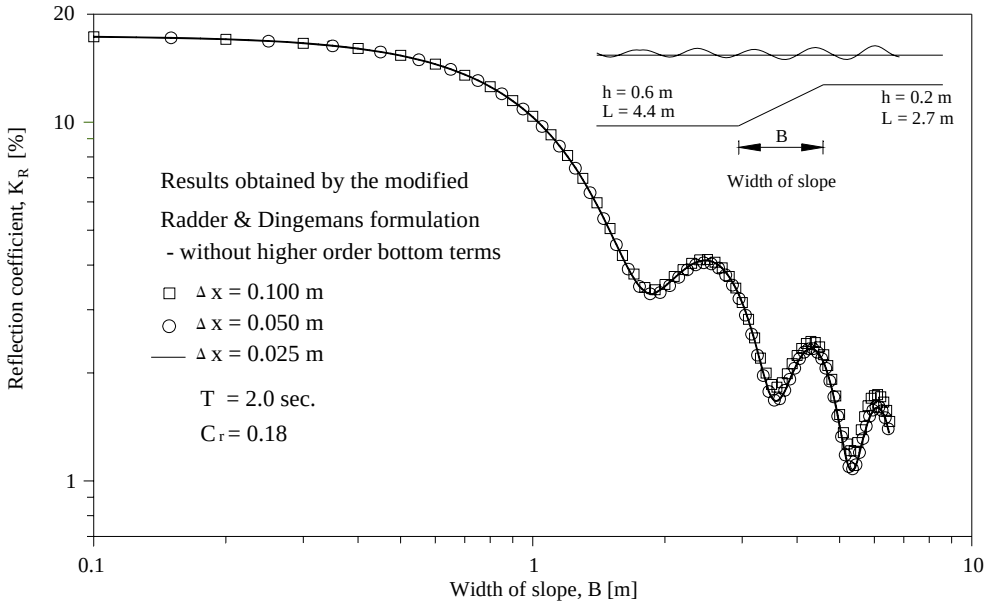

Figure 12: *Influence on the wave reflection regarding the spatial discretisation.*

It is seen that the solution becomes slightly affected by discretisation errors when the grid size increases. Using only 27 elements per minimum wavelength, i.e. Δx = 0.10 m, the numerical solution differs from the solution using 54 elements and 108 elements, which are alike. A number of 30-50 elements per minimum wavelength seem to assure a satisfactorily spatial discretisation.

7.3 Generation of irregular waves

In order to investigate the applicability of the time-dependent wave equations provided by Radder and Dingemans with the inclusion of higher-order bottom terms and energy dissipation, numerical tests are conducted. To verify that the generation of irregular waves is correct the JONSWAP spectrum is used as an input target spectrum generated in a numerical layout with constant water depth. Finally, the wave transformation of waves propagating over a sloping bed is studied with the inclusion of wave energy dissipation due to bottom friction and wave breaking.

The modified equations by Radder and Dingemans are used from this point of regarding use of the numerical wave model.

7.3.1 Generation of a wave spectrum

So far only regular waves have been tested. In the following examples the time-dependent equations of the extended refraction-diffraction equation given by Radder and Dingemans are used for simulation of irregular wave propagation.

The frequency spectrum of incident waves, $S_\eta(f)$, is taken as the JONSWAP spectrum with the input parameters; H_s = 5 m, T_p = 10 sec. and a peak enhancement factor $\gamma_p = 3.3$. The water depth is kept constant at h = 20 m. The simulation of wave elevation series is based on random phases.

To ensure numerical stability and accuracy, the frequency range of the incident waves are chosen so the frequency components of lower densities are excluded. The considered frequency range is 0.075 Hz and 0.175 Hz, which covers 93% of the total energy and yields a generated significant wave height of H_{m0} = 4.82 m. The significant wave height is denoted H_{m0} when this parameter is based on the energy density spectrum.

The numerical layout is similar to the layout shown in Figure 9 but without a slope. Still, no dissipation of wave energy is introduced in the computational domain. The thickness of the sponge layers at both ends are $3 \times L_{max}$, where L_{max} is calculated after the cut-off frequency f_{min} = 0.075 Hz. The inner computational domain is $10.5 \times L_{max}$. The grid size is Δx = 2 m and the time step is Δt = 0.033 sec. yielding a maximum Courant number of C_r =0.18 corresponding to the cut-off frequency, f_{min} = 0.075 Hz.

Surface elevation time-series of irregular waves are generated for a period of $500 \times T_p$. The elevation is measured $6.5 \times L_{max}$ down-wave the wave generation point from $50 \times T_p$ to $500 \times T_p$, yielding approximately 150,000 time steps.

In order to estimate the coefficients $\bar{k}$, $\overline{C}$ and $\overline{C}_g$ in Eq.(57) the peak frequency, f_p, of the spectrum is chosen as the so-called wave carrier frequency. Propagation of waves

with a wave frequency different from the wave carrier frequency the exact solutions of the wavelength, phase speed and group velocity in the numerical calculations will not be exact. The error using a wave carrier frequency in the calculations becomes smaller the narrower the spectrum is chosen. The error influences the propagation of waves and thereby yields erroneous values of the wave energy transportation. The influence of this is studied later in the present chapter.

A Fourier Transformation is used for spectral analysis of the generated time series. The spectrum is discretised by introducing 35 degrees of freedom, i.e. 35 wave frequencies. The 150,000 wave elevations are processed in 45 sub-series.

Figure 13 shows the comparison between the generated JONSWAP spectrum and the measured spectrum in the numerical wave model. The generated spectrum is similar to the target spectrum yielding the predicted significant wave height of 4.82 m after the frequency components of lower densities are excluded. The generated wave elevations are hereafter added to the generation point. The measured energy spectrum down-wave is measured at $6.5 \times L_{max}$, but does not change during the propagation from the generation point. The influence of using a single wave carrier frequency in the propagation of waves is seen to yield acceptable results. The spectrum of the simulated water surface waves is almost the same as the generated spectrum and the energy densities are equal. This proves the model's ability to generate irregular waves for a relatively narrow spectrum with a carrier frequency chosen at the peak frequency.

The wave energy, which is neglected due to cut-off of the lower densities, shall be taken into consideration when numerical results are compared with laboratory tests. The cut-off energy shall be added to the target spectrum in order to generate energy equivalent to the desired target energy spectrum.

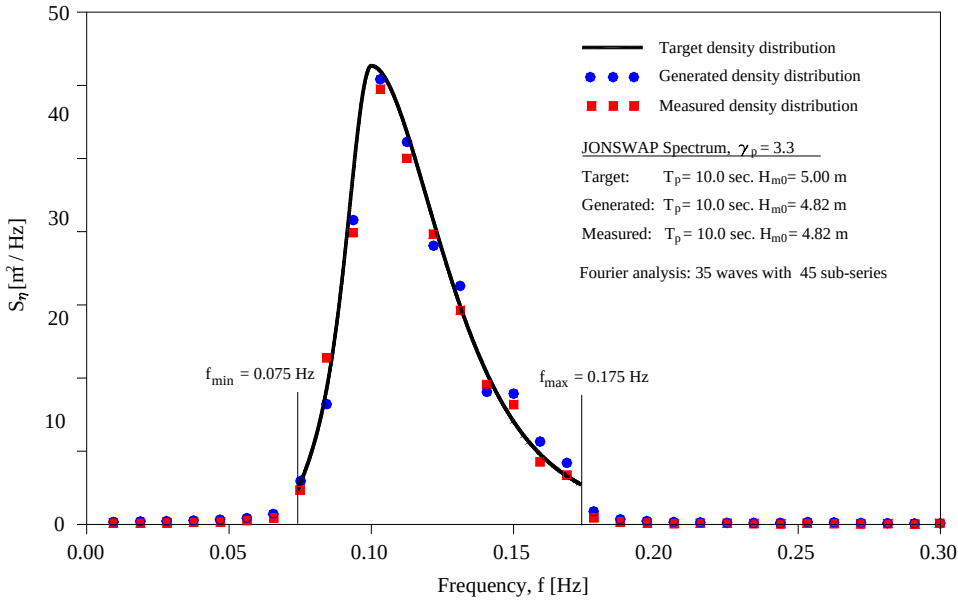

Figure 13: *Comparison of generated spectrum and measured spectrum, respectively.*

7.3.2 Irregular waves propagating over a slope

Irregular waves propagating over a steep sloping bed are tested in the present wave model. This case includes the higher-order bottom terms in the calculations and no wave energy dissipation is included. The objective is to clarify the ability of the model to propagate irregular waves over a steep bottom using a wave carrier frequency.

It should be noted that Suh et al. [1997] showed with a similar model that it is possible to simulate the transmission of irregular waves propagating over a ripple patch. Using a single carrier frequency in a relatively narrow spectrum they found similar results compared to a Finite Element solution. For a broad spectrum accurate results could be obtained when the frequency range was divided into several bands and model each of them with a respective carrier frequency.

The numerical layout is shown in Figure 14. A slope is introduced with a seaward water depth of 20 m and a water depth on the reef-plateau of 6 m. The grid size is Δx = 2 m and the time step is Δt = 0.033 sec. yielding a maximum Courant number of C_r = 0.18 corresponding to the cut-off frequency, f_{min} = 0.075 Hz.

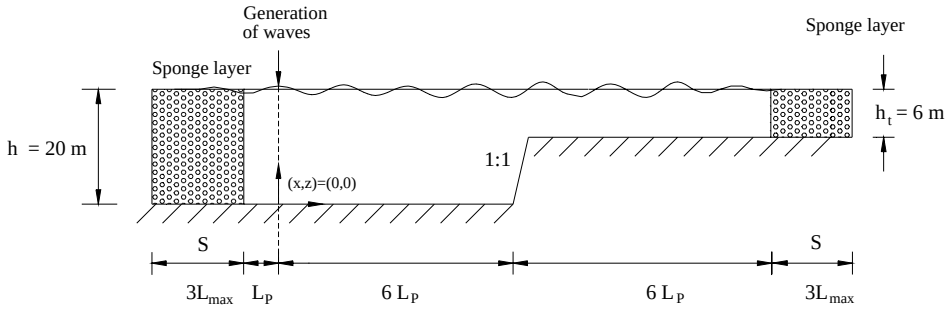

Figure 14: *Numerical layout for irregular waves propagating a steep bottom slope.*

Before irregular waves are generated a regular wave with H = 5 m and T = 10 sec. is propagated in the model. This exercise is almost similar to the test performed in Section 7.2.1, but instead the energy transport is focused upon. The width of the slope is 14 m, i.e. a steepness of 1:1. After a start-up simulation period of $25 \times T$, wave amplitudes in the region between $x = L_p$ and $x = 2 \times L_p$ are found and the reflection coefficient according to Eq.(72) is estimated as K_r = 0.20. The definition of the reflection coefficient and the transmission coefficient K_t is introduced as

$$K_r = \frac{H_r}{H_i}, \quad K_t = \frac{H_t}{H_i} \tag{73}$$

where H_i is the incident wave height. H_r is the reflected wave height and H_t is the transmitted wave height.

To test whether the energy transport in the model is fulfilled, the viewpoint of energy flux is obtained. Other results in the present test are

- $C_{g\ (h=20\text{m})}$ = 9.27 m/sec.
- $C_{g\ (h=6\text{m})}$ = 6.78 m/sec.
- H_t = 5.73 m

The wave carrier frequency is chosen as the peak frequency. It is noted that the transmission coefficient is K_t =1.14, which is above unity because the waves are shoaling on the reef-plateau. The total energy flux is equal to the reflected and the transmitted energy flux. The energy flux in a regular wave is

$$P = E\,C_g = \frac{1}{8}\rho_w\, g H^2 C_g \tag{74}$$

The reflected wave height is

$$H_r = \sqrt{\frac{1/8\,\rho_w\, g\left(H_i^2 C_{g(h=20m)} - H_t^2 C_{g(h=6m)}\right)}{1/8\,\rho_w\, g\, C_{g(h=20m)}}}$$

$$= \sqrt{\frac{H_i^2 C_{g(h=20m)} - H_t^2 C_{g(h=6m)}}{C_{g(h=20m)}}} \qquad (75)$$

In the present test the reflected wave height according to Eq.(75) is H_r = 1.01 m, yielding a reflection coefficient of K_r = 0.20, which is equal to the coefficient estimated by use of Eq.(72).

It is seen that the propagation of a regular wave is described correctly in the wave model. Eq.(75) is presented to show that energy conservation is fulfilled in the present test, no energy dissipation is introduced. A similar test is performed with irregular waves.

The frequency spectrum of the incident seaward waves, $S_\eta(f)$, is again taken as the JONSWAP spectrum with the input parameters; H_s = 5 m, T_p = 10 sec. and a peak enhancement factor of $\gamma_p = 3.3$.

The cut-off frequencies yield a reduced significant wave height of H_{mo} = 4.82 m.

The wave energy spectrum is measured before and after the waves pass the slope with a steepness of 1:1 as shown in Figure 14. No dissipation of energy is introduced in the test.

The results obtained are depicted in Figure 15. The graph shows values before and after the reef-plateau of the significant wave height, H_{mo}. The significant wave height is calculated using a Fourier analysis.

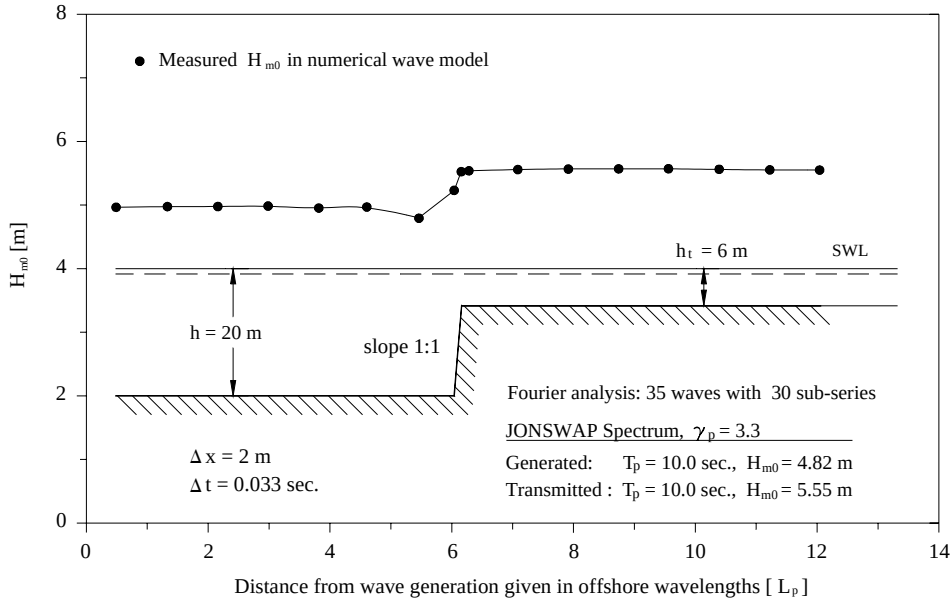

Figure 15: *Measured significant wave height for waves propagating a steep slope.*

The significant wave height calculated seaward the slope is slightly higher than the generated significant wave height due to the reflection from the slope. The wave carrier frequency is equal to the spectral peak period. The average transmitted significant wave height is H_{mo}= 5.55 m. Using Eq.(75) an estimate of the reflection coefficient is K_r = 0.15. This estimate is based on the group velocities after the peak period at the relevant water depths. Figure 16 shows the generated spectrum and the transmitted spectrum at the reef-plateau. The transmitted spectrum is measured 10.5 times the seaward wavelength after the wave generation point.

The energy flux is calculated by integrating the energy spectrum over the respective wave group velocities at each frequency as

$$P = \sum_{f_{\min} \le f \le f_{\max}} \rho_w \, g \, S_\eta \, \Delta f \, C_g \tag{76}$$

By using only one wave carrier frequency in the model equations an error is made. The size of the error depends on the difference between the respective frequencies of the waves in the spectrum and the chosen wave carrier frequency.

The error can be estimated in this example by calculating the incident flux and the transmitted flux after the spectra shown in Figure 16. The incident flux is calculated as 116 kW and the transmitted flux after Eq.(76) is 120 kW. The transmitted flux is

slightly higher than the incident wave energy flux. Furthermore, the reflection from the slope should reduce the transmitted energy flux even more. The narrower the spectrum is the less the error will be. The test shows that the calculated transported energy density using one wave carrier frequency is satisfactory, but care should be taken when the energy flux is considered. Depending on the width of the spectrum, the energy flux should be calculated using several wave carrier frequencies.

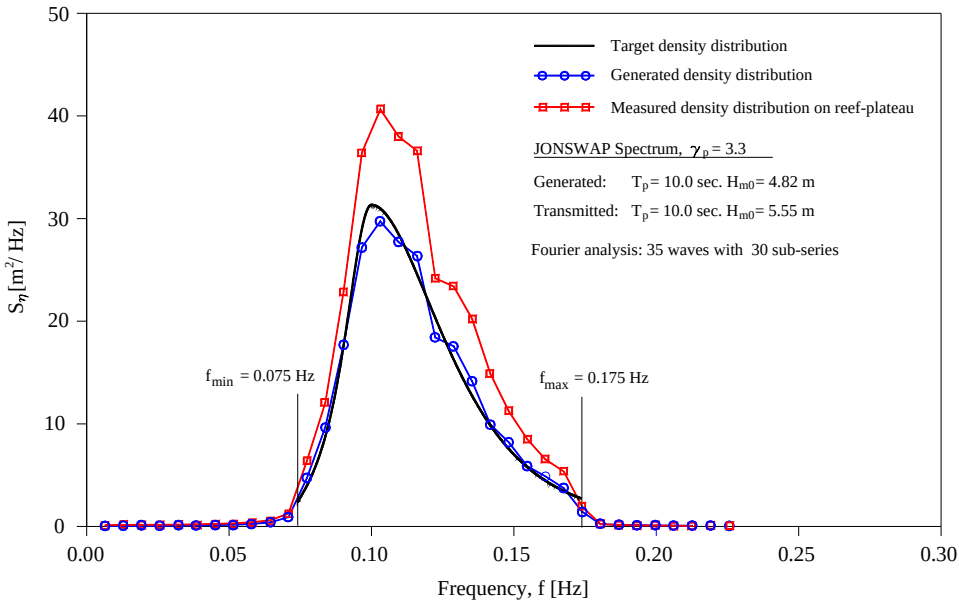

Figure 16: *Comparison between the generated and transmitted spectrum.*

7.3.3 Inclusion of wave energy dissipation due to wave breaking

Wave breaking is introduced in Eq.(51) by including the wave dissipation term

$$W_b = \frac{\varepsilon_b}{E} = \frac{\alpha_0 \, \overline{\omega}}{\pi \, h} \left(\frac{H_{\max}^3}{H_{rms}^2} \right) \left(\frac{\sqrt{gh}}{\overline{C}} \right) Q_b \tag{77}$$

H_{rms} is estimated as $H_{rms} = \sqrt{8} \, \sigma_\eta$. The variance of the wave elevation, σ_η, is straightforward to calculate in the wave model, which is a time-domain model. The variance is estimated on basis of the preceding 100 waves. 100 waves is a number, which gives a relatively acceptable statistical estimate. The numerical solution is not sensitive whether H_{rms} is estimated on basis of 50 waves or 200 waves.

The maximum wave height is the key parameter to estimate. The present test is presented in order to describe and verify the wave model regarding the model ability to include the wave energy dissipation due to breaking of waves. The maximum wave height before breaking of the wave is taken as $H_{\max} = \gamma \, h_t$, where the breaker index is $\gamma = 0.6$. The water depth on the shallow reef is h_t = 6 m, which yields a maximum allowable wave height before breaking of H_{max} = 3.6 m.

The numerical layout is similar to the tests described in Section 7.3.2. Only dissipation due to wave breaking is included and is only included from the start of the reef-slope. The wave energy spectrum is measured on the reef-plateau approximately 1.5 “shallow” wavelengths from the slope. In Figure 17 the results from tests with various values of α_0 are presented.

The fraction of waves breaking is related to the parameter Q_b, see Eq.(47). The fraction of waves breaking will vary along the reef-plateau as the wave energy is dissipated, and thereby attenuating the waves. The average value of Q_b, measured at the point of measurement, is given in Figure 17 for different values of α_0. This value will vary slightly because the waves are irregular and the measured and updated root-mean-square wave height varies. Because the fraction of breaking waves is indirectly related to α_0, the effect of a higher value of α_0 is minor above a certain value. This is illustrated by the relatively small damping applied to the energy density spectrum when raising α_0 from 1.0 to 1.5.

It is already mentioned that α_0 is of the order $0(1)$ [Massel and Gourlay, 2000]. The periodic bore model is reported to underestimate the breaking, especially for waves breaking at shallow conditions. It is mainly the assumption that the wave heights are Rayleigh-distributed, also after breaking, which causes some errors. The effect of α_0

is to compensate for this underestimation and it can be expected that α_0 is not below 1.0.

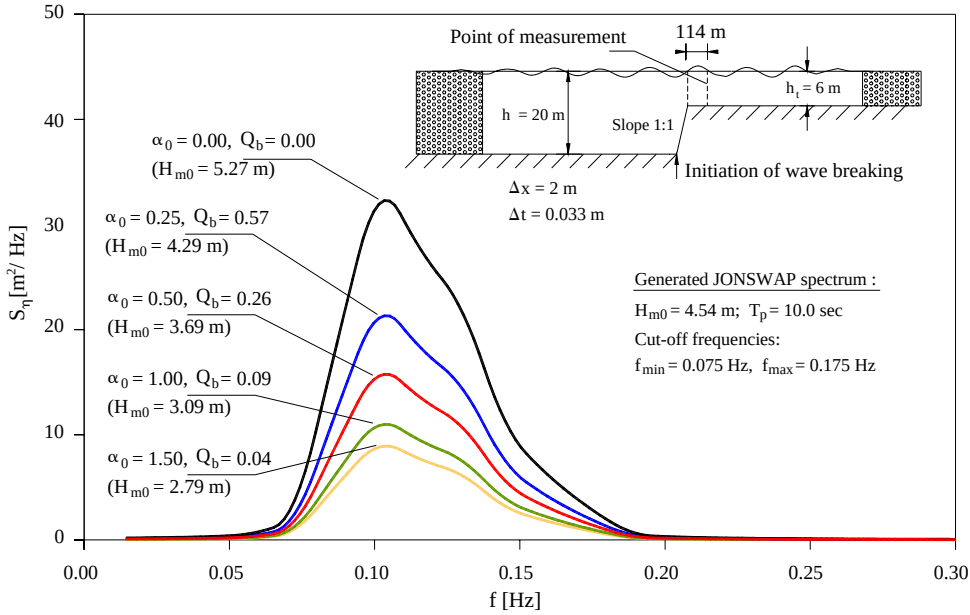

Figure 17: *The damping of the wave energy spectrum using different values of α_0.*

It is observed that using α_0 = 1.0 the energy dissipated after approximately a distance of 1.5 times the wavelength at the reef-plateau, is almost 2/3 of the total incident wave energy.

7.3.4 Inclusion of wave energy dissipation due to bottom friction

The damping term due to the bottom friction is introduced in Section 5.5 as Eq.(51)

$$W_f = \frac{\varepsilon_f}{E} = \frac{16 f_r}{3\pi} \frac{|U|^3}{g H_{rms}^2} \tag{78}$$

Values of the wave energy friction factor, f_r, are for breaking waves over a steep coral reef in the order of 0.1-1.0, Gerritsen [1981]. Nelson [1996] reported values between 0.1-0.2 for waves propagating along a rough coral reef-plateau without the waves breaking. For small scale models using a smooth seabed made of mortar or similar it is expected that the friction will be around 0.01. This is a value often mentioned by other authors.

The estimation of the amplitude of the seabed velocity U is the key parameter regarding inclusion of the energy dissipation due to bottom friction for irregular waves and has been chosen to be calculated according to Eq.(49). The average wave height in the wave train is used and estimated as $H_{mean} = 2.5\sigma_{\eta}$. This seems to comply well with the fact that the wave dissipation friction factor, f_r, is an averaged value. It seems that Nelson [1996] used the significant wave height in order to calculate the friction factor, f_r, which seems to yield too large values in the present model. This is described later. The purpose of this test is to describe and show that the wave model is capable of including the wave energy dissipation due to the bottom friction. The choice of the size of the friction factor f_r, is still not clear and should be studied further. Furthermore, using the present model the friction factor has to be calibrated or evaluated based on the fact that the average wave height of the irregular wave train is used to calculate the rate of energy dissipation. In the further use of the wave model the contribution of wave energy due to the bottom friction is assumed very small because the experimental tests are simulated and the friction is expected to be relatively small in the scale flume tests. Still, it is shown that the wave model is capable of introducing the effect of bottom friction in the numerical calculations and an approach is suggested.

The numerical layout and the waves generated are similar to the tests performed in Section 7.3.2. Dissipation due to bottom friction is included only from the start of the reef-slope. The wave energy spectrum is measured on the reef-plateau 114 m after the reef-edge. Figure 18 illustrates how the size of the friction factor influences the energy density spectrum.

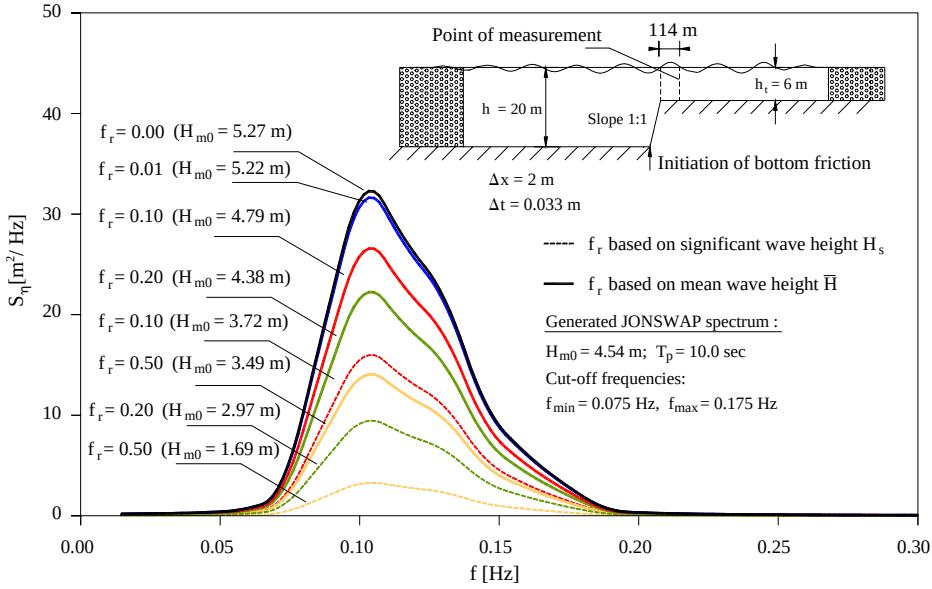

Figure 18: *The damping of the wave energy spectrum at different values of f_r.*

It is observed that inclusion of the bottom friction dissipation reduces the wave energy density spectrum. Choosing f_r = 0.01 has little or no effect on the wave energy spectrum measured 1.5 wavelength after the reef. The damping of the waves due to a friction factor of f_r = 0.1 is minor but has some effect on the wave energy spectrum, approximately 17 % of the wave energy is dissipated due to bottom friction. The effect is very high if f_r = 0.5.

The results are also shown when the amplitude of the seabed velocity is based on the significant wave height being, $H_s = 4.0\sigma_\eta$. It is seen that choosing f_r = 0.01 has a significant effect on the wave energy spectrum and the wave energy dissipated due to bottom friction is approximately 50%, a value being unrealistically high.

CHAPTER 8 PRESENTATION OF EXPERIMENTAL TESTS

Experimental tests are performed in the hydraulic laboratory in order to obtain measurements of waves breaking over steep bottom slopes. The object of the tests is to establish formulae to predict the transmitted wave energy density and transmitted wave energy flux.

A second objective performing the tests is to calibrate the numerical model on basis of the data obtained. Information is needed regarding a breaking criterion for controlling the wave breaking, i.e. a criterion describing the initiation and ending of extracting energy from the waves. Furthermore, the results of the tests are used to calibrate the unknown wave energy dissipation parameter for breaking waves, α_0.

8.1 Description of experimental tests in a scale wave flume

In November 2000 the author performed a large series of regular and irregular tests at the hydraulic laboratories of Aalborg University.

A 23 m long and 1.5 m wide wave flume was used for the simulation of waves breaking over a steep reef-slope. The water depth range in front of the reef-slope was between 0.56-0.71 m. The height of the slope was 0.38 m yielding a water depth of 0.18-0.33 m on the horizontal reef-plateau. Between the wave generator and the slope an approximated “deep” water depth was provided with a horizontal bottom. The length of the reef-plateau was 14 m in order to provide enough length for the waves to reform after breaking. The waves were dissipated after the reef-plateau by a mild sloping gravel beach.

The structure was built using concrete blocks. The energy dissipation due to wave breaking was focused upon and the bottom friction was therefore minimised by applying a layer of thick plastic on top of the concrete blocks. The pressure from the propagating waves removed the air bubbles being trapped in the structure beneath the layer of plastic after few minutes.

Figure 19 shows a picture of the wave flume being built and Figure 20 shows one of the simulated reef-slopes made of a thick metal plate.

Figure 19: *Construction of the 'reef' in the wave flume.*

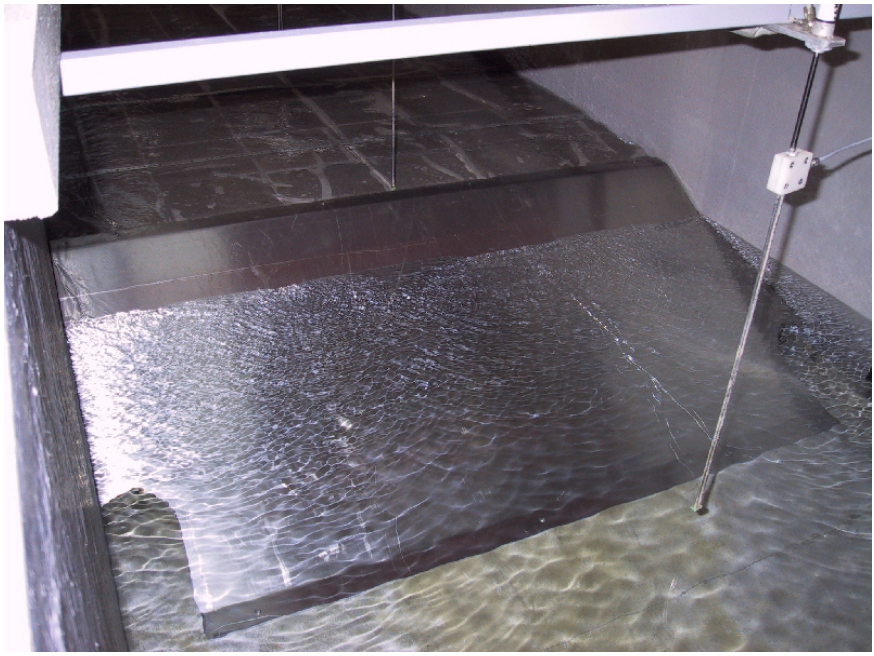

Figure 20: *A metal plate was used to simulate the reef slope.*

A schematic sketch of the layout in the wave flume and the location of 14 wave gauges are shown in Figure 21. The wave gauges were placed in order to identify the transformation of the waves as they propagated in the wave flume.

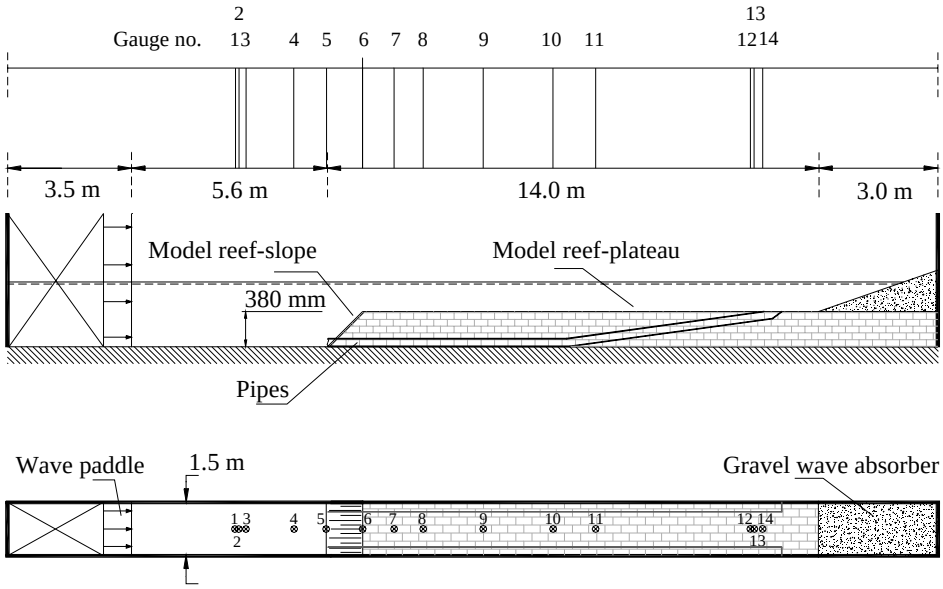

Figure 21: *Experimental layout in the hydraulic laboratory.*

To avoid the effect of water being pumped over the reef-plateau and thereby raising the water level because of the vertical end wall, a return flow system was provided by pipes connecting the reservoir in front of the slope. The pipes were placed beneath the concrete blocks and connected to the water reservoir on the reef-plateau close to the gravel slope. It is noted that the effect of the pipes was not evaluated in detail.

Due to wave reflection from the waves being reflected from the steep slope an active wave absorption system was used to avoid re-reflection of waves from the wave generator. The absorption system was developed at Aalborg University and described in details by Frigaard et al. [1994]. Wave gauges in front of the wave generator were used to correct the signal sent to the generator, modifying the motion of the vertical wave paddle. It is verified later in this thesis that this ensured that the incident waves were controlled with relatively good accuracy. Without the utility of active absorption the tests would have to be limited to milder slopes constructed with an absorbent material.

The layout of the model, especially the relative small width of the wave flume being 1.5 m, ensures that no or minimum resonant cross oscillations were present.

Four different layouts of the reef-slope were used with the inclinations 1:0.5, 1:1, 1:2 and an additional S-formed ‘reef-slope’ with a straight section with the inclination of 1:1. The slopes are depicted in Figure 22.

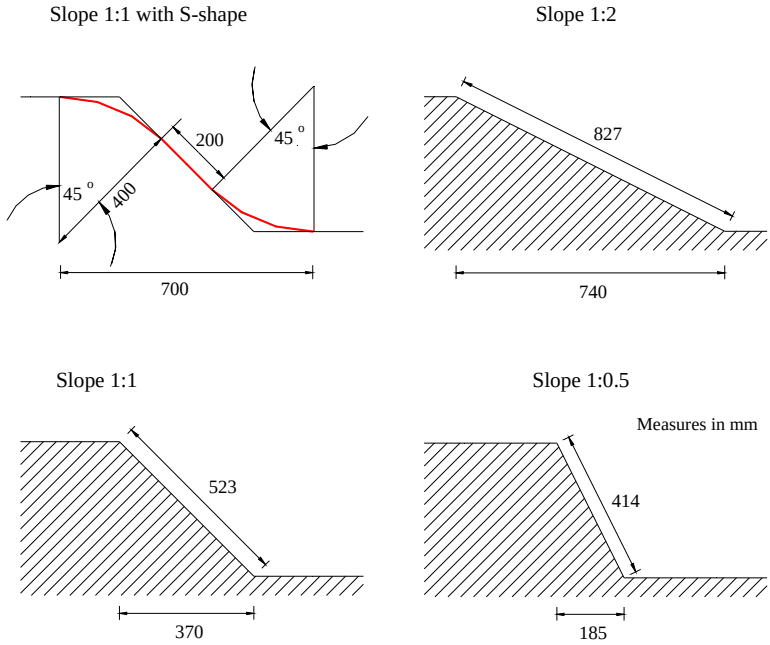

Figure 22: *Layout of the slopes used in the experimental tests.*

8.2 Measurements

The waves were measured at 14 locations along the flume with capacitance gauges. Frequent calibration of the wave gauges was provided. The use of these gauges was considered to be very reliable as regards their linearity. Some drift was observed during start-up due to stirring up the salts dissolved in the flume water. Measurements were performed after a long warm-up period. All data was stored and analysed online. The following measurements were made in the laboratory.

- Surface elevations along the flume centre line.
- Water levels.
- Breaker type and surf zone width using video.

The tests were performed in two phases as:

- Generation of regular waves to establish threshold values for wave breaking.
- Generation of irregular waves to evaluate the wave energy dissipation.

The incident wave height of the regular waves was obtained as an average from the gauges between the wave generator and the slope to ensure that the active absorption system yielded reasonable values. Incident wave heights of the irregular wave trains were calculated by using the technique for separation of incident waves and reflected waves as proposed by Mansard and Funke [1980].

The wave-induced water level set-up along the reef slope and the reef-plateau is a phenomena associated with the waves breaking. It was originally the aim to measure this parameter. Unfortunately, it appeared that more advanced equipment than the used wave gauges for determination of the wave set-up was needed. The measured set-up was small compared to the actual water depth and several repetition tests showed a relatively large deviation in the set-up from the measurements of the wave gauges. As previously mentioned, it is not know if the insignificant levels of set-up was influenced by the return flow system adopted in the experimental model. Without the return flow system it was clear that water was being pumped over the reef-plateau and thereby raising the water level unrealistic. It was not possible to quantify the pumping effect and the wave set-up, but the raising of the water level was mainly caused be the pumping effect. If the small levels of set-up were to be measured then sensitive gauges should have been installed on the seabed.

It is believed that the experimental model was modelled to reflect the most realistic scenario possible. In nature, platform reefs surrounded by the ocean, or fringing reefs and lagoons with significant outlet channels, the water being pumped onto the reef plateau can escape over the leeward edge of the reef or through the outlet channels. Indeed, in many apparently two dimensional fringing reef situations an outlet channel at one end of the reef system will provide an outlet for water impounded on the reef-top by wave set-up. In such situations wave-induced flows develop and the magnitude of the set-up on the reef will be much less in the two dimensional situation, Gourley [1996a].

Irregular waves were generated based on a JONSWAP spectrum with a peak enhancement factor of $\gamma_p = 3.3$. The wave elevation was measured with a sampling period of 20 Hz, i.e. the surface position was stored 20 times per second.

In total 301 tests with regular waves were performed and 110 tests with irregular waves. This included 10 repeated tests, i.e. the wave parameters and layout in the flume were similar for several of the tests. This was done in order to investigate the sensitivity of the tests in relation to the measured wave energy spectres. The irregular wave trains consisted of 650 waves to represent the test. In addition to the waves measured, a warm-up period represented by 50 waves was generated. The duration of

each test was found as the peak period of the generated spectrum multiplied a number of 650 waves.

Table 2 and Table 3 summarise the used combinations of parameters of generated regular waves and irregular waves, respectively. The range is given as key parameters being the wave steepness, H/L, and the non-dimensional wave height H/h_t. The wavelength is calculated using the linear dispersion relation $\omega^2 = gk\tanh(kh)$.

For regular waves the parameters referenced are

H	incident seaward wave height
T	incident wave period
L	wavelength based on T
h	seaward water depth
h_t	water depth on the reef-plateau
a	steepness of the slope

For irregular waves the parameters referenced are

H_s	incident significant spectral seaward wave height
T_p	peak period based on the incident wave spectrum
L_p	wavelength based on T_p
h	seaward water depth
h_t	water depth on the reef-plateau
a	steepness of the slope

The incident significant wave height is denoted H_s as the wave parameter used when generating waves based on the JONSWAP spectrum. The significant wave height on the reef-plateau is calculated from the wave energy density spectrum and referred as H_{m0}.

h_t [m]	L [m]	H/L [-]	H/h_t [-]	$H/(gT^2)$ [-]
0.205-0.325	1.5-6.4	0.005-0.137	0.09-1.02	0.0004-0.0214

H [m]	T [Sec]	h [m]	Slope (1:a) [-]	Number of tests [-]
0.210	1.0-1.4-1.8-2.2-2.6	0.585	1-1(s)-2	14
0.190	1.0-1.4-1.8-2.2-2.6	0.585-0.655	1-1(s)-2	28
0.173	1.0-1.4-1.8-2.2-2.6	0.585-0.655	1-1(s)-2	24
0.160	1.0-1.4-1.8-2.2-2.6	0.705	1-1(s)	9
0.157	1.0-1.4-1.8-2.2-2.6	0.585-0.655	1-1(s)-2	26
0.145	1.0-1.4-1.8-2.2-2.6	0.705	1-1(s)	9
0.140	1.0-1.4-1.8-2.2-2.6	0.585-0.655	1-1(s)-2	23
0.130	1.0-1.4-1.8-2.2-2.6	0.705	1-1(s)	10
0.120	1.0-1.4-1.8-2.2-2.6	0.585-0.655-0.705	1-1(s)-2	40
0.100	1.0-1.4-1.8-2.2-2.6	0.655-0.705	1-1(s)	15
0.090	1.4--2.6	0.585-0.705	1-1(s)-2	5
0.085	1.8	0.585	1-1(s)-2	3
0.070	2.2	0.585	1-1(s)-2	3
0.060	2.6	0.585	1-1(s)-2	3
0.050	2.2-2.6	0.585	1-1(s)-2	6
0.030	2.6	0.585	1-1(s)-2	3
0.03-0.21	1.0-1.4-1.8-2.2-2.6	0.585-0.655-0.705	0.5	80
				301

Table 2: *Regular waves tested in the wave flume. The S-formed slope is denoted (s).*

h_t [m]	L_p [m]	H_s/L_p [-]	H_s/h_t [-]	$H_s/(gT_p^2)$ [-]
0.205-0.275	2.7-6.2	0.016-0.078	0.36-1.02	0.0015-0.0109

H_s [m]	T_p [sec]	h [m]	Slope (1:a) [-]	Number of tests [-]
0.21	1.4-1.8-2.2	0.585-0.655	0.5-1-1(s)-2	18
0.19	1.4-1.8-2.2	0.585-0.655	0.5-1-1(s)-2	18
0.16	1.4-1.8-2.2	0.585-0.655	0.5-1-1(s)-2	18
0.13	1.4-1.8-2.2	0.585-0.655	0.5-1-1(s)-2	18
0.09-0.10	1.4-1.8-2.2	0.585-0.655	0.5-1-1(s)-2	18
0.10-0.13-0.19-0.21	2.6	0.655	1(s)	5
0.19	1.8-2.4	0.655	2	2
0.16	1.4-2.4	0.655	2	2
0.13	2.4	0.655	2	1
				100

Table 3: *Irregular waves tested in the wave flume. The S-formed slope is denoted (s).*

The procedure by separating incident and reflected waves using the method of Mansard and Funke can induce errors. Therefore, the target incident wave parameters are always referred to as seaward wave parameters. In general there is a match between the parameters of the generated wave and the measured seaward wave.

Minor deviations of the smallest waves were observed. The tests based on the smallest target wave height, H_{m0} = 0.10 m, in some few instances, were corrected less than 10% based on the measurements in front of the wave paddle. They were in fact measured slightly higher.

Figure 23 shows the breaking of a wave propagating the reef-slope during a test.

Figure 23: *Breaking of a wave propagating the steep reef-slope during the tests.*

CHAPTER 9 EXPERIMENTAL RESULTS

Data obtained during the experimental tests are analysed and presented in this chapter. The objective is to establish a criterion for wave breaking and to study the statistical properties of the waves. Such results have to be obtained in order to control the wave breaking in the wave model. The experimental results will form basis for the development of the wave model and the developed formulae, i.e. two approaches to describe the wave energy dissipated.

9.1 Wave energy dissipation along the reef

In the flume test the waves propagate over the reef-slope and if they break, they break either immediately on the reef-crest or shortly after the edge between wave gauge No. 6 and wave gauge No. 7. In general they break as plunging waves and then propagate over the reef-plateau as a succession of bores before they reform into stable oscillatory waves approximately at wave gauge No. 10. For knowledge of the rate of wave energy dissipation along the reef-plateau Figure 24 is presented.

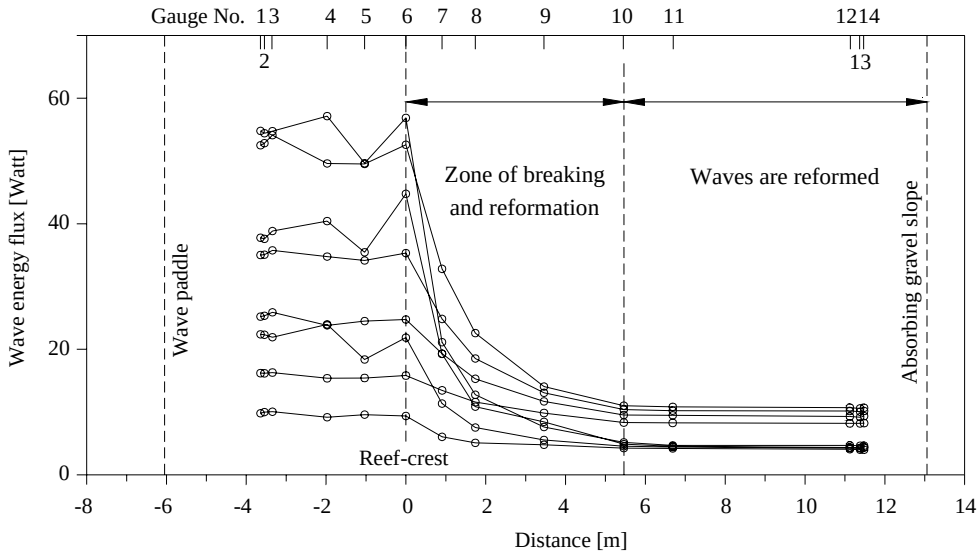

Figure 24: *Wave energy flux measured along the wave flume for irregular waves.*

The graph shows the decay of wave energy flux along the 1.5 m wide wave flume for a number of 8 representative tests at two different water depths. Regarding the 8 tests shown in Figure 24, the reflected waves are not separated when calculating the wave height in front of the reef-slope. It is noted that the waves are all reformed at wave gauge no. 10. The measured energy flux in front of the reef-slope is influenced by

wave reflection and the fact that the group velocity at the reef-crest is calculated based on the water depth at the reef-plateau.

It is emphasised that experimental measured estimates of wave energy density and wave energy flux are based on measured energy spectra. The energy spectra are obtained using a Fourier analysis performed on the measured elevations. The wave energy density is measured directly. It is more difficult to measure the wave energy flux, which is based on the group velocity. The group velocity is not a directly measurable quantity (as the wave height) but needs input of the water depth and a wave frequency. The measured wave energy flux referred in all experimental tests is estimated accordingly to Eq.(76).

9.2 The maximum transmitted wave height

The maximum possible ratio of wave height to a constant depth of water is about 0.8, both theoretical and experimentally. This value is often used for engineering practice in order to determine a design wave height. In Section 4.1 the estimation of the maximum possible wave height before breaking is discussed.

The following graphs present results of regular and irregular waves measured immediately after the reef-edge at wave gauge No. 7. The waves have just initiated wave breaking or in the very early stage of wave breaking at the location of wave gauge No. 7. Results are also presented obtained at wave gauge No. 11, where all the waves are reformed into stable waves. In Figure 21 and Figure 24 the positions of the two wave gauges are seen.

The range of regular waves is chosen in such a way that the waves are both breaking and non-breaking in order to identify a threshold of breaking. The wave breaking is determined visually, but also recorded on video in case of any re-evaluation. It is noted that it is easy to determine whether the regular waves are breaking or non-breaking.

In all irregular wave trains generated breaking waves occurred. The smallest chosen incident wave height combined with the deepest water depth on the reef-plateau yielded mildly breaking waves. The largest incident wave height combined with the shallowest water depth yielded significant breaking of all waves.

The regular wave parameters depicted in Figure 25 and Figure 26 are the measured non-dimensional wave height and the wavelength at wave gauge No. 7 and wave gauge No. 11 versus the so called non-linearity parameter F_{c0}. Notice that the non-linearity parameter is depicted on a logarithmic axis. F_{c0} is based on the incident seaward wave parameters and the water depth at the reef-plateau. The non-linearity parameter is described in Section 5.5.1 as a suitable parameter for classifying wave transformation on a coral reef. The parameter is also known to describe and classify waves. It is repeated that if F_{c0} is less than 10 then deep-water waves are expected and

values between 10-500 characterise transitional waves. Values above 500 indicate shallow water waves. Massel and Gourlay [2000] reported that the value of energy dissipation for waves with F_{c0} less than approximately 100 was negligibly small.

The range of the non-linearity parameter is 40-1500 for regular waves and 120-950 for irregular waves. This means that the irregular waves generated are expected to be transitional waves and shallow water waves. The non-linearity parameter F_{c0} did not exceed 1000, which is expected to violate the refraction-diffraction equation, which the wave model is based on.

9.2.1 Results obtained for regular waves propagating a steep slope

The regular wave height is measured by a zero-downcrossing analysis and is given as the average wave height. As expected the deviation of the regular waves is negligible.

The non-dimensional wave height measured at wave gauge No. 7 immediately after the reef-crest shows that the maximum non-dimensional wave height reaches a maximum value of approximately 0.8. This happens for waves generated with F_{c0} larger than 1000, which are the largest waves generated at the most shallow water depths. These waves are very shallow water waves and are turbulent breaking waves attenuating rapidly with the distance from the reef-edge. The non-breaking waves comply with the envelope proposed by Nelson [1994] until a value of F_{c0} in the range 100-200. Hereafter the maximum non-dimensional wave height is no larger than 0.4. For waves propagating in shallow waters with a horizontal seabed the upper limit value found by Nelson [1994] is 0.55. For waves propagating a steep slope with shallow water conditions at the reef-plateau, it is indicated from the present experimental tests that the maximum ratio of wave height over local water depth is approximately 0.4.

The bottom graph in Figure 25 shows the breaking waves differentiated regarding the steepness of slope used in the tests. Because all the slopes, with exception of the steepest slope 1:0.5 for some of the ranges, are tested using the same waves and water depth, it is possible to compare these results. On the bottom graph in Figure 25 it is indicated for the largest values of F_{c0} that the highest ratio of non-dimensional wave height is obtained with the flatter slope of 1:2 and then the non-dimensional wave height decreases as the slope steepness increases. This seems to be most pronounced for the shallow water waves.

The waves are all reformed at gauges No. 10 and No. 11 and the breaking process is ended. The results are depicted in Figure 26. It is observed that the waves are attenuated significantly during the breaking process. All the non-breaking waves seem to have a higher non-dimensional wave height than the waves exposed to breaking. The maximum ratio of the non-breaking waves is almost unchanged for waves with F_{c0} being less than 100. For waves not breaking, where F_{c0} is larger than 200, the non-dimensional wave height is decreased. This is because these waves are

shoaling when propagating into the shallow waters and decrease again when they are reformed. The difference in non-dimensional wave height along the reef-plateau is not pronounced for waves at larger water depths i.e. $F_{c0} < 100$.

In the bottom graph in Figure 26 the breaking waves are again differentiated due to the steepness of the used reef-slope. Any trends are now difficult to identify, i.e. the steepness of the reef-slope has only a weak influence on the reformed non-dimensional wave height.

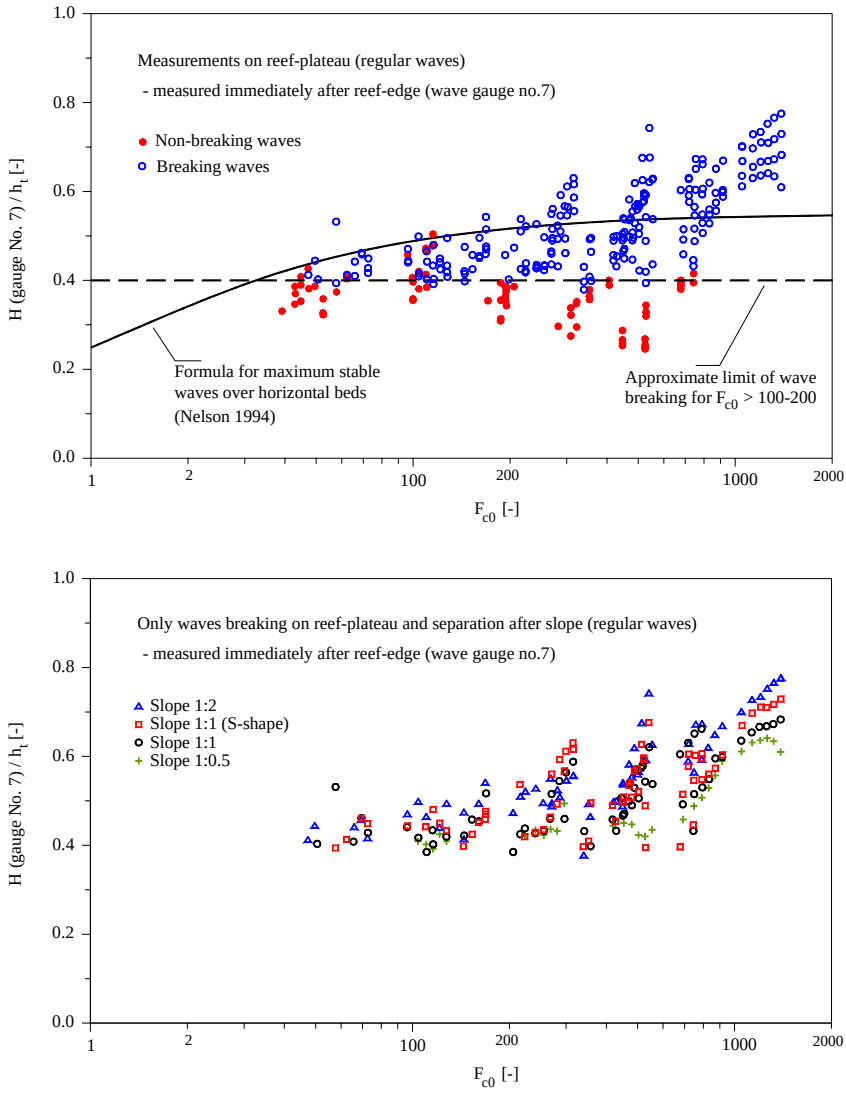

Figure 25: *Non-dimensional parameters of regular waves on the reef-slope.*

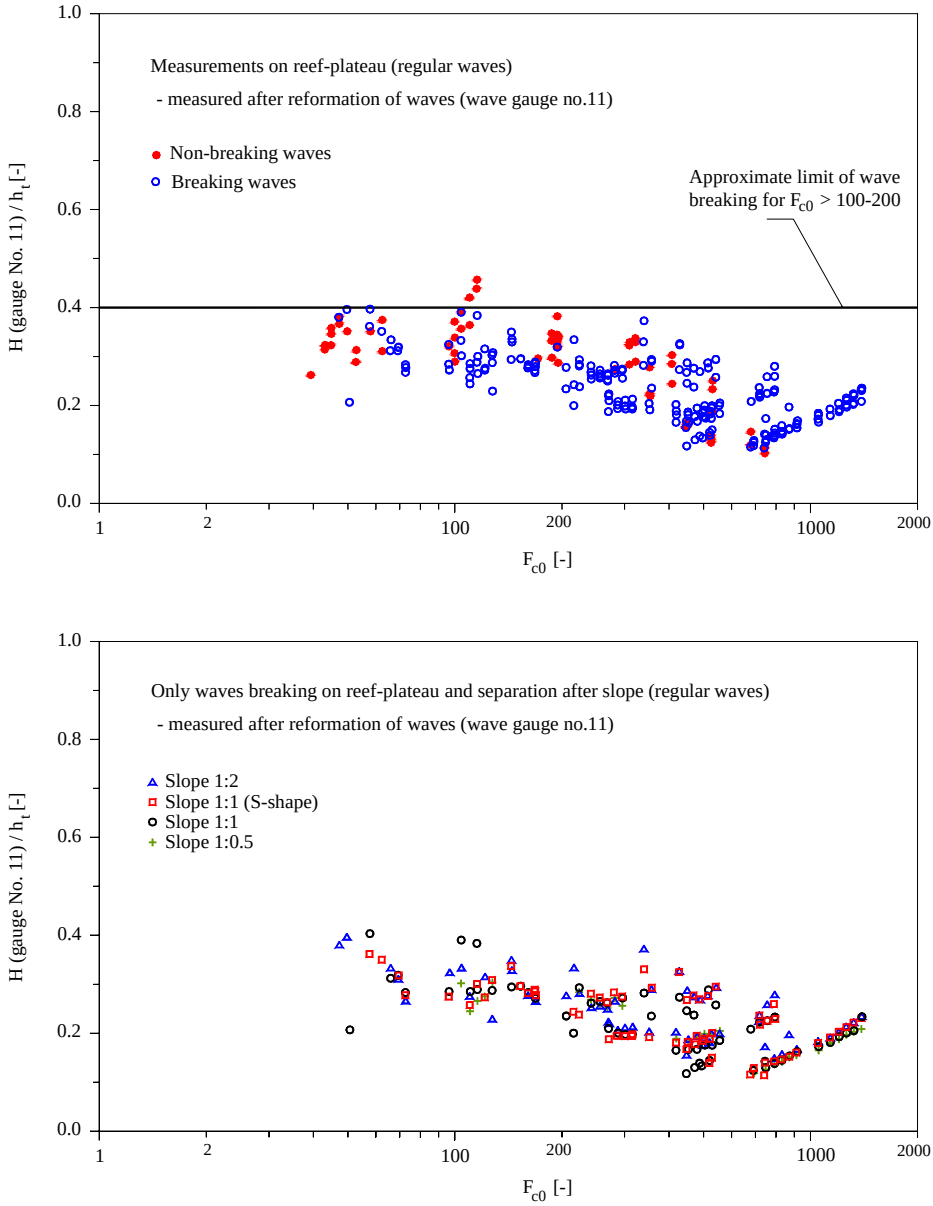

Figure 26: *Non-dimensional parameters after reformation of regular waves.*

9.2.2 Irregular waves

The maximum wave height in the irregular wave train is discussed in the following. Furthermore, the wave height distribution of the reformed waves is studied. A zero-downcrossing analysis is used to estimate the wave heights in order to obtain the wave height distribution and a Fourier analysis is used to obtain the significant wave height based on wave energy spectrum.

The results of the tests generating irregular waves are depicted in Figure 27. In the top graph the measurements are obtained at wave gauge No. 7, where wave breaking is initiated. The non-dimensional significant wave height increases for higher values of F_{c0}. Similar to the results obtained for the regular waves, the maximum ratio of the non-dimensional significant wave height is approximately 0.8. A minor influence of the steepness of the slope is observed. The bottom graph shows the results after the irregular waves are reformed and measured at wave gauge No. 11. The non-dimensional wave height is reduced to a value between 0.31 and 0.37. It is noted that this value is rather constant for different wave parameters and slopes used.

The results of the non-dimensional significant wave height passing the steep reef without breaking complies with the observations made by Hardy et al. [1990], that the maximum ratio of the significant wave height passing a coral reef is 0.4. This was based on experimental measurements.

Assuming a Rayleigh distribution of the wave heights, the non-dimensional ratio of the highest wave height will be 1.8 times higher in the irregular wave train consisting of 650 waves, i.e. $\sqrt{\ln 650/2} = 1.8$. The wave height distribution will after the wave breaking process not be a Rayleigh distribution, because primarily the largest waves are breaking. An analysis of the wave height distribution measured at wave gauge No. 11 in the irregular wave trains is depicted in Figure 28 for representative tests. It is shown that the wave height distributions do not follow a Rayleigh distribution, because the larger waves are not appearing with the probability as expected if the wave heights followed a Rayleigh distribution. The deviation from the Rayleigh distribution does not depend of the value of F_{c0}.

A further analysis of the relationship between the parameters H_{m0}, H_s and H_{max} can be seen from the top graph in Figure 29, where various ratios are depicted against the non-linearity parameter F_{c0}. It is noted that all the waves are reformed. For high values of F_{c0} it is observed that the ratio between H_{m0} and H_s is reduced from 1.0 to approximately 0.85. That is, H_{m0} is slightly underestimated for high values of F_{c0} regarding the definition of the significant wave height as the average of 1/3 of the largest wave heights.

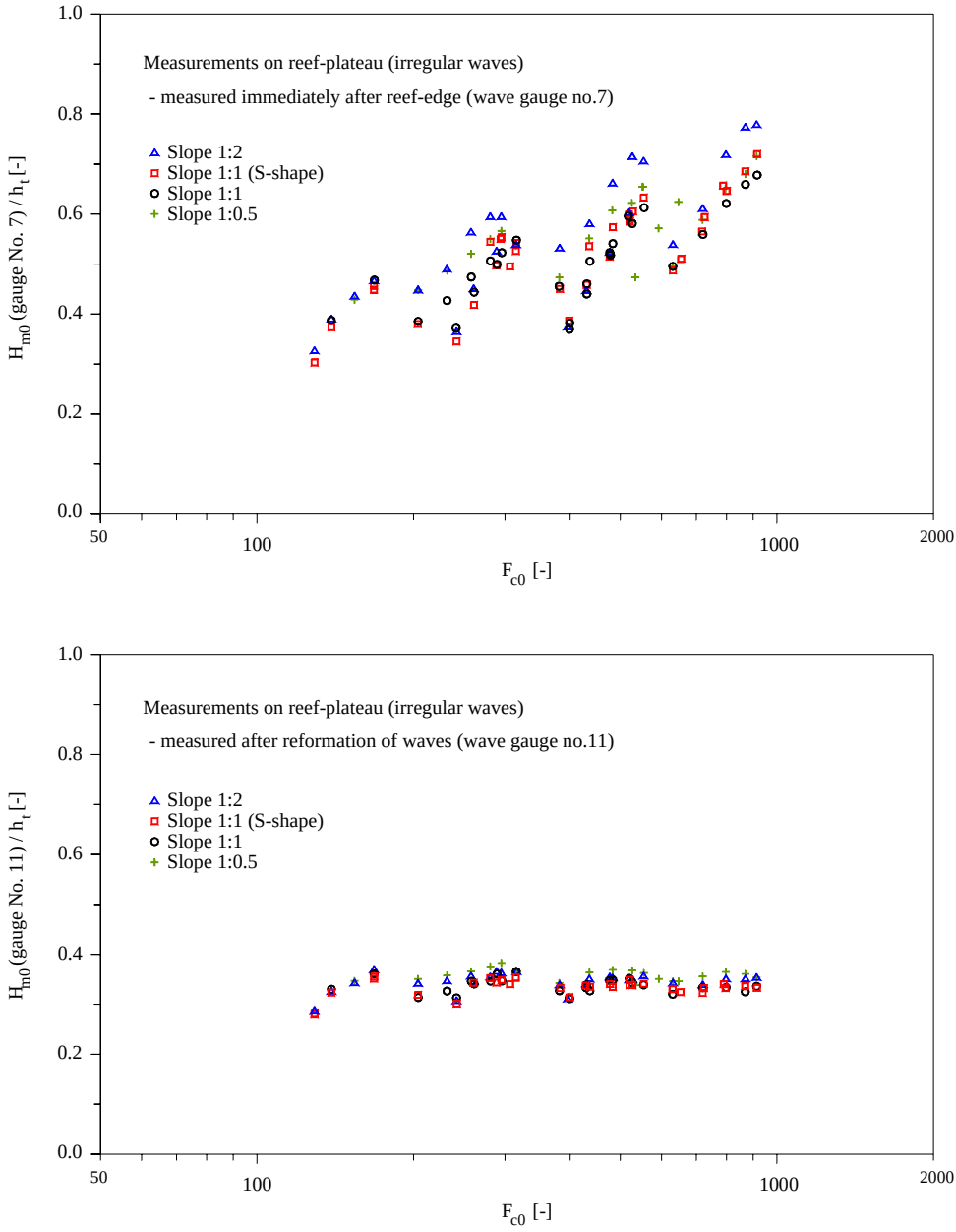

Figure 27: *Tests with irregular waves depicted using non-dimensional parameters.*

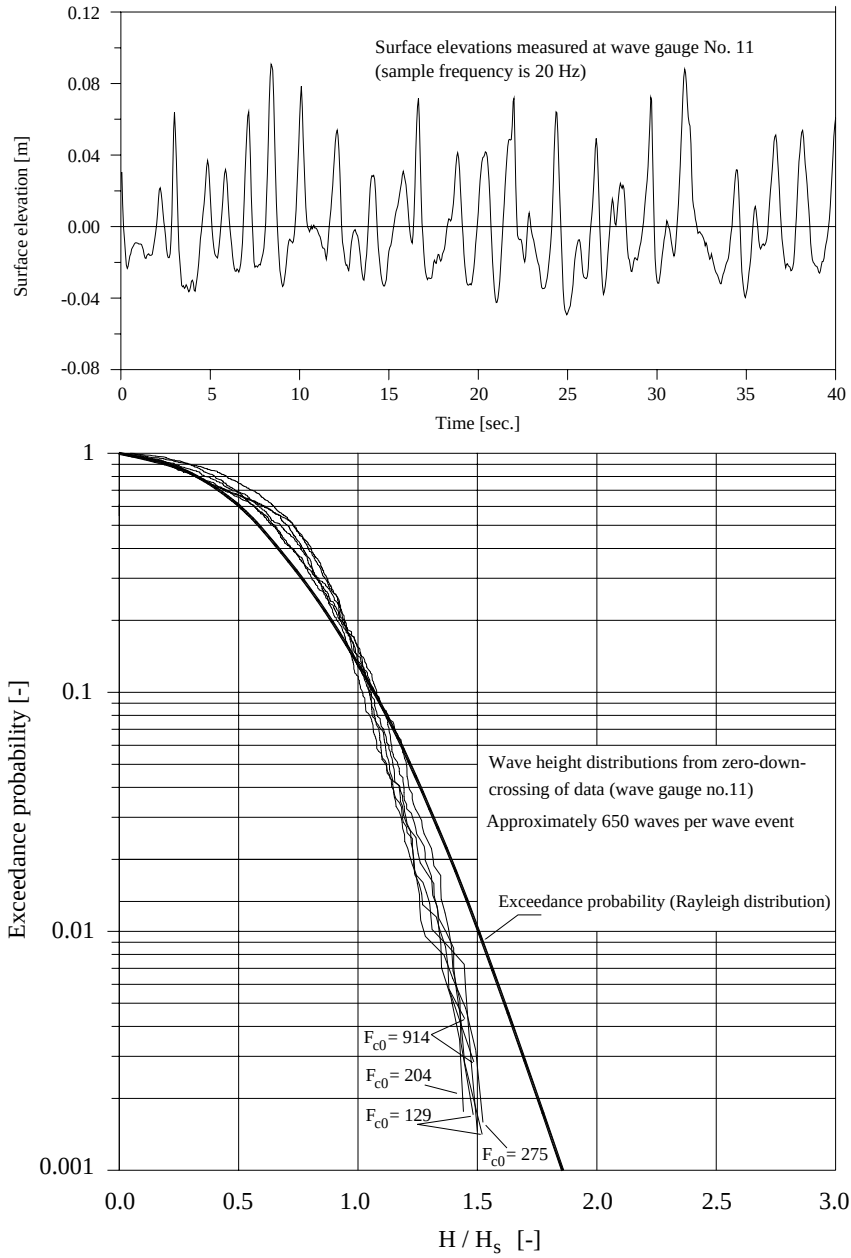

Figure 28: *Measured surface elevation at wave gauge No. 11 and several distributions of zero-downcrossing wave heights.*

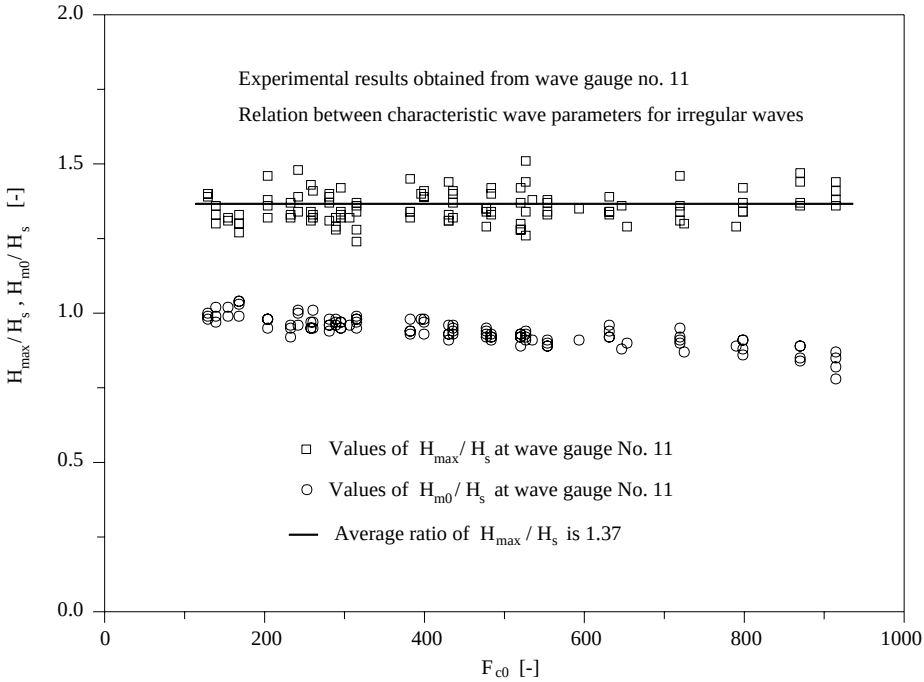

Figure 29: *Depicted values of the ratio between the spectral significant wave height, H_{mo}, and the statistical wave heights, H_s and H_{max}.*

In Figure 29 the relation between the significant wave height and the maximum wave height in the wave train is depicted. These wave heights are determined from the zero-downcrossing analysis. An average value of 1.37 is evaluated. If the waves are Rayleigh distributed a value of 1.8 should have been obtained in the case of 650 waves.

In the top graph in Figure 30 the ratio of the maximum wave height to the reef-plateau water depth in each of the respective wave trains is depicted. The ratio varies from 0.4 to 0.6. There is a tendency of a higher maximum wave height ratio for high values of F_{c0}. A best fit by assuming a linear trend is

$$\frac{H_{\max}}{h_t} = 0.438 + 1.28 \cdot 10^{-4} \cdot F_{c0} \tag{79}$$

In the bottom graph in Figure 30 the ratio of the root-mean-square wave height and the maximum wave height is depicted for reformed waves measured at wave gauge No. 11. An average value of 0.55 is estimated.

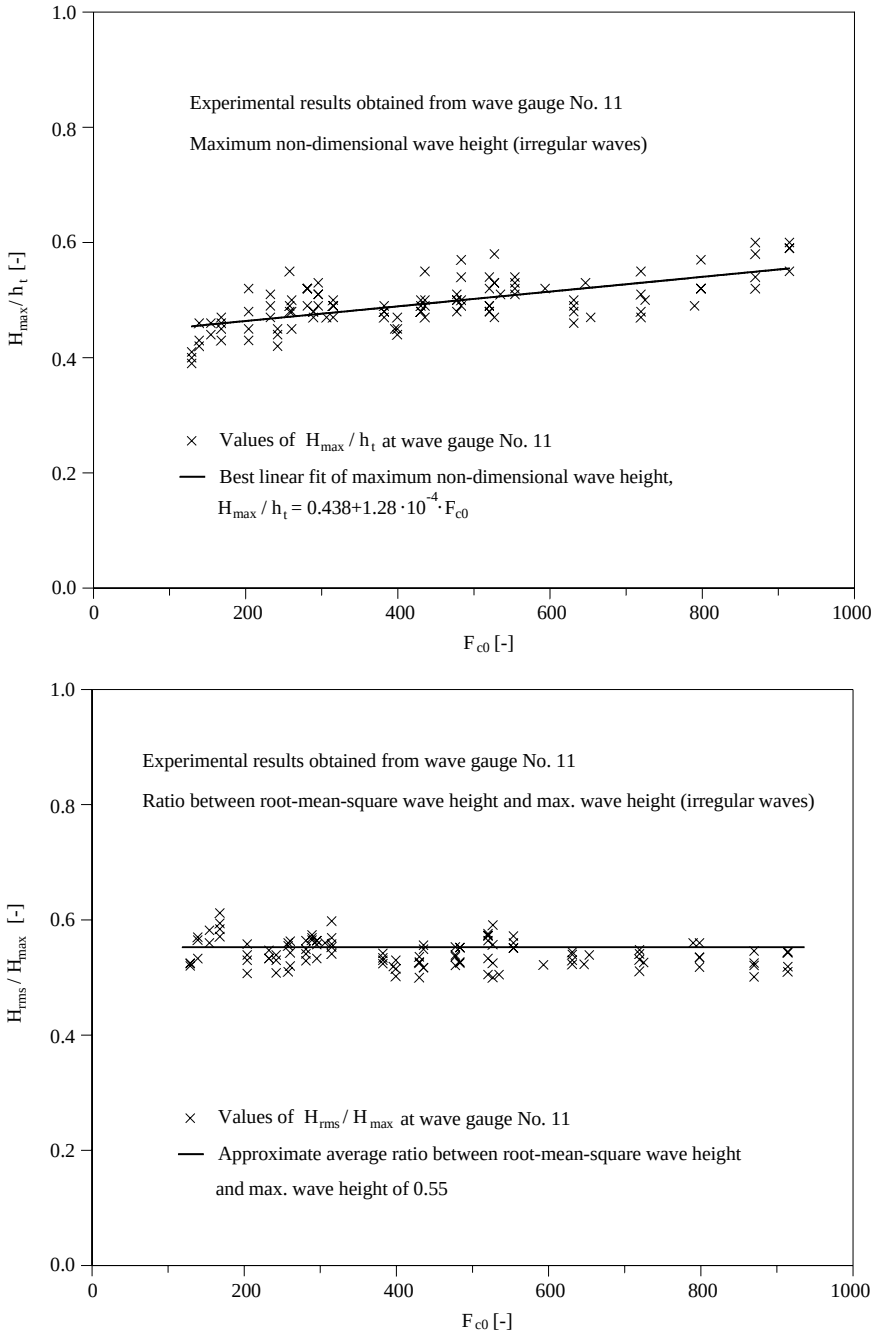

Figure 30: *Top graph shows ratio of non-dimensional maximum wave height. Bottom graph shows the ratio between the root-mean-square and the maximum wave height.*

Sulaiman et al. [1994] performed experiments regarding the maximum wave heights on the horizontal reef at Samur Beach in Bali. For a non-dimensional water depth range of $0.17 \cdot 10^{-4} < h_t / gT^2 < 0.17$ Sulaiman concluded that the ratio of maximum wave height to water depth is always smaller than 0.6. The range used in the present tests is $31 \cdot 10^{-4} < h_t / gT^2 < 0.04$, which is a lesser range than the tests performed by Sulaiman. The ratio of 0.6 compares well with the results obtained in the present tests.

Regarding the reformed waves measured at wave gauge No. 11 it is summarised that the maximum non-dimensional wave height, H_{max}/h_t, within the range of irregular waves generated varies between 0.4-0.6. An average value of 0.5 seems to cover a large range of wave parameters. The ratio of H_{rms}/H_{max} is approximately 0.55. The ratio between the significant wave height and the maximum wave height based on the distribution of waves is on average 1.37. The ratio between the significant wave height based on the energy spectrum and the significant wave height based on the wave height distribution varies between 1.0 and 0.85.

These obtained relations between the characteristic wave heights are found useful later when the wave model is calibrated to the experimental tests.

In the following the spectral significant wave height, H_{m0}, is the parameter focused upon, because it is a practical parameter often used and it is connected to the energy density in the waves.

9.3 Wave energy dissipation due to the reef-slope

The energy flux is introduced in the following as a parameter used to evaluate the experimental tests even further. The energy flux is calculated by integrating the energy spectrum over the respective wave group velocities at each frequency. In Figure 31 and Figure 32 the transmitted energy flux is depicted for all the tests performed at water depths on the reef-plateau of 0.205 m and 0.275 m, respectively. The flux is measured at wave gauge No. 11, where the reformed waves are identified. It is noted that waves seem to be reformed already at wave gauge No. 10. The transmitted energy flux is normalised with the incident energy flux generated. The energy flux is depicted after the wave steepness, where the wave steepness is calculated using the incident significant wave height and the wavelength based on the incident spectral peak period.

Each figure shows results for a different steepness of the slope. The curved lines are drawn by hand to indicate tests with the same incident peak wave period. There is less transmitted energy flux available as the water depth on the reef-plateau decreases, i.e. the change between Figure 31 and Figure 32. There is a clear trend of the results of the normalised transmitted wave energy flux regarding the incident wave height, incident peak wave period and the water depth on the reef-plateau. An important

observation is that the steepness of the slope in the range 1:2 to 1:0.5 has no significant influence on the transmission of energy flux after waves are reformed. This includes different forms of the slope as the S-shaped slope. This observation is confirmed by comparing with the graphs depicted in Section 9.2.1and Section 9.2.2.

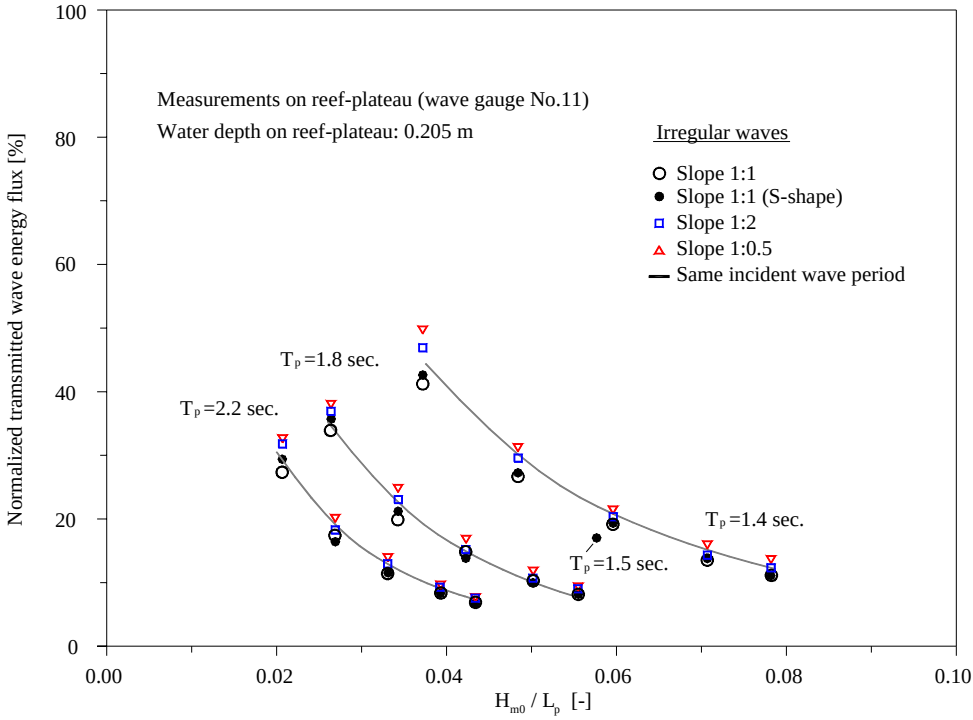

Figure 31: *Transmitted wave energy flux regarding irregular waves, h_t= 0.205 m.*

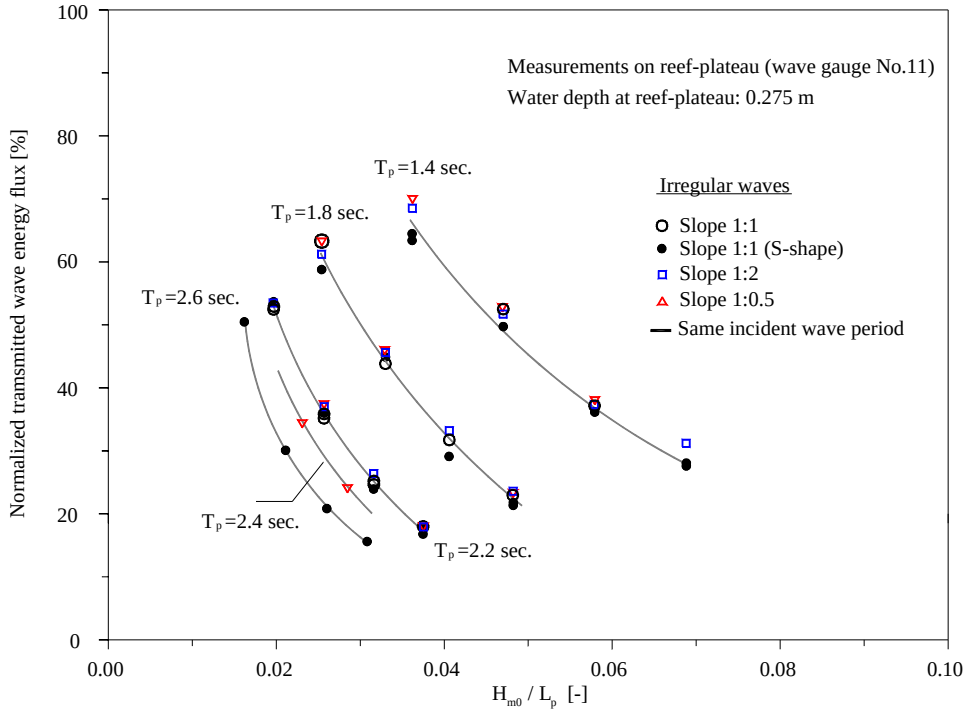

Figure 32: Transmitted wave energy flux regarding irregular waves, h_t = 0.275 m.

Several tests are repeated and the scatter observed is insignificant as shown in Figure 32, where 5 tests are repeated associated with the peak period being 2.2 sec. and 2 tests are repeated using a peak period of 1.4 sec.

To conclude, the transmitted wave energy flux depends on the seaward incident wave height, the peak wave period and the water depth on the reef-plateau. Figure 33 shows the influence of the water depth. The dependence is weak regarding the reef-slope when this is steeper than 1:2. It shall be noted that the reflected wave energy depends on the steepness of the slope. When waves start to break the wave reflection from the slope decreases. Apparently, the amount of wave energy reflected, when the waves are breaking due to the steepness of the slope, is not significant compared to the amount of energy dissipated in the wave breaking process.

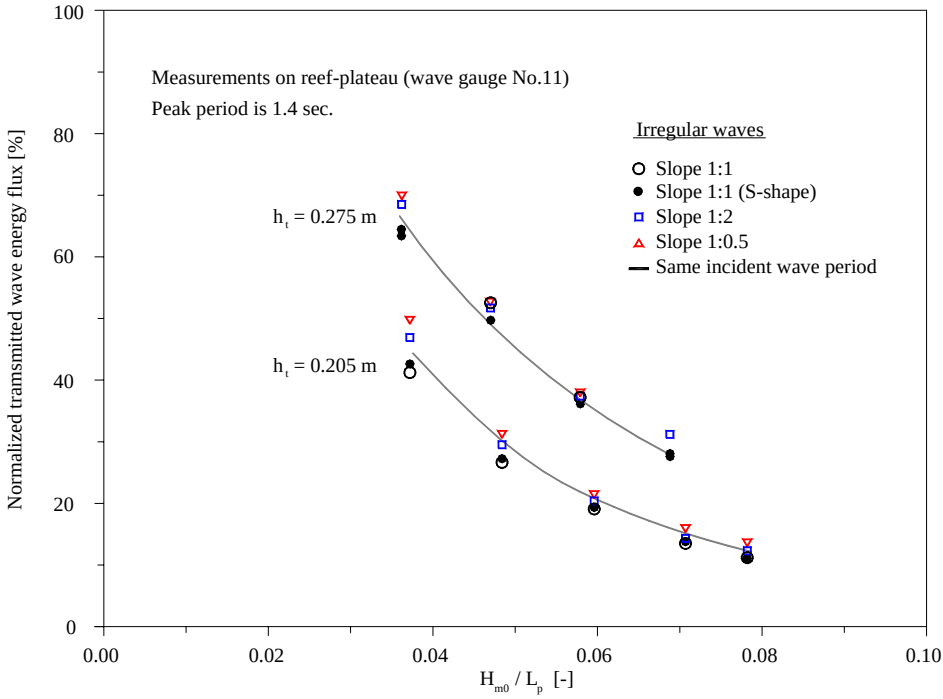

Figure 33: Transmitted wave energy flux regarding irregular waves, h_t = 0.275 m.

9.4 Changes of the wave energy spectrum along the reef-plateau

The change in the shape of the wave energy spectrum along the reef-plateau is of interest when deducing the reformed wave parameters, i.e. the spectral significant wave height and the spectral peak period. In Figure 34 two representative wave energy spectra at different wave conditions are shown. For each wave condition the wave energy spectrum is shown before and after passing the steep reef-slope.

The incident spectrum is measured at the wave gauges No. 1, 2 and 3, where separation of incident and reflected waves is performed. The reformed wave spectrum is measured at wave gauge No. 11.

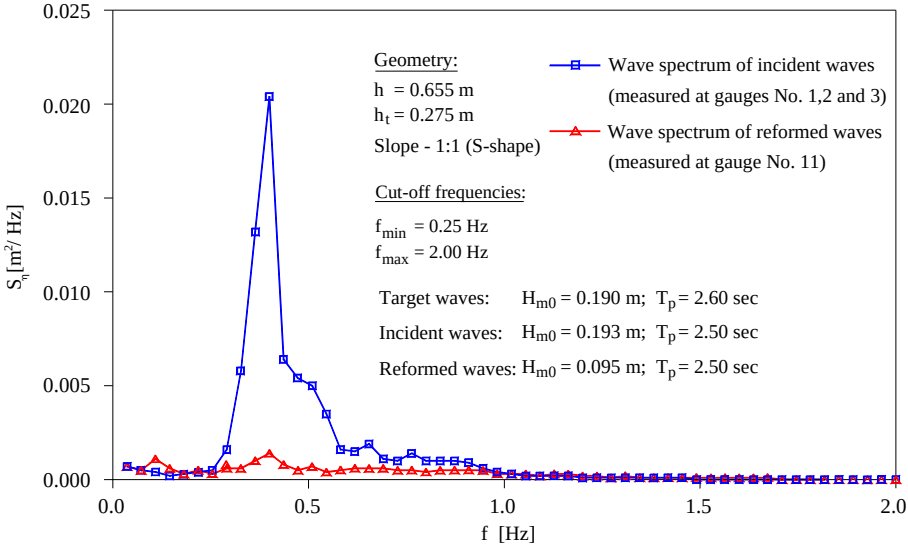

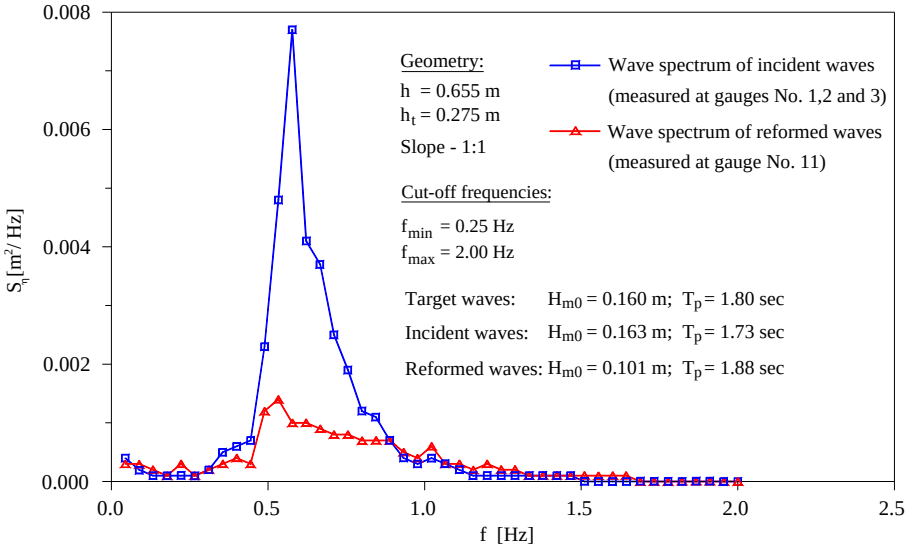

Figure 34: *Representative wave energy spectra along the reef-plateau.*

It is observed that the targeted and the measured spectrum comply with each other regarding the generated wave density, i.e. the measured incident wave height and the measured peak wave period are quite similar with the targeted waves generated. The results are representative for all tests. It is clear that the energy peak in the spectrum is levelled out. This implies that the reformed wave spectrum is broad compared to the incident waves. A best estimate of the peak period in the reformed spectrum seems still to be the peak period of the incident waves.

CHAPTER 10 WAVE ENERGY TRANSMISSION FORMULAE

Formulae predicting transmission of wave energy density and wave energy flux of irregular, breaking waves over a steep slope are presented in the following. The formulae are non-dimensional and are valid for incident head-on waves. The parameters focused upon are the transmitted wave energy density and the transmitted wave energy flux along the reef-plateau, respectively. The transmitted wave energy density is directly related to the transmitted wave height as shown in Eq.(80) and will be referred to only indirectly by the transmitted wave height.

With knowledge of the transmitted energy density it is possible to estimate the reformed wave height on the reef-plateau. Because the wave height is a practical parameter, which is often used and referred to, such a formula is useful. Knowledge about the transmitted energy flux is no less valuable and a formula for this is also provided. Wave energy flux is not often a parameter referred to, but it is an important parameter because the energy flux contains information of the remaining transported energy. As an example the widely utilised CERC formula (SPM 1984) for estimating the potential longshore sand transport rate is based on the assumption that the transport rate is proportional to the energy flux. If only the transmitted wave height is known on the reef-plateau, the information of the energy flux is lost because information of the wave frequencies is lost.

It is noted that the formula of transmitted wave height is based on a constant water depth on the reef-plateau. If the water depth changes on the reef-plateau or a lagoon follow, then the wave height will change depending on the water depth. The transmitted wave energy flux will remain the same after the breaking is finalised, assumed there will be no additional loss of energy.

The energy dissipation present in the tests is due to wave breaking and dissipation due to bottom friction. Dissipation due to bottom friction is not significant along the breaking zone of the waves, because the reef used in the tests is considered smooth. The dissipation is expected to be larger if a relatively rough reef is considered.

The wave energy density transmission is related to the wave height transmission coefficient by

$$K_{t,H} = \sqrt{\frac{E_t}{E_i}} = \frac{H_t}{H_i} \tag{80}$$

where E_t is the density of the transmitted energy spectrum and E_i is the incident wave energy density. H_i and H_t is the significant incident wave height and the significant wave height transmitted on the reef-slope. The transmission coefficient can be larger

than 1.0 if the waves are shoaling on the reef without any breaking taking place. Similar, a transmission coefficient regarding the wave energy flux is expressed as

$$K_{t,P} = \sqrt{\frac{P_t}{P_i}} \tag{81}$$

where P_i and P_t are the incident wave energy flux and the wave energy flux transmitted on the reef-slope, respectively. It is chosen to apply a square-root-sign in Eq.(81) in order to make an analogy to Eq.(80) because the wave energy flux is more related to the wave energy than then wave height.

The following formulae are based on results obtained from the tests performed in the hydraulic laboratory as described in Section 8.1. With reference to Figure 21 the data obtained from the wave gauges No. 7, 8, 9 and 10 on the reef-plateau are used. After wave gauge No. 10 all the waves seem to be reformed, when comparing to the following four wave gauges, i.e. the wave gauges No. 11, 12, 13 and 14.

So far, results from wave gauge No. 11 are often referenced. It is emphasised that the results obtained from wave gauge No. 10 and wave gauge No. 11 are comparable.

In total 110 tests were performed, with measurements from four wave gauges a total of 440 series of irregular waves were obtained. The varying parameters were the incident wave height, wave period, water depth and the steepness of the reef-slope. A Fourier analysis was applied in order to obtain the wave energy spectra for each test. The values of significant wave height and the wave energy flux were deducted based on the wave energy spectra. All data are presented in Appendix D.

The distance from the slope and down-wave the reef is denoted X, see also Figure 35. The exact distances of the gauges within the zone of wave breaking are

- Gauge No. 7: $X = 0.90$ m
- Gauge No. 8: $X = 1.74$ m
- Gauge No. 9: $X = 3.10$ m
- Gauge No. 10: $X = 5.46$ m

Wave gauge No. 7, which is nearest to the reef-edge, is close to the point where the largest waves initiate wave breaking. Therefore, a few of the tests yield transmission coefficients at wave gauge No. 7 that are higher than 1.0 because the waves are shoaling when they propagate the steep reef-slope. The energy dissipation rate is highest within the first part of the wave breaking zone, see also Figure 24. In order to include the development of the energy dissipation along the slope in the formulae, it is important to use the measurements at wave gauge No. 7. These measurements represent threshold values, where waves initiate wave breaking. Inclusion of these

data introduces more scatter between predicted and measured values compared to the scatter obtained from the wave gauges at a greater distance from the reef-slope.

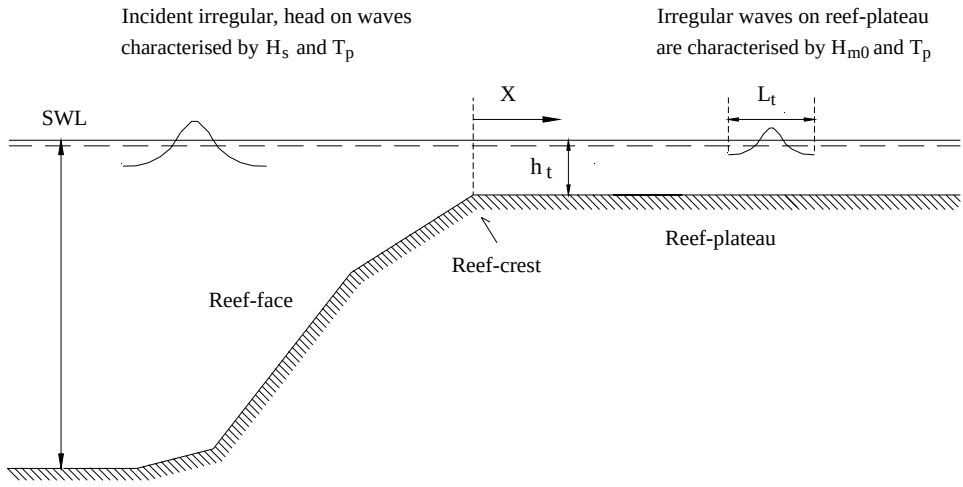

Figure 35: *Definitions related to wave energy transmission formulae.*

10.1 Transmission of wave energy flux

An expression of the rate of transmitted wave energy flux of breaking, irregular waves propagating a steep slope is obtained using the relation between the wave energy flux off-shore the reef-slope and outside the zone of wave breaking, as

$$\frac{P_t}{P_i} = \frac{\frac{1}{8}\rho_w\, g\, H_t^2\, \overline{C}_{g,t}}{\frac{1}{8}\rho_w\, g\, H_s^2\, \overline{C}_{g,o}} = \frac{H_t^2\, \overline{C}_{g,t}}{H_s^2\, \overline{C}_{g,o}} \tag{82}$$

where $\overline{C}_{g,o}$ and $\overline{C}_{g,t}$ are the wave group velocity, based on the incident seaward spectral peak period, and the spectral peak period at the reef-plateau, respectively. It is noted that Eq.(82) is based on first order linear wave theory.

The incident wave spectrum simulated in the laboratory is relatively narrow and the energy flux can be represented using a characteristic frequency to represent the wave group velocity. The transmitted wave height in Eq.(82) is not known, but is measured in the experimental tests. It is assumed that the transmitted wave height is related to a constant ratio of the water depth on the reef-plateau, i.e.

$$H_t = \gamma \cdot h_t \tag{83}$$

The breaker index, γ, is the ratio of the water depth yielding the maximum allowable significant wave height on the reef-plateau. The parameter is described in Section 4.1 and introduced in Eq.(4). This relation between the significant wave height and the water depth at the reef-plateau is confirmed by the bottom graph depicted in Figure 27, where the reformed significant wave height, H_{m0}, on the reef-plateau have a breaker index between 0.3-0.4 at wave gauge No. 11 for a wide range of values of F_{c0} .

Inserting Eq.(82) into Eq.(83) and assuming that the group velocity seaward equals the group velocity in deep water the following expression of the transmission coefficient for wave energy flux is obtained as

$$K_{t,P} = \sqrt{\frac{4\pi\gamma^2 h_t^2 \overline{C}_{g,t}}{H_s^2 g T_P}} \tag{84}$$

where the wave group velocity on the reef-plateau is calculated as

$$\overline{C}_{g,t} = 0.5 \cdot \overline{C}_t \left(1 + \frac{2\overline{k}_t h_t}{\sinh 2\overline{k}_t h_t} \right) \tag{85}$$

where $\overline{C}_t$ is the wave phase velocity and $\overline{k}_t$ is the wave number on the reef-plateau calculated after the peak period of the incident waves.

In the experiments the water depth in front of the reef is finite and the water depth on the reef is shallow. Therefore, it is more consistent relating to the experimental data to use the expression for the group velocity in finite water depth seaward the reef. Similar, it is more consistent to use the group velocity at shallow water $\left(\overline{C}_{g,t} = \sqrt{g h_t}\right)$ on the reef. Surprisingly, using the deep-water group velocity seaward the reef in combination with the group velocity for finite water, Eq.(85), on the reef yielded a marginally better fit and have therefore been adopted. It is noted that the difference is not significant.

Figure 36 shows the correlation between the formulae given by Eq.(84) and the estimated wave energy flux at wave gauge No. 10. As mentioned previously, the wave energy flux is based on the wave height and period measured. A calibration of formula Eq.(84) based on the experimental results indicates that $\gamma = 0.33$ yields the best fit.

Eq.(85) is based on use of the peak frequency for calculation of the wave group velocity. If a broad frequency range represents the incident wave spectrum, it is not clear how this will affect the accuracy of Eq.(84). Unfortunately, no other wave energy spectra are generated besides the JONSWAP spectrum. As observed in Figure 34 the spectrum obtained after the waves are reformed is no longer represented by a peaked spectrum, but is levelled out on both sides of the peak period. Using the incident peak period when calculating the wave group velocity on the shallow reef is therefore not expected to influence the accuracy of the formula regarding the shape of the incident spectrum.

The correlation between the 110 experimental obtained data and the calibrated Eq.(84) is good. The standard deviation of the wave transmission coefficient is 0.025 and a 90% confidence interval estimate yields $K_{t,P} = \pm 0.04$.

Limits of validity of Eq.(84) are discussed later but the only restriction to the formula is requirements regarding the incident wave height being large enough to cause wave breaking.

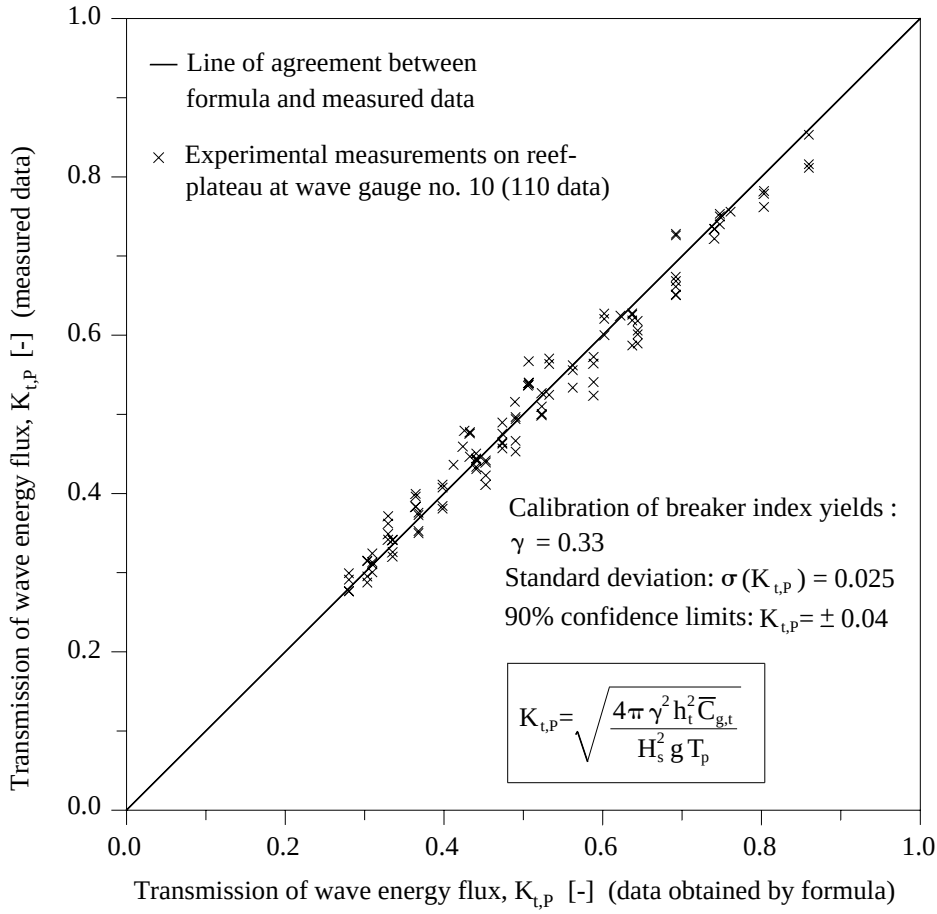

Figure 36: *Comparison between measured values of the reformed transmitted wave flux coefficient and corresponding values estimated by Eq.(84).*

10.2 Transmission of wave energy flux along the reef-plateau

The total transmission of energy flux from waves propagating from deeper water until waves are reformed down-wave the reef-plateau is determined by Eq.(84). By inclusion of a contribution to the total transmitted wave energy flux depending on the length from the reef-slope, X, a formula predicting the transmitted wave energy flux is proposed using an expression representing the contribution as

$$\tanh\left(\kappa\left[\frac{X}{L_t}\right]^{-\zeta}\right) \tag{86}$$

where the wavelength on the reef-plateau, $L_{t,}$ is calculated based on the peak period and without approximation to shallow water conditions.

Without the hyperbolic tangent function the prediction of the transmitted wave energy flux increases to infinity, as the ratio of X/L_t becomes zero. The formula predicting the transmission coefficient along the reef-plateau, according to Eq.(86), should not be used outside the minimum value of the tested range, i.e. the requirement using Eq.(86) is that $X/L_t > 0.22$. It is noted that within the tested range of parameters the effect of the hyperbolic tangent function is minor, but is used because it ensures that the expression will not exceed unity.

The final expression of the transmission coefficient of wave energy flux along the reef-plateau is

$$K_{t,P} = \sqrt{\frac{4\pi\gamma^2 h_t^2 C_{g,t}}{H_s^2 g T_P} + \tanh\left(\kappa\left[\frac{X}{L_t}\right]^{-\zeta}\right)} \tag{87}$$

The breaker index is kept unchanged as $\gamma = 0.33$. A calibration of Eq.(87) based on the 440 data obtained from the experimental tests yields an estimate of the coefficients as $\kappa = 0.06$ and $\zeta = 1.5$.

The standard deviation of the wave transmission coefficient is 0.04 and a 90% confidence interval estimate yields $K_{t,P} = \pm 0.07$. Figure 37 shows the correlation between the results predicted by the formula in Eq.(87) and the measured wave energy flux at wave gauges No. 7, 8, 9 and 10.

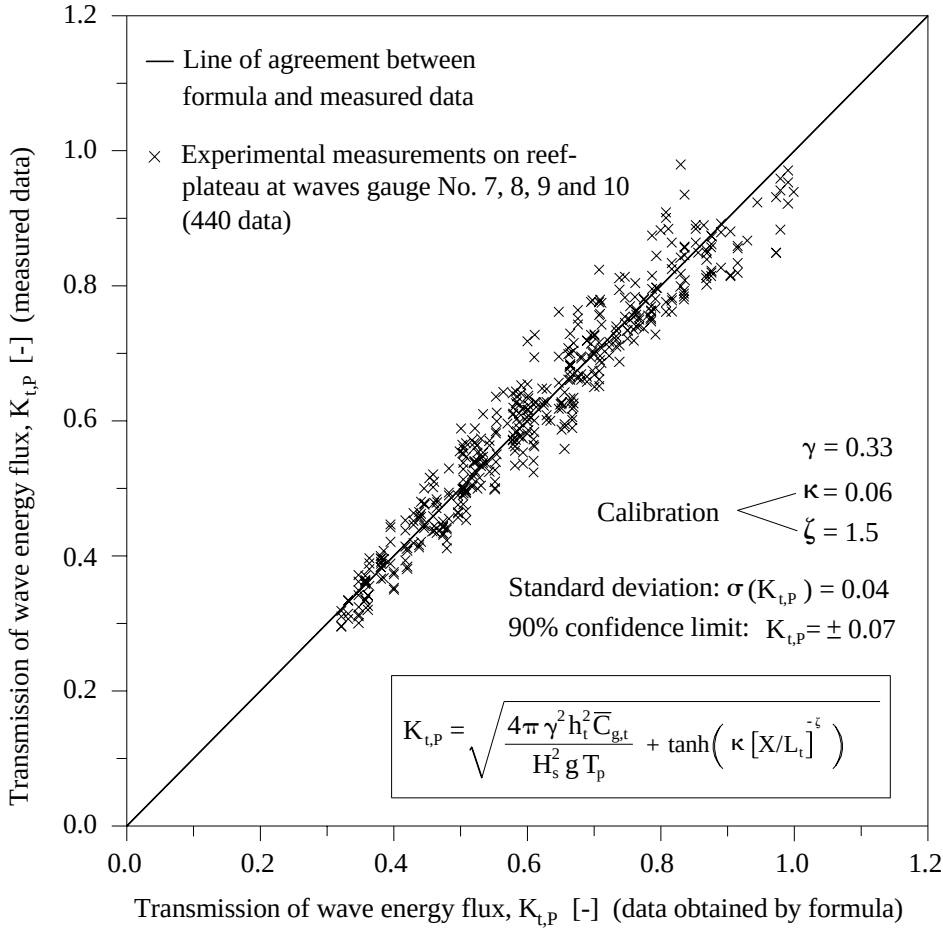

Figure 37: *Comparison between measured values of the transmitted wave flux coefficient along the reef-plateau and corresponding values estimated by Eq.(87).*

10.3 Transmission of significant wave height

An expression of the rate of transmitted significant wave height is based on a constant ratio between the significant wave height and the water depth at the reef-plateau (the breaker index) by assuming that the reformed wave height on the reef-plateau is determined only by the water depth. The same assumption was applied when deriving a formula for the transmission of wave energy flux. Assuming a constant breaker index the wave height transmission can be written as

$$K_{t,H} = \frac{\gamma\, h_t}{H_s} \tag{88}$$

A calibration of formula Eq. (88) based on the experimental results yields $\gamma = 0.36$.

The standard deviation of the wave transmission coefficient is 0.04 and a 90% confidence interval estimate yields $K_{t,H} = \pm 0.06$.

It is expected that the breaker index calibrated in Section 10.1 as $\gamma = 0.33$ when deriving the formula for estimation of the wave energy flux, is similar with the breaker index calibrated when deriving a formula for estimation of the transmitted wave height. The breaker index estimated in the previous section might be influenced by other parameters and should be regarded more as a constant rather than a real breaker index, although, it is noted that the two coefficients are of the same size. In fact, the two values do not yield a significant visual difference when interchanged and depicted, i.e. if the value $\gamma = 0.36$ is used in Eq.(84) and depicted similar to the graph presented in Figure 36. It is chosen to keep two different values in the respective formulae.

Figure 38 shows the correlation between the estimates provided by Eq.(88) and the measured wave height coefficients at wave gauge No. 10. The clear deviation of the highest transmission coefficients being estimated higher than actually measured is related to the smaller waves with the incident wave parameters H_s = 0.11 m and a largest water depth on the reef-plateau being h_t = 0.275 m. This yields a non-dimensional wave height on the reef-plateau being H_s/h_t = 0.4, which is the lowest non-dimensional wave height applied in the tests. These waves are mildly breaking and a threshold of initiation of wave breaking is reached. It is therefore required that the non-dimensional significant wave height shall exceed a ratio of 0.4 to ensure a sufficient fraction of waves breaking. In other words, if the ratio of the incident significant wave height and the water depth on the shallow reef is less than 0.4 the waves will not experience significant wave breaking and the expressions are no longer valid. This limit of validity applies to all the formula derived.

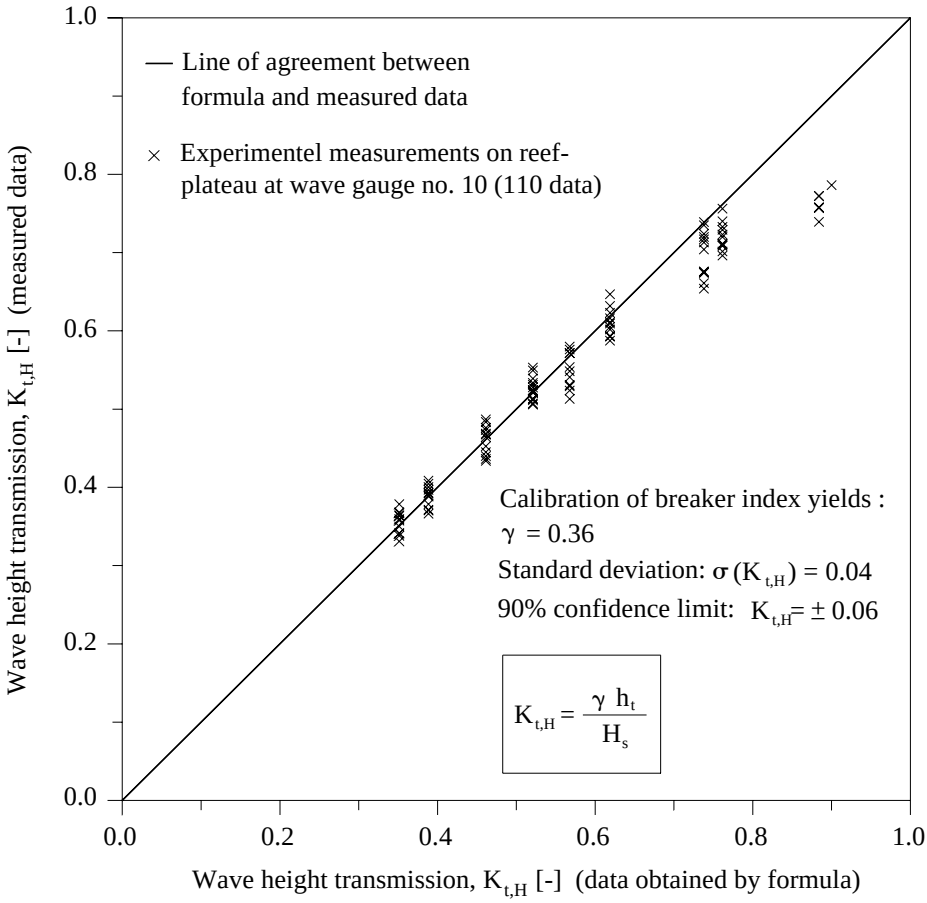

Figure 38: *Comparison between measured values of the reformed transmitted wave height coefficient and corresponding values estimated by Eq.(88).*

10.4 Transmission of significant wave height along the reef-plateau

Assuming that the loss of wave energy flux and wave energy density is closely correlated, the same expression as Eq.(88) is used to represent the contribution to transmitted wave energy flux. The formula for predicting the transmission coefficient along the reef-plateau becomes

$$K_{t,H} = \sqrt{\left(\frac{\gamma\, h_t}{H_s}\right)^2 + \tanh\left(\kappa\left[\frac{X}{L_t}\right]^{-\zeta}\right)} \qquad (89)$$

The breaker index is maintained as γ = 0.36. A calibration of Eq.(89) based on the experimental obtained data yields the coefficients κ = 0.06 and ζ =1.5. That is, the same coefficients describing the contribution to the transmitted wave energy density are found when comparing with the formula describing transmitted wave energy flux along the reef-plateau. The standard deviation of the wave transmission coefficient is 0.06 and a 90% confidence interval estimate yielding $K_{t,H} = \pm 0.09$. Figure 39 shows the correlation between the formula given by Eq.(89) and measured wave height transmission coefficients at wave gauges No. 7, 8, 9 and 10.

The confidence limits regarding all above mentioned formulae are found on basis of the distribution curves of the error between measured values and values predicted by the respective formulae, see Appendix F.

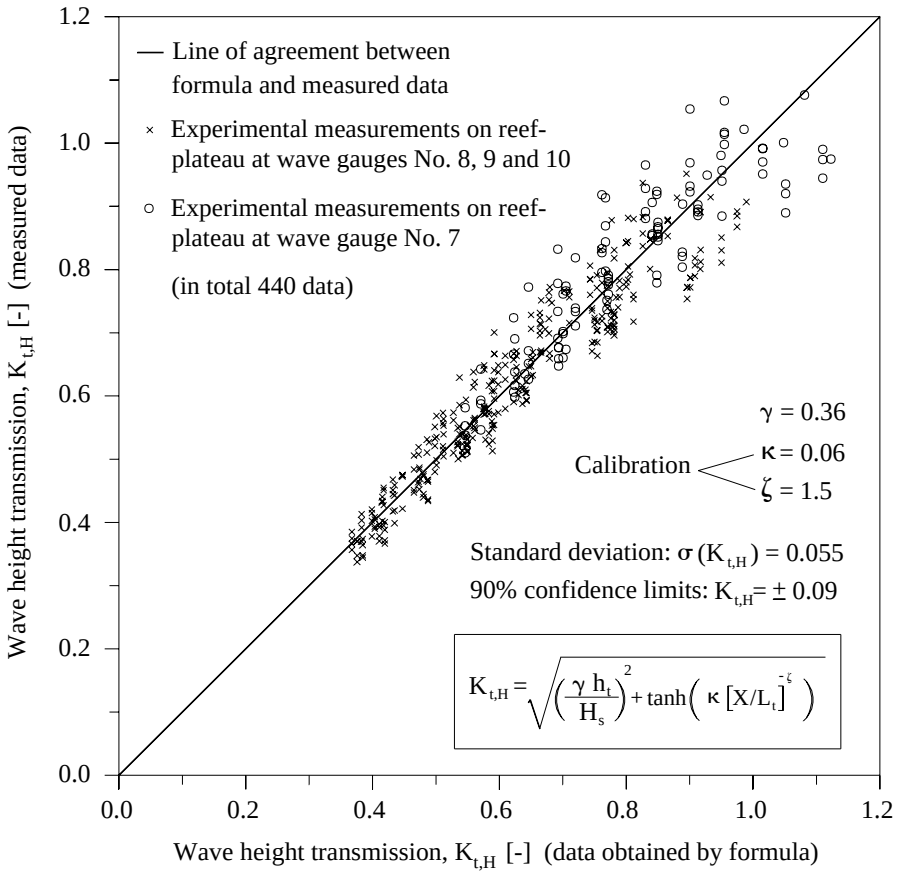

Figure 39: *Comparison between measured values of the wave height transmission coefficient along the reef-plateau and corresponding values obtained from Eq.(89).*

CHAPTER 11 VERIFICATION OF THE WAVE BREAKING MODEL

The wave model based on the extended Mild-Slope formulation has so far been verified regarding propagation of irregular waves over steep slopes. The periodic bore model is chosen to simulate the process of waves breaking and the related loss of wave energy. In the following the wave model developed is further verified based on the knowledge and results obtained from the experimental wave flume tests with special emphasis on the unknown parameter α_0, which governs the intensity of loss of energy and the resulting wave height attenuation. The aim is to show that the model can reproduce the loss of wave energy for waves propagating over a steep reef and breaking on a shallow reef-plateau. By use of the experimental data α_0 is calibrated and thereby establishing a wave-breaking model to be used without any prior estimation of α_0 based on experimental tests.

So far, it is indicated that the steepness of the reef does not significantly influence the wave breaking process on the reef plateau for very steep slopes, i.e. reefs with a slope steeper than approximately 1:2. The waves do not break on the slope but immediately after. In the following the wave model is tested by generating irregular waves propagating over a milder slope. This set-up has been tested in the laboratory by other researchers and experimental data are available. The model shows good agreement choosing α_0 in the range of 1.0-1.5. For steeper slopes the model is calibrated with respect to α_0, based on the experimental data obtained in this study. It is found that some modification to the approach proposed by Battjes and Janssen [1978] yields good results and establishes a method for simulation of waves breaking over steep slopes. Furthermore, it is shown that the parameter α_0 can be more accurately estimated based on the knowledge of the incident wave parameters and the water depth on the shallow reef. For this purpose the non-linearity parameter F_{c0} is used as an important parameter in the estimation of the parameter α_0.

11.1 Numerical simulation of waves breaking over a mild slope

The wave model is tested for a set-up where the steepness is mild compared to the slopes used in the experimental tests as described in Section 8.1. The model set-up and resulting experimental data used in the following are obtained from Thorkilsen et al. [1991]. Thorkilsen et al. performed wave flume tests with irregular waves propagating a bar. The bar consisted of a fore-slope of 1:20 followed by a milder slope of 1:33. The off-bar water depth was 0.55 m with a water depth of 0.10 m at the bar-plateau. The generated waves are described by a JONSWAP spectrum with random phase assignment and a peak enhancement factor of γ_p = 3.3. One test is chosen for comparison with the present wave-breaking model. The incident significant wave height is H_s = 0.14 m with a peak period of T_p = 1.8 sec.

The wave breaking model by Battjes and Janssen [1978] is applied as described in Section 5.5. The maximum allowed wave height used to establish the probability of wave breaking, Q_b, is 0.8 times the local water depth as recommended for shallow water conditions by Battjes and Janssen [1978]. On the flat plateau of the bar the water depth is 0.10 m, which yields a maximum wave height of 0.08 m. Along the slopes the maximum allowed wave height is higher because of greater water depth compared to the reef-plateau. The root-mean-square wave height, which is continuously estimated in the wave model and used to estimate Q_b, is estimated on basis of a length of the wave train of 100 wave periods after the peak period T_p. In other words, the root-mean square wave height is always estimated on basis of the preceding 100 wave periods. It is noted that the results are not especially sensible to this length, but a length of more than 50 waves is found to give good results. Furthermore, this "window" should not be too long in order to make the model capable of reflecting changes, especially if the incidentally generated waves for a period change. As described in Section 7.3.2 the generated incident wave spectrum is subject to a cut-off regarding the frequencies far from the chosen wave carrier period. The wave carrier period is chosen similar to the wave peak period, with a minimum cut-off frequency of 0.74 times the peak frequency and a maximum cut-off frequency of 1.74 times the peak frequency. The reduction of the spectrum yields also a reduction of the generated energy in the wave model. In order to compensate for this reduction, the spectrum generated is H_s = 0.146 m, which corresponds to an incident wave height of H_{m0} = 0.140 m.

As described in Section 5.2 the wave model is based on an extended refraction-diffraction equation and takes into account the rapidly varying topography and steep slopes as introduced by Massel [1993; 1996a]. It shall be noted that this extension to the model has no influence on the results compared to neglecting these contributions. This is because the bar is mildly sloping and the refraction coefficient is relatively small.

The width of one element in the numerical model is Δx = 0.1 m and the time step is Δt = 0.01 sec. This yields a maximum Courant number of C_r = 0.19 based on the minimum cut-off frequency at the off-bar water depth in front of the slope. The spatial resolution is on average approximately 30 elements regarding the wavelengths experienced on the bar-plateau, but can be as low as 10 elements based on the maximum cut-off frequency and the water depth at the shallow bar-plateau. Tests have also been made with the double spacing using Δx = 0.2 m and Δt = 0.02 sec. The results using different spacing in the model are comparable within a few percentages of the measured wave heights, which ensures that resolution errors do not influence the evaluation of the test. In Section 7.2.2 the spacing requirement suggested, based on a test with regular waves propagating a plane slope, is between 30 and 50 elements per minimum wavelength. The effect of occasionally having a less spatial discretisation than 30 elements as in the present test has only a minor influence on the results.

The experimental set-up by Thorkilsen et al. [1991] is shown in Figure 40 along with the experimental results and the numerical results obtained with the present wave model. Thorkilsen et al. presented wave heights calculated on basis of the root-mean-square wave height. The presented wave heights are transformed to significant wave heights assuming that the wave heights are Rayleigh-distributed. The referenced numerical values are likewise given as the significant wave height based on the root-mean-square estimate.

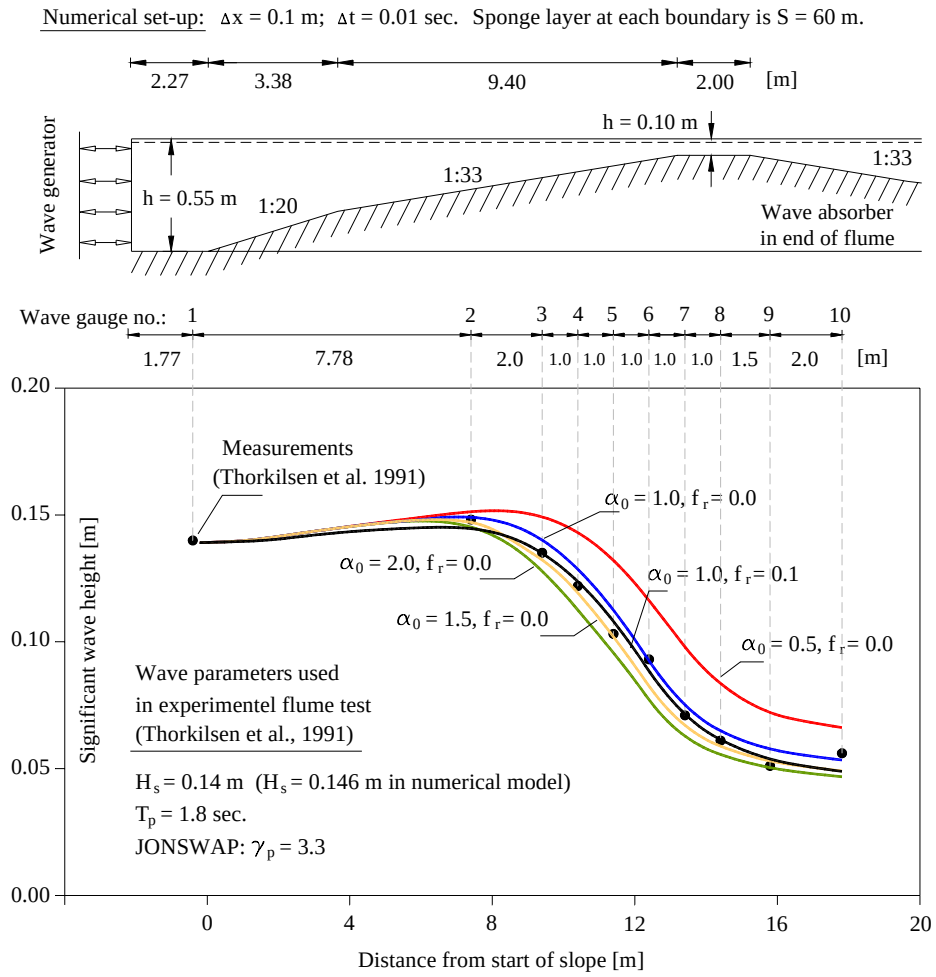

Figure 40: *Description of layout and results obtained in a small wave flume set-up used in experimental tests performed by Thorkilsen et al. [1991].*

By use of the numerical model the significant wave height is calculated along the slope for α_0 in the range 0.5-2.0. Furthermore, wave energy dissipation due to bed

friction is introduced in one test. The wave energy dissipation due to bed friction is introduced as described in Section 7.3.4. In the model the contribution to energy dissipation from bed friction is initiated at the fore-slope of the bar in order to maintain a significant wave height of 0.14 m at wave gauge No. 1. It is noted that the location and numbering of the wave gauges has no relation to the wave gauges referred to frequently in the present test and used for the experimental tests performed during this thesis.

It is seen from Figure 40 that correlation between the numerical results and the experimental data compares well when α_0 is chosen in the range 1.0-1.5. The rate of dissipation of the wave energy reflected in attenuation of the significant wave height does not follow the linear ratio of α_0 because the dissipation depends also on the probability of wave breaking, Q_b. By introducing the bed friction in combination with $\alpha_0 = 1.0$, the numerical results come even closer to the experimental data. It shall be noted that applying a wave energy friction factor with the value $f_r = 0.1$ is done without any knowledge of the experimental conditions and possible scaling errors compared to the value proposed by Nelson [1996]. It is expected that wave energy dissipation due to bed friction is of minor influence in these experimental tests. It is concluded that the wave-breaking model can predict the wave energy dissipation for irregular waves breaking over a mild slope well. The value of α_0 is in the order of 1 for waves breaking at mild slopes.

11.2 Numerical simulation of experimental test results

The objective in the following is to evaluate the dissipation coefficient α_0 for waves breaking over steep slopes. The tests performed in the experimental tests are used to calibrate the dissipation coefficient.

The numerical layout of the wave model in order to simulate the wave flume tests is shown in Figure 41.

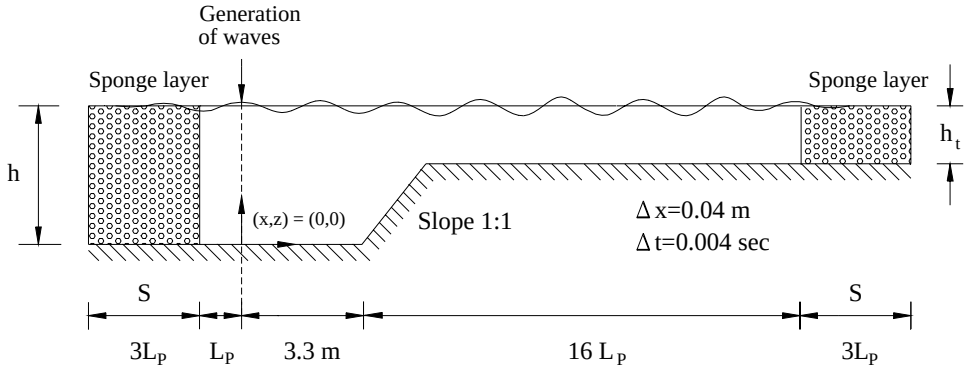

Figure 41: *Layout of the numerical model.*

Based on the knowledge obtained from former numerical test cases the resolution of the model is $\Delta x = 0.04$ m and the time step is $\Delta t = 0.004$ sec. The slope is 1:1. The number of waves generated will be equivalent to 650. The width of the seaward sponge layer is $3 \times L_p$, where L_p is based on the seaward incident peak period. In the down-wave direction the width of the sponge layer is likewise $3 \times L_p$. Waves are generated at a distance of L_p away from the absorbing seaward sponge layer. To provide enough length on the reef-plateau for the waves to reform a length of $16 \times L_p$ is provided in the model. It is observed in Figure 24 that the waves are reformed already at wave gauge No. 10. The distance between the generation line and start of the slope is 3.3 m equivalent to the distance used in the laboratory. The wave energy density is measured equivalent to the locations of the wave gauges No. 7, 8, 9 and 10.

Based on the performed experimental tests the dissipation term α_0 is evaluated in the following. The aim is to find a relation between α_0 and the characteristic wave parameters and the water depth on the reef-plateau. It is already verified that the steepness of the slope, within the range examined, has minor influence on the wave breaking process when compared with the influence from the water depth, wave height and the period, respectively. In the following the parameter α_0 will be calibrated only to the reformed wave height measured at wave gauge No. 10, where the waves are reformed. Hereafter, it is verified that the numerical derived wave

heights at the wave gauges No. 7, 8 and 9 comply with the experimental tests. It is later shown that the calculated wave height along the reef-plateau comply well with the experimental results.

In the tests performed in the laboratory the dissipation on the reef-plateau due to bottom friction is believed to be of significantly less influence to the total wave energy dissipation compared with the actual wave breaking. It is not possible to extract the exact ratio of contribution to the dissipation regarding the experimental tests with breaking waves. Without presenting results, it is indicated that regarding regular waves, which did not break, reformed at approximately the predicted wave height with the same period as the incident period. An exact estimate of the ratio of energy dissipation due to bottom friction is difficult to give because of the uncertainty of the small amount of reflection from the gravel slope on the reef-plateau. For waves not breaking, it is estimated that the dissipation did not exceed even one percentages of the total incident energy flux. In the numerical model it is chosen to simulate the bottom friction with a friction dissipation coefficient of $f_r = 0.01$, which is shown in Section 7.3.4 to yield a minor contribution to the total wave dissipation. To summarise, the energy dissipation due to bottom friction is included but has insignificant influence on the calibration of α_0. The dissipation due to bottom friction is included along the entire region while the dissipation due to wave breaking is only included from the steep slope and along the reef-plateau. It is noted that no waves experienced breaking before passing the reef-edge.

The breaking process is described using a modification of the Battjes and Janssen [1978] periodic bore model. Estimation of the root-mean-square wave height, H_{rms}, is most important, because it is indirectly controlling the rate of wave breaking. It has been chosen to estimate the root-mean-square wave height on basis of the preceding 100 waves obtained in the wave model, which in Section 11.1 yielded realistic results compared to field measurements of the wave energy dissipation along a coral reef.

Battjes and Janssen [1978] used a maximum non-dimensional wave height of $H_{max}/h_t = 0.80$ corresponding to waves breaking in shallow waters of constant depth. The maximum non-dimensional wave height measured at the reef-plateau during the experimental tests varies between 0.4 and 0.6 depending on the non-linearity parameter, F_{c0}, see also Section 9.2.2. These values were measured at a location where the waves were reformed.

Figure 42 shows the results of a calibration applied to a test with significant wave breaking. The incident significant wave height is $H_s = 0.21$ m and the water depth on the reef-plateau is $h_t = 0.205$ m, which yields the highest value of $F_{c0} = 914$ among all the irregular tests performed in the laboratory. The results are obtained as the transmitted wave heights and are compared with the actual measured wave heights along the reef-plateau and furthermore the wave height estimated by the formulae obtained for transmitted wave energy density, i.e. Eq.(89). As already mentioned, the

calibration of the numerical model is performed in such a way that the wave height obtained from the numerical wave model at wave gauge No. 10 is similar to the actually measured wave height. Two lines are given as results obtained with the numerical model. One dashed line (both dashed lines indicate numerical results) is reflecting the results strictly following the approach described in Section 5.5 on how to include wave breaking by introduction of the fraction of breaking waves, Q_b, as

$$W_f = \frac{\varepsilon_b}{E} = \frac{\alpha_0 \, \overline{\omega}}{\pi h} \left(\frac{H_{\max}^3}{H_{rms}^2} \right) \left(\frac{\sqrt{gh}}{\overline{C}} \right) Q_b \tag{90}$$

This graph is denoted in Figure 42 by the approach proposed by Battjes and Janssen [1978], except that the maximum allowable ratio of maximum wave height over water depth at the reef-plateau is taken as 0.5 instead of 0.8, this applies in all the numerical tests. The maximum wave height can be evaluated as the average ratio, $H_{max}/h_t = 0.5$, from the top graph in Figure 30. It is noted that several approaches were tested in choosing the ratio of the maximum allowable wave height over the water depth. The use of Eq.(79) yielded results which did not comply well to the relation between F_{c0} and α_0 compared with using $H_{max}/h_t = 0.5$.

An additional graph in Figure 42 reflects a modified approach taking into account the results obtained in this thesis. The approach evaluates Eq.(90) differently if the actual root-mean-square wave height, which is continuously updated in the numerical wave model, gets unreasonably large compared to the maximum wave height measured in the respective tests. The knowledge obtained in Section 9.2.2 that the ratio between H_{rms} and H_{max} is approximately 0.55, is used, i.e.

$$\begin{aligned} & H_{rms} \le 0.55 \, H_{\max} \Rightarrow W_f = \frac{\alpha_0 \, \overline{\omega}}{\pi h} \left(\frac{H_{\max}^3}{H_{rms}^2} \right) \left(\frac{\sqrt{gh}}{\overline{C}} \right) Q_b \\ & \textit{else} \\ & H_{rms} > 0.55 \, H_{\max} \Rightarrow W_f = \frac{\alpha_0 \, \overline{\omega}}{\pi h} \left(H_{rms} \right) \left(\frac{\sqrt{gh}}{\overline{C}} \right) \quad \{ Q_b = 1.0 \} \end{aligned} \tag{91}$$

The effect of this modification is seen in the following test.

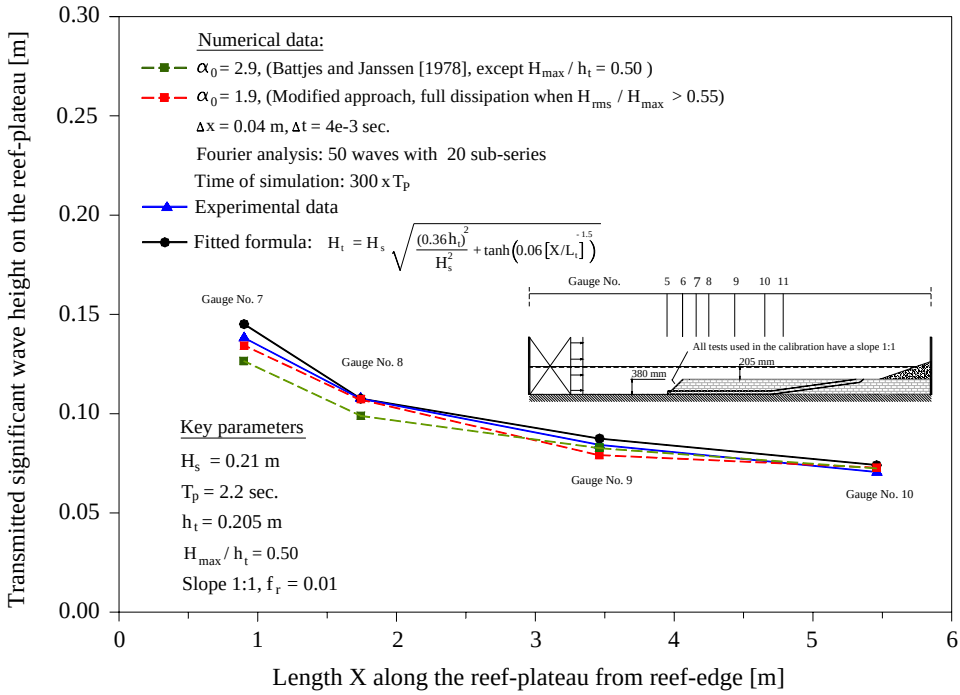

Figure 42: *Transmitted significant wave height along the reef.*

It is seen that during significant wave breaking, Eq.(90), denoted Battjes and Janssen [1998] in Figure 42, does not predict the transmitted wave height as well as the slightly modified approach during the early wave breaking process, i.e. at the two first wave gauges. Furthermore, the α_0 parameter has to be as high as 2.9 compared with a value of α_0 = 1.9 in the case of the modified approach.

At the two first gauges the root-mean-square is measured higher than 0.55 H_{max}, and yields more dissipation according to Eq.(90), where the modified approach dictates that full wave breaking should be applied because the root-mean-square wave height exceeds a ratio of 0.55 H_{max}. Both approaches seem to compare well with the experimental data before wave dissipation is ended, which is mainly due to the calibration of the α_0-values. At the two last wave gauges the modified approach still apply maximum wave breaking (Q_b = 1.0) because the root mean square wave height is close to 0.55 H_{max} which is the reason why α_0 = 1.9 instead of α_0 = 2.9 in the not modified approach.

Without presenting results it was experienced that in the early stage of wave breaking the root-mean-square wave height can exceed H_{max} in the wave model. In such case the term $H_{\max}^3 / H_{rms}^2$ in Eq.(90) becomes unreasonably small. This is another reason to

apply the modified approach and is especially associated with the fact that when the slope is very steep it is not always possible to dissipate sufficient wave energy using the bore model as proposed by Battjes at al.

It can be concluded that if the root-mean-square wave height controls the rate of wave breaking, when the ratio of the root-mean-square wave height and the maximum wave height exceeds 0.55, the predictions improve in the case of high values of F_{c0} associated with waves breaking over a steep bottom slope. It should also be noted that the predicted transmitted wave heights obtained from the formulae given in Eq.(89) compare well with the experimental data.

11.2.1 Formula to predict the coefficient α_0

In order to obtain a relation between the coefficient α_0 and the wave parameters characterising the incident wave climate it is chosen to use the relation suggested by Massel and Gourlay [2000], and described briefly in Section 5.5.1. It is later shown that inclusion of the non-dimensional significant wave height in a new proposed formula as H_s / h_t improves the correlation to the experimental data.

It is already shown that α_0 does not depend significantly on the steepness of the reef-slope and the following basic relationship is assumed to be in the form

$$\begin{aligned} &\alpha_0 = 0 \;\; if\, F_{c0} \le F_{c0}^{(\lim)} \\ &\alpha_0 = a\left(F_{c0} - F_{c0}^{(\lim)}\right)^b \;\; if\; F_{c0} > F_{c0}^{(\lim)} \end{aligned} \tag{92}$$

where a and b are fitted parameters and $F_{c0}^{(\lim)}$ is the threshold value of the parameter F_{c0}, where the observed or calculated value of energy dissipation is negligibly small [Massel and Gourlay, 2000]. Massel and Gourlay obtained values of α_0 in the order of $0(1)$ and found a threshold value, $F_{c0}^{(\lim)}$, approximately equal to 100. Typical values of the fitted parameters were found as a = 0.025 and b = 0.52.

The fitted parameters a and b are not expected to be comparable with the ones obtained in this study, mainly due to the modified approach applied.

Each test performed with a slope steepness of 1:1 is simulated in the numerical model. The parameter α_0 is used as the calibration parameter in order to obtain comparable results between the experimental data and the numerical results.

In the top graph in Figure 43 the calibrated values of α_0 are shown depicted against Eq.(92), where a calibration of the parameters a, b and $F_{c0}^{(\lim)}$ have been performed. It is seen that Eq.(92) is not capable of predicting the parameter α_0 calculated based on

the modified approach for irregular waves breaking on a reef-plateau with a steep bottom slope. A best calibration of Eq.(92) is estimated as

$$\alpha_0 = 0.025\left(F_{c0} - 100\right)^{0.72} \tag{93}$$

where the threshold value $F_{c0}^{(\lim)} = 100$ and $a = 0.025$ are similar to the values found by Massel and Gourlay [2000]. The fitted parameter b=0.72 is found to be somewhat higher.

In the bottom graph in Figure 43 the calibrated values of α_0 are shown depicted against Eq.(94), where a calibration have been performed to a new proposed formula.

$$\alpha_0 = \frac{F_{c0}^{A}}{B}\frac{h_t}{H_s} \Rightarrow (\textit{fitted values inserted}) \quad \alpha_0 = \frac{F_{c0}^{0.77}}{100}\frac{h_t}{H_s} \tag{94}$$

The non-dimensional significant wave height is included as $\left(H_s/h_t\right)^{-1}$ and the threshold value $F_{c0}^{(\lim)}$ is not included. The parameters A = 0.07 and B = 100 are obtained by a best fit between the formula and the numerically obtained and calibrated values of α_0. It shall be noted that the formula is only valid within the range of tests performed, i.e. for F_{c0} higher than 100, which is recognised as a threshold value irregular waves breaking. Furthermore, F_{c0} shall be less than 1000, which is the limit of the capacity of the wave model.

To summarise, the numerical model is able to predict the transmitted wave height for irregular waves breaking over a steep reef with satisfactory accuracy. The wave height can be predicted along the reef during the breaking process. Utilising Eq. (94), to estimate the parameter α_0, numerical simulations can predict the transmitted wave height without any use of experimental tests in order to calibrate α_0.

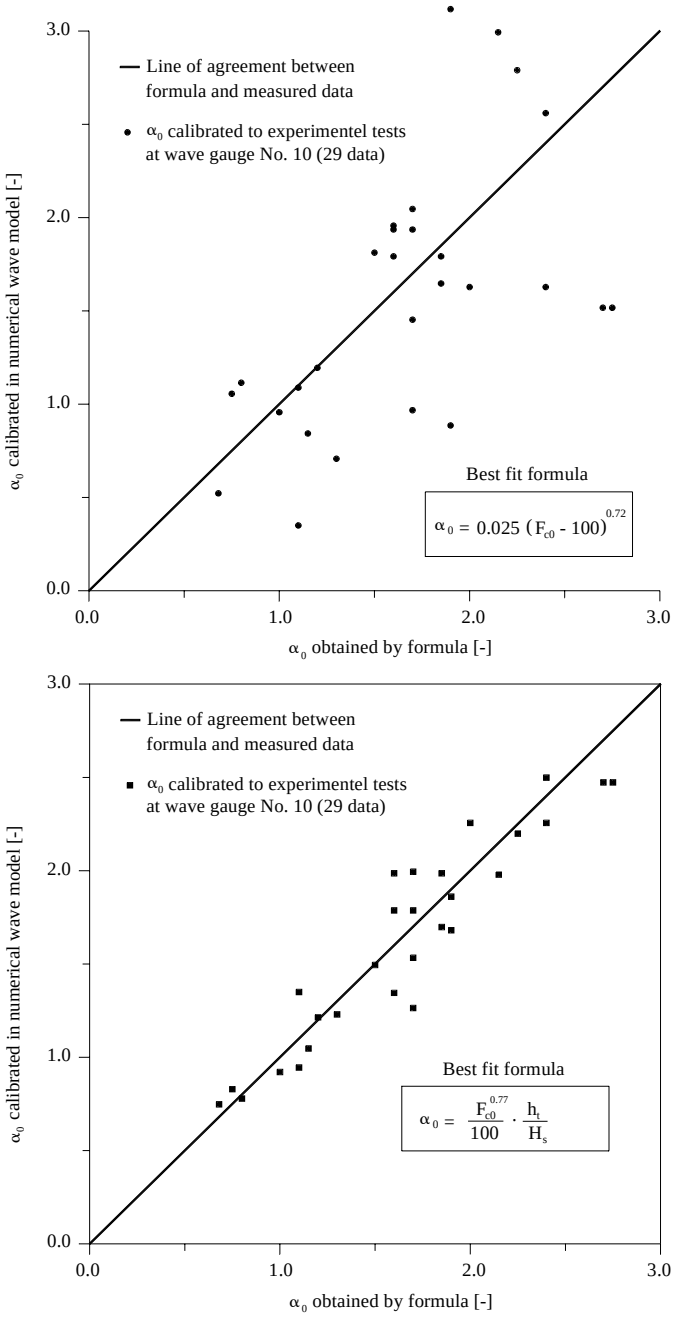

Figure 43: *Comparison between calculated and measured values of α_0 calibrated against two different formulae.*

CHAPTER 12 CONCLUSIONS

The objective of this thesis is to develop tools to predict the transmission of wave energy of breaking, irregular waves propagating over a steep submerged bottom slope. The developed tools are several formulae and a simple numerical wave model. Both approaches are calibrated against the results from the experimental tests and have been shown to provide realistic results.

A review of the research regarding waves breaking over steep slopes has been performed and existing breaking formulae are presented. The parameters expected to have an influence on the wave transformation regarding waves breaking over steep bottom slopes are the wave parameters being the spectral incident significant wave height and the peak period. Furthermore, the water depth on the reef-plateau and the steepness of the reef-slope are referenced parameters.

A number of 301 tests with regular waves and 110 with irregular waves have been performed at the hydraulic laboratories at Aalborg University in order to measure the wave energy dissipation of breaking waves propagating over a steep bottom slope. At 14 locations along the flume the waves were measured yielding information of the wave energy dissipation. The wave parameters, slope steepness and the water depth were varied.

Regarding important results obtained in the experimental tests it is summarised that the maximum non-dimensional wave height, H_{max}/h_t, within the range of irregular waves generated varies between 0.4-0.6. An average value of 0.5 seems to cover a large range of wave parameters. The ratio of H_{rms}/H_{max} is approximately 0.55. The ratio between the significant wave height and the maximum wave height based on the distribution of waves is on average 1.37. The ratio between the significant wave height based on the energy spectrum and the significant wave height based on the wave height distribution varies between 1.0 and 0.85.

Based on tests with irregular waves the transmitted wave energy depends on the seaward incident wave height, the peak wave period and the water depth on the reef-plateau. Compared to these parameters, the transmitted values of wave energy flux and wave energy density depend only slightly on the steepness of the slope within the range of slopes tested, i.e. 1:2 – 1:0.5.

Non-dimensional formulae are provided using a theoretical approach and calibrated to experimental data. One set of formulae predicts the transmission of wave energy flux. The second set of formulae predicts the transmission of wave heights, which is directly related to the energy density.

A simple numerical model simulating the wave energy dissipation of irregular waves propagating over a rapidly varying seabed is developed. The model is verified in

several cases when compared to the theoretical solution. The propagation of waves in the model is based on the extended refraction and diffraction equation provided by Massel [1993] and takes into account the higher-order bottom terms. The extended refraction and diffraction equation is an extension of the classical Mild-Slope equation. The classical Mild-Slope equation is limited to milder slopes than applied in this study. A modified formulation by Radder and Dingemans is used and verified. The second order bottom terms provided by Massel [1993] are added yielding a coupled equation suitable to be solved using a numerical approach. A numerical solver of the equations is based on the Adams-Bashforth-Moulton scheme, which is a predictor-corrector method.

Two wave energy dissipation processes are simulated, one being the wave energy dissipation due to breaking of waves, which is the main source of energy dissipation, and the other the wave energy dissipation due to bottom friction. The periodic bore model approach for description of the energy dissipated during wave breaking is selected and implemented in the numerical model. A commonly referenced and acknowledged expression for the energy dissipation due to bottom friction is implemented.

Results to be noted and obtained in several test examples are the importance of the higher-order bottom terms. A test regarding the reflection of waves from a plane slope improves the solution significantly. This is also the case for even milder slopes than 1:3, which is a commonly referenced limit for the application of the classical Mild-Slope equation. The numerical model developed is also capable of generating two-dimensional monochromatic waves and other researchers have demonstrated the possibility of generating directional waves. This knowledge yields a basis for the possibility of developing a model capable of generating irregular, dissipating, directional waves propagating over a rapidly varying bottom. The present model deals only with one-dimensional irregular, dissipating propagating waves. Waves are generated internally in the numerical model with sponge layers placed at the outside boundaries for absorption of the reflected wave energy. The numerical scheme is tested for errors regarding the time step and the step in space. The experimental tests are used to calibrate the numerical wave energy dissipation model via the parameter α_0, which controls the intensity of the energy dissipation due to wave breaking. A similar approach as proposed by Massel and Gourlay [2000] is used with some modifications. The parameter, α_0 shows a correlation to a Swart and Loubster type parameter or the so-called non-linearity parameter. Development of a formula is based on formula suggested by Massel and Gourlay [2000], but with some modifications as including the non-dimensional significant wave height. The formula providing α_0 is presented based on a calibration of experimental data. To summarise, the numerical model developed is able to predict the experimental data very well and energy dissipation due to wave breaking can be introduced in the numerical model as

$$W_f = \frac{\alpha_0 \, \overline{\omega}}{\pi \, h} \left(\frac{H_{\max}^3}{H_{rms}^2} \right) \left(\frac{\sqrt{gh}}{\overline{C}} \right) Q_b \tag{95}$$

where the parameter α_0 can be estimated based on the non-linearity parameter F_{c0} as

$$\alpha_0 = \frac{F_{c0}^{0.77}}{100} \frac{h_t}{H_s} \tag{96}$$

The wave model is only verified in the range of F_{c0} = [100-1000]. F_{c0} = 100 is the threshold of waves breaking and F_{c0} = 1000 is the limit of the wave model, where the extended refraction-diffraction model provides realistic results.

The periodic bore model approach for description of the energy dissipated, Eq.(95), is modified compared to the original proposed model by Battjes and Janssen [1978]. The maximum wave height is determined as H_{max}/h_t = 0.5 instead of a ratio being 0.8. Furthermore, when the ratio between the root-mean-square wave height obtained in the numerical model and the maximum wave height exceeds 0.55, i.e. when H_{rms}/H_{max} > 0.55, then the fraction of waves breaking, Q_b, is set to 1.0 and $H_{\max}^3 / H_{rms}^2$ is set to H_{rms}.

Beside the numerical wave model, formula have been developed based on a theoretical approach and calibrated to the experimental tests. These are summarised in the following.

(In Appendix H similar formulae are provided based on expressions having a more physical meaning. Appendix H is written after the Ph.D. thesis was presented and the Ph.D. degree awarded in February 2003.)

Transmission of wave energy flux along reef-plateau:

$$K_{t,P} = \sqrt{\frac{4\pi\gamma^2 h_t^2 C_{g,t}}{H_s^2 g T_P} + \tanh\left(0.06\left[\frac{X}{L_t}\right]^{-1.5}\right)}\ ,\ \gamma = 0.33.$$

Standard deviation is $\sigma(K_{t,P}) = 0.04$. The 90% confidence level is $K_{t,P} = \pm 0.07$. Limit is $X/L_t > 0.22$ and $H_s/h_t > 0.4$

Transmission of wave energy flux on reef-plateau – after reformation of waves:

$$K_{t,P} = \sqrt{\frac{4\pi\gamma^2 h_t^2 C_{g,t}}{H_s^2 g T_P}}\ ,\quad \gamma = 0.33$$

Standard deviation is $\sigma(K_{t,P}) = 0.025$. The 90% confidence level is $K_{t,P} = \pm 0.04$. Limit is $H_s/h_t > 0.4$

Wave height transmission along reef-plateau:

$$K_{t,H} = \sqrt{\left(\frac{\gamma h_t}{H_s}\right)^2 + \tanh\left(0.06\left[\frac{X}{L_t}\right]^{-1.5}\right)}\ ,\ \gamma = 0.36.$$

Standard deviation is $\sigma(K_{t,H}) = 0.055$. The 90% confidence level is $K_{t,H} = \pm 0.09$. Limit is $X/L_t > 0.22$ and $H_s/h_t > 0.4$

Wave height transmission on reef-plateau – after reformation of waves:

$$K_{t,H} = \frac{\gamma h_t}{H_s},\quad \gamma = 0.36$$

Standard deviation is $\sigma(K_{t,H}) = 0.04$. The 90% confidence level is $K_{t,H} = \pm 0.06$. Limit is $H_s/h_t > 0.4$

REFERENCES

Ahrens J.P., (1987)
Characteristics of reef breakwaters. Tech. Rep CERC-87-17 US Army Corp. Eng. p. 45.

Article 1, (1999)
Beach Erosion Facts. Halama Association Research Findings.

Athanassoulis, G.A and Belibassakis, K.A (1999)
A Consistent Coupled-Mode Theory for the propagation of small-amplitude water waves over variable bathymetry regions. Journal Fluid Mech. vol. 389, pp. 275-301, 1999.

Battjes, J.A. and Janssen, J.P.F.M., (1978)
Energy loss and set-up due to breaking of irregular waves. Proc. 16th Coastal Eng. Conf., Hamburg, 1: pp. 563-587.

Berkhoff, J.C.W., (1972)
Computation of combined refraction-diffraction. Proc. 13th International Conference Coastal Eng. Vancouver.

Booij N., (1983)
A note on the accuracy of the Mild-Slope equation. Coastal Engineering 1983; 7: pp. 191-203.

Bowen, A.J., Inman, D.L and Simmons, V.P., (1968)
Wave set-down and set-up. J. Geophys. Res., 73: pp. 2569-2577.

Brorsen, M., Helm-Petersen, J., (1998)
On the reflection of short-crested waves in numerical models. Proc. 26th Coastal Eng. Conf., Copenhagen 1998. pp. 394 - 407.

Copeland, G.J.M., (1985)
A practical alternative to the Mild-Slope wave equation. Coastal Eng. 9, pp. 125-149.

Dally, W.R. Dean, R.G. and Dalrymple, R.A., (1985)
Wave height variation across beaches of arbitrary profile. Jour. Geoph. Res., 90: pp. 10,917-11,927

Danel, P., (1952)
On the limiting clapotis, Gravity waves, US Department of Commerce, National Bureau of Standards, Circular 521, pp. 35-45.

Dingemans, M.W., (1997)
Water Wave Propagation Over Uneven Bottoms. World Scientific Publishing Company, Incorporated.

Frigaard P., Christensen M., (1994)
An absorbing wave-maker based on digital filters. Proceedings 24th ICCE. Kobe, Japan. Vol. 1, pp. 168-180.

Galvin, C. J., (1969)
Breaker travel and choice of design wave height, J. Waterways Harbour Div., ASCE 9, WW2, pp. 175-200.

Gerritsen F., (1981)
Wave attenuation and wave set-up on a coastal reef. Univ. Hawaii. Look Lab. Tech. Rep. No. 48, p. 416.

Goda, Y., (1964)
Wave forces on a vertical circular cylinder: Experiments and a proposed method of wave force computation, Report of the Port and Harbour Research Institute. Ministry of Transportation, No. 8, p. 74.

Goda, Y., (1970)
A synthesis of breaker indices, Trans. JSCE 2: pp. 227-230.

Goda, Y., (1974)
New wave pressure formula for composite breakwater. Proc. 14th Coastal Eng. Conf., ASCE, pp. 1702-1720.

Gourlay, M.R., (1994)
Wave transformation on a coral reef. Coastal Eng., 23: pp. 17-42.

Gourlay, M.R., (1996a)
Wave set-up on coral reefs: 1. Set-up and wave-generated flow on an idealised two dimensional horizontal reef. Coastal Eng. 27 (3-4).

Gourlay, M.R., (1996b)
Wave set-up on coral reefs: 2. Set-up on coral reefs with various profiles. Coastal Eng. 28, pp. 17-55.

Hansen, J. B. and Svendsen, I. A., (1979)
Regular waves in shoaling water experimental data, Series Paper No. 21, Institute of Hydrodynamics and Hydraulic Engineering, Technical University of Denmark, p. 243.

Hardy, T., Young, I.R., Nelson, R.C., Gourlay, M.R., (1990)
Wave attenuation on an offshore coral reef. Proc. 22nd Coastal Eng. Conf., Delft, 1990,1, pp. 330-344.

Hardy, T., Young, I.R., Nelson, R.C., Gourlay, M.R., (1996)
Field study of wave attenuation on an offshore coral reef. J. Geophys. Res. 101, pp. 14,311-14,326.

Hattori, M. and Aono, T., (1985)
Experimental study of turbulence structures under breaking waves, Coastal Engineering Japan 28: pp. 97-116.

Hopley, D., (1982)
The Geomorphology of the Great Barrier Reef. Quaternart Development of Coral Reefs. Wiley, New York, p. 453.

Horikawa, K. and Kuo, C.T., (1966)
A study of wave transformation inside the surf zone, Proc. 10th Coastal Engineering Conf., ASCE, pp. 217-233.

Hwung, H.H., Chyan, J. M. and Chung, Y. C., (1992)
Energy dissipation and air bubbles mixing inside surf zone, Proc. 23rd Coastal Engineering Conference., ASCE, pp. 308-321.

IAHR/PIANC: Intern. Ass. for Hydraulic Research/Permanent Intern. Ass. of Navigation Congresses.
List of Sea State parameters. Supplement to Bulletin No. 52, Brussel.

Iversen, H. W., (1952)
Laboratory study of breakers, Gravity Waves, Circular 52, US Bureau of Standards, pp. 9-32.

Iwagaki, Y., Sakai, T., Tsukioka, K. and Sawai, N., (1974)
Relationship between vertical distribution of water particle velocity and type of breakers on beaches, Coastal Eng. Japa, JSCE 17: pp. 51-58.

Jensen, M.S., (2001)
A study of coastal zone problems related to coral-sand beaches in East Africa – with special attention to coastal erosion. A report supported and published by DANIDA (56 pages).

Jonsson, I.G., (1963)
Measurements in the turbulent wave boundary layer. Proc. 10th IAHR Congress, Vol. 1: pp. 85-92.

Jonsson, I.G., (1966)
Wave boundary layers and friction factors. Proc. 10th Coastal Engineering Conference, ASCE, Vol. 1: pp. 127-148.

Kamphuis, J. W., (1975)
Friction factors under oscillatory waves. J. Waterways Harbours & Coastal Engineering. ASCE, 1975, 101: pp. 135-144.

Kamphuis, J. W., (1991)
Incipient wave breaking, Coastal Eng. 15: pp. 185-203.

Kirby, J.T., Lee. C., Rasmussen, C., (1992)
Time-dependent solutions of the Mild-Slope wave equations. In: Proc. 23rd Int. Conf. Coastal Eng., pp.391-404.

Kono, T. Tsukayama S., (1980)
Wave transformation on reef and some consideration on its application to field. Coastal Eng. Japan 23: pp.45-57.

Lamb, H., (1932)
Hydrodynamics. Dover Publ., New York

Larsen. J., Dancy. H., (1983)
Open boundaries in short wave simulations – a new approach. Coastal Eng. 7. pp.285-297.

Lee, C., Suh. K.D., (1998)
Internal generation of waves for time-dependent Mild-Slope equations. Coastal Eng. 34. pp. 35-57.

Lee, C., Park, Woo Sun, Cho, Young-sik, Suh, Kyung Doug, (1998)
Hyperbolic Mild-Slope equations extended to account for rapidly varying topography. Coastal Eng. 34. pp. 243-257.

Lee TT, Black K.P, (1978)
The energy spectra of surf waves on a coral reef. Proc. 16th. Coastal Eng. Conference Hamburg, Germany, pp. 588-608.

Lippmann, T.C., Brookins, A.H., Thornton , E.B., (1996)
Wave energy transformation on natural profiles. Coastal Eng. 27, pp. 1-20.

Longuet-Higgins, M.S., (1952)
On the statistical distribution of heights of sea waves. Journal Mar. Res., 11: pp. 245-266.

Madsen, P.A and Larsen, J., (1987)
An efficient finite-difference approach to the Mild-Slope equation. Coastal engineering, 11. pp. 329-351.

Mansard, E.P.D., Funke, E.R., (1980)
The measurement of incident and reflected spectra using least squares method. In: Proc. 17th Coastal Eng. Conf., Sydney, Vol. 1, pp. 154-172.

Maruyama, K., Sakakiyama, T., Kajima, R., Saito, S. and Shimizu, T. (1983)
Experimental study on wave height and particle velocity near the surf zone using a large flume, Civil Engineers Laboratory Report No. 382034, The Central Research Institute of Electric Power Industry, Chiba, Japan (in Japanese).

Massel, S.R., Belberova, D.Z., (1990)
Parameterization of the dissipation mechanisms in the surface waves induced by wind. Arch. Mech. 42, pp. 515-530.

Massel, S.R., (1993)
Extended refraction-diffraction equation for surface waves. Coastal Eng. 19, pp. 97-126.

Massel, S.R., (1996a)
Ocean surface waves: Their Physics and Prediction. World Scientific.

Massel, S.R., (1996b)
On the largest wave height in water of constant depth. Ocean Eng. 23: pp. 553-573.

Massel, S.R., Brinkman, R.M., (1998)
Measurement and modelling of wave propagation and breaking at steep slopes. Recent Advances in Marine Science and Technology, 98, Honolulu, pp. 27-36.

Massel, S.R., Gourlay M.R., (2000)
On the modelling of wave breaking and set-up on coral reefs. Coastal Engineering, 39 (2000). pp. 1-27.

McCowan, J., (1894)
On the highest waves of permanent type, Philosophical Magazine, Edinburgh 38, Ser. 5, pp. 351-358.

Miche, R., (1944)
Movements ondulatoires des mere en profondeur constante on decroissante, Ann. Des Ponts et Chaussees, Chap . 114, pp. 131-164, 270-292, and 369-406.

Mitsuyasu, H., (1962)
Experimental study on wave force against a wall, Report of the Transportation Technical Research Institute, No. 47, p. 39 (in Japanese).

Mizuguchi, M. (1980)
An heuristic model of wave height distribution in the surf zone, Proc. 17th Coastal Eng. Conf., ASCE, pp. 278-289.

Munk, W., Sargent M.C., (1948)
Adjustment of Bikini Atoll to ocean waves. Trans Am. Geophys. Union 29: pp. 855-860.

Nadaoka, K., Kondoh, T. and Tanaka, N., (1982)
The structure of velocity field within the surf zone revealed by means of a laser-doppler anemometry, Port and Harbour Research Institute 21, 2, pp. 50-102 (in Japanese).

Nagayama, S., (1983)
Study on the change of wave height and energy in the surf zone, Bach. Thesis, Civil Engineering, Yokohama National University, Japan, pp. 24-35.

Nelson, R.C., (1983)
Wave heights in depth limited conditions. Proc. 6th Australian Conference on Coastal and Ocean Engineering.

Nelson, R.C., and Lesleighter, E.J., (1985)
Breaker height attenuation over platform coral reefs. Proc. 7th Australian Conf. on Coastal and Ocean Eng., Christchurch, 1: pp. 9-16

Nelson, R.C., (1994)
Depth limited design wave heights in very flat regions. Coastal Engineering 23, pp: 43-59.

Nelson, R.C., (1996)
Hydraulic roughness of coral reef platforms. Appl. Ocean Res. 18, pp. 265-274.

Oceanspace Issue 165, (1999)

Okayasu, A., Shibaya, T. and Mimura, N., (1986)
Velocity field under plunging waves, Proc. 20th Coastal Engineering. Conf., ASCE, pp. 660-674.

Okayasu, A., Shibaya, T. and Horikawa, K., (1988)
Verification of undertow in the surf zone, Proc.21st Coastal Engineering. Conf., ASCE, pp. 478-491.

Ostendorf, D. W. and Madsen, O. S., (1979)
Analysis of longshore current and associated sediment transport in the surf zone, Report No. 241, Department of Civil Engineering, MIT, p. 169.

Ozaki, A., Sasaki, M. and Usui, Y. , (1977)
Study on rip currents: Experimental observation of nearshore circulation on a sloping bottom, Coastal Eng. Japan, JSCE 20: pp. 147-158.

Radder, A.C., Dingemans, M.W., (1985)
Canonical equations for almost periodic, weakly nonlinear gravity waves. Wave motion 7, pp. 473-485.

Rattanapitikon, W., Shibayama, T., (2000)
Verification and modification of breaker height formulae. Coastal Engineering Journal, Vol. 42, No. 4, pp. 389-406.

Peregrine. D.H., (1967)
Long waves on a beach. J. Fluid Mech. 27, pp. 815-827.

Roberts, H.H, Murray, S.P. and Suhayda, J.N., (1975)
Physical processes in a fringing reef system. J.Mar. Res., 33: pp. 233-258.

Roberts H.H., Murray S.P., Suhayda J.N., (1977)
Physical processes in a fore-reef shelf environment. 3rd Int. Coral Reef Symp. University of Miami, Fla. pp. 507-515.

Roberts H.H., (1980)
Physical processes and sediment flux through reef lagoon systems. Proc. Coastal Eng, pp. 1-17.

Roberts H.H., Suhayda J.N., (1983)
Wave-current interactions on a shallow reef (Nicaragua, Central America). Coral Reefs 1: pp. 209-214.

Porter, D., Staziker, D.J., (1995)
Extensions of the Mild-Slope equation. J. Fluid Mech. 300, pp. 367-384.

Saeki, H. and Sasaki, M., (1973)
A study of the deformation of waves after breaking, Proc. 20th Japanese Conf. Coastal Eng., JSCE, pp. 559-564 (in Japanese).

Sato, S., Fukuhama, M. and Horikawa, Kk., (1988)
Measurements of the near-bottom velocities in random waves on a constant slope, Coastal Eng. Japan, JSCE 31, 2, pp.219-229.

Sato, S., Isayama, T. and Shibayama, T., (1989)
Long-wave component in near bottom velocity under random waves on a gentle slope, Coastal Eng. Japan, JSCE 32, 2, pp. 149-159.
Sato, S., Homma, Kand Shibayama, T., (1990)
Laboratory study on sand suspension due to breaking waves, Coastal Eng. Japan, JSCE 33, 2, pp. 219-231.

Seelig, W.N., (1983)
Laboratory study of reef-lagoon system hydraulics. J.Waterw., Ports, Coastal, Ocean Eng. 109, pp. 380-391.

Shore protection manual, (1984).
4th ed., 2 Vol, U.S. Army Engineer Waterways Experiment Station, U.S. Government Printing Office, Washington, DC.

Singamsetti, S.R. and Wind, H.G., (1980)
Characteristics of breaking and shoaling periodic waves normally incident on to plane beaches of constant slope, Report M1371, Delft Hydraulic Laboratory, Delft, The Netherlands, p. 142.

Smith, J. M. and Kraus, N. C. (1990)
Laboratory study on macro-features of wave breaking over bars and artificial reefs, Technical Report CERC-90-12, WES, US Army Corps of Engineers, p. 232.

Souther, D.W., Lindén O., (2000)
The health and future of coral reef systems. Ocean & Coastal Management 43. pp. 657-688.

Stive, M. J. F., (1984)
Energy dissipation in wave breaking on gentle slopes, Coastal Eng. 8: pp. 99-127.

Stokes, G.G., (1847)
On the theory of oscillatory waves. Trans. Camb. Phil. Soc., 8: pp. 441-455.

Stokes, G.G., (1880)
Considerations relative to the greatest height of oscillatory waves, which can be propagated without change of form. Mathematical and Physical Papers.

Suhayda J.N., Roberts H.H., (1977)
Wave action and sediment transport on fringing reefs. Proc. 3rd Int. Coral Reef Symp, University of Miami, Fla., pp. 65-70.

Suh. K.D., Lee C., Park W.S., (1997)
Time-dependent equations for wave propagation on rapidly varying topography. Coastal Eng. 32. pp. 91-117.

Sulaiman, D.M., Tsutsui, S., Yoshioka, H., Yamashita, T., Oshiro, S. and Tsuchiya, Y., (1994)
Prediction of the maximum wave on the coral reef. Proc. 24th Coastal Eng. Conf., Kobe.

Swart, D.H. and Loubser, C.C., (1978)
Vocoidal theory for full non-breaking waves. Proc. 16th Coastal Eng. Conf., Hamburg, 1978, 1: pp. 467-486.

Tait, R.J. (1972)
Wave set-up on coral reefs. Journal of Geophysical Research. 78, pp. 7834-7844.
Thorkilsen, M., Rosing, N. and Shchaeffer, H.A., (1991)
Experimental investigation of waves breaking over a bar. Extended abstract. In: Proc. of Mid-term Workshop of the MAST G6-M project, Edinburgh.

Thornton, E.B. and Guza, R.T., (1983)
Transformation of wave height distribution. Journal Geoph. Res., pp. 5925-5938.

Ting, C. K. and Kirby, J. T., (1994)
Observation of undertow and turbulence in a laboratory surf zone, Coastal Eng. 24: pp. 51-80.

Walker, J. R., (1974)
Wave transformations over a sloping bottom and over a three-dimensional shoal, Miscellaneous Report No. 11, University of Hawaii, Look Lab-75-11, Honolulu, Hawaii, USA.

Vernon, J.E.N., (1986)
Corals of Australia and the Indo-Pacific. Univ. Hawaii Press, Honolulu, p. 644.

Visser, P. J., (1982)
The proper longshore current in a wave basin, Report No. 82-1, Laboratory of Fluid Mechanics, Department of Civil Engineering, Delft University of Technology, Delft, The Netherlands, p. 86.

Wilkinson C.R., (1993)
Coral reefs of the world are facing widespread devastation. Proceedings of 7th International Coral Reef Symposium, vol. 1, 1993. pp. 11-21.

Young, I.R., (1989)
Wave transformation over coral reefs. J.Geophys. Res. 94, pp. 9779-9789.

APPENDIX A: NOTATION USED IN THE THESIS

SYMBOL	DEFINITION	UNITS
A	Wave height amplitude	m
a	Steepness of bottom slope as 1:a, where a =1/tan(β_s)	-
B	Width of reef-slope	m
b	Ratio used in wave breaking dissipation model = H_{rms}/H_{max}	-
C	Wave celerity, (= L/T)	m/sec
C_g	Group velocity, $C_g = 0.5 \cdot C \cdot \left(1 + \frac{2 \cdot k \cdot h}{\sinh(2 \cdot k \cdot h)}\right)$	m/sec
$\overline{C}$	Wave celerity associated with the wave carrier frequency	m/sec
$\overline{C}_g$	Group velocity associated with the wave carrier frequency	m/sec
$\overline{C}_e$	Energy velocity of waves associated with the wave carrier frequency	m/sec
$C_{g,t}$	Energy velocity of waves associated with the wave carrier frequency on the reef-plateau (not necessarily equal to shallow water conditions)	m/sec
C_r	Courant number after energy velocity, (= $C_e \Delta t / \Delta x$)	m/sec
D	Energy per unit span dissipated in a hydraulic bore	W/sec
d	Distance along the sponge layer in the numerical model	m
D_s	Damping coefficient in numerical model	s^{-1}
E	Total wave energy per unit of the wave front over one wavelength	J
E_i	Incident wave energy	J
E_t	Transmitted wave energy	J
F_c	Swart and Loubser type parameter for classifying wave transformation	-
F_{c0}	Swart and Loubser type parameter (non-linearity parameter) for classifying wave transformation based on off-shore wave parameters	-
$F()$	Notation associated with Adam-Bashforth-Moulton's method	-
f	Wave frequency	Hz
f_{min}	Cut-off frequency for minimum wave frequency in spectrum	Hz
f_{max}	Cut-off frequency for maximum wave frequency in spectrum	Hz
f_p	Frequency corresponding to the peak spectral frequency	Hz
Δf	Frequency band regarding spectral resolution	Hz
f_r	Wave energy dissipation factor	-
$G()$	Notation associated with Adam-Bashforth-Moulton's method	-
g	Gravitational acceleration being 9.81 m/sec^2	m/sec^2
h	Local water depth	m
h_b	Water depth at wave breaking	m
h_t	Still water depth on reef-plateau	m
H	Wave height	m
$\hat{H}$	Modal value used in connection with Battjes et al's wave breaking model	m
H_b	Breaking wave height	m
H_0	Deep-water wave height	m
H_i	Incident wave height	m
$H_{1/3}$	Alternative denotation for significant wave height	m
H_{max}	Maximum wave height in a wave train	m
H_{mean}	Mean wave height in a wave train	m
H_{m0}	Spectral estimate of significant wave height	m
H_s	Significant wave height based on wave height distribution	m

SYMBOL	DEFINITION	UNITS
H_r	Reflected water wave height	m
H_{rms}	Root-mean-square wave height	m
H_t	Transmitted wave height	m
$I_{1\text{-}5}$	Parameters in expression of higher-order bottom effects	-
K_r	Wave height reflection coefficient ($=H_r/H_i$)	-
K_t	Wave height transmission coefficient ($=H_t/H_i$)	-
$K_{t,H}$	Wave height transmission coefficient associated irregular waves	-
$K_{t,P}$	Wave energy flux transmission coefficient associated irregular waves	-
k	Wave number ($=2\pi/L$)	m^{-1}
$\overline{k}$	Wave number associated with the wave carrier frequency	m^{-1}
k_h	The derivative of k relating to h ($=\partial k/\partial h$)	m^{-2}
k_{hh}	$(=\partial^2 k/\partial h^2)$	m^{-3}
L	Wavelength ($=C\cdot T$)	m
L_b	Wavelength of breaking waves	m
L_{max}	Maximum wavelength often associated with highest spectral frequency	m
L_o	Deep water wavelength ($=g\cdot T^2/2\pi$)	m
L_p	Wavelength based on peak wave period	m
L_t	Wavelength on reef-plateau (not necessarily equal shallow water wave length)	m
m_0	The variance of wave elevations (1^{st} order moment in energy spectrum)	m^2
P	Wave energy flux per unit wave front	J/(m sec)
P_i	Incident wave energy flux per unit wave front	J/(m sec)
P_t	Transmitted wave energy flux per unit wave front	J/(m sec)
Q	Vertically integrated function in Copeland's Mild-Slope formulation	m^2/sec^2
Q_b	Fraction of wave breaking	-
R_1, R_2	Parameters determining higher-order bottom effects	-
$S_\eta(f)$	Wave energy density spectrum	m^2sec
S	Thickness of sponge layer in numerical model	m
SWL	Still water level	-
T	Water wave period	sec
T_p	Water wave period corresponding to peak of wave spectrum	sec
t	Time	sec
Δt	Time step in numerical model	sec
U	Amplitude of the bed velocity variations	m/sec
u_b	Instantaneous bed velocity	m/sec
$U_{1\text{-}3}$	Parameters in expression of higher-order bottom effects	-
$W_{1\text{-}6}$	Parameters in expression of higher-order bottom effects	-
W_t	Total damping factor	s^{-1}
W_b	Damping factor due to wave breaking	s^{-1}
W_f	Damping factor due to bottom friction	s^{-1}
x, y	Horizontal spatial co-ordinates in numerical model	m
X	Distance on the reef-plateau from the reef-edge	m
Δx	Grid spacing or distance between two nodes in the numerical model	m
Y_1, Y_2	Depths used to define the periodic bore model	m
z	Vertical coordinate. Measured vertically upwards from still water level	m
α	Coefficient describing the intensity of wave breaking	-

SYMBOL	DEFINITION	UNITS
α_0	Coefficient describing the intensity of wave breaking (= α^3)	-
β_s	Angle of reef-slope or bottom slope	rad
β	Coefficient related to the steepness and the peakness of the crest and flatness of the wave trough	-
ε_t	Total energy dissipation rate per unit area in waves	W/m^2
ε_f	Energy dissipation rate per unit area in waves due to bottom friction	W/m^2
ε_b	Energy dissipation rate per unit area in waves due to wave breaking	W/m^2
γ	Breaker index introduced by Battjes and Janssen in expression for breaker height formula	-
γ_p	Peak enhancement factor in JONSWAP spectrum	-
η^*	Surface elevation to be added to generate waves in numerical model	m
η	Displacement of the free surface relative to still water level	m
φ	Velocity potential at the mean water level	m^2/sec
λ	$(= \omega^2/g)$	sec/m
κ	Parameter fitted to formula	-
ζ	Parameter fitted to formula	-
π	Constant (=3.14159)	-
θ	Angle related to wave direction, normal incident waves (= 0º)	º
ρ_w	Density of water	kg/m^3
σ	Statistical parameter - standard deviation	-
σ_η	Standard deviation of the wave elevation	m
ψ	Constant related to the periodic bore model	-
τ	Instantaneous bed shear stress	$kg/(sec^2 m)$
ω	Angular wave frequency $(= 2\pi / T)$	rad/sec
$\overline{\omega}$	Angular wave frequency associated with the wave carrier frequency	rad/sec
ω_{max}	Maximal angular water wave frequency	rad/sec

APPENDIX B: COMPONENTS OF TERMS R_1 AND R_2

$$W_1 = -2\lambda + 2\frac{k_h}{k} + 2\frac{khk_h}{\lambda} - 4\frac{\lambda\ hk_h}{k} + \frac{hk_{hh}}{k} + \frac{h^2k_h^2}{\lambda} - 2\frac{\lambda\ h^2k_h^2}{k^2}$$

$$W_2 = 2k - 2\frac{k_h}{\lambda} + 2hk_h$$

$$W_3 = 2k_h - \frac{k_{hh}}{\lambda} + 2\frac{hk_h^2}{k}$$

$$W_4 = -2\frac{kk_h}{\lambda}$$

$$W_5 = -\frac{k_h^2}{\lambda}$$

$$W_6 = 1 + \frac{hk_h}{k}$$

$$U_1 = 1 + \frac{hk_h}{k}$$

$$U_2 = -\frac{k}{\lambda}$$

$$U_3 = -\frac{k_h}{\lambda}$$

$$I_1 = \int_{-h}^{0} \cosh^2 k(h+z)\, dz$$

$$I_2 = \int_{-h}^{0} \cosh\, k(h+z) \sinh k(h+z)\, dz$$

$$I_3 = \int_{-h}^{0} (h+z) \cosh\, k(h+z) \sinh\, k(h+z)\, dz$$

$$I_4 = \int_{-h}^{0} (h+z) \cosh^2 k(h+z)\, dz$$

$$I_5 = \int_{-h}^{0} (h+z)^2 \cosh^2 k(h+z)\, dz$$

$$k_h = \frac{\partial k}{\partial h} = -\frac{\lambda\, k}{\lambda\, h + \sinh^2 kh}$$

$$k_{hh} = \frac{\partial^2 k}{\partial h^2} = -\frac{\lambda\, k_h}{\lambda\, h + \sinh^2 kh}\left(2 + \frac{k + hk_h}{\lambda}\sinh 2kh\right)$$

$$\lambda = \frac{\omega^2}{g} = -k \tanh kh$$

APPENDIX C: A MODIFIED COPELAND MODEL

Following, the hyperbolic mild-slope equation formulated by Copeland [1985] is modified to include the higher-order bottom terms. The hyperbolic approach is a practical alternative to the elliptic extended mild-slope equation by Massel [1993].

The modified Copeland formulation is easily implemented numerically and reduces the computing time. This formulation shall only be used when generating regular waves, because the energy transport regarding irregular waves is not treated correctly [Suh, et al., 1997]. The method is developed in order to make comparisons with the modified Radder and Dingemans formulation, which is described in the thesis.

The elliptic extended mild-slope equation is recasted into the form of a pair of first-order equations, which constitute a hyperbolic system. The resulting model includes higher-order bottom effects proportional to the square of the bottom slope and to the bottom curvature. Without these higher-order bottom terms, the model presented in the following is reduced to the model originally outlined by Copeland [1985].

Model equations

The extended mild-slope equation by Massel [1993] without the non-propagating modes is given by

$$\nabla \cdot \left(CC_g \nabla \varphi \right) + \omega^2 \left\{ \frac{C_g}{C} - R_1 \left(\nabla h \right)^2 - R_2 \nabla^2 h \right\} \varphi = 0 \tag{C1}$$

where φ is the velocity potential at mean water level, C and C_g are the phase speed and group velocity, respectively, of a wave with the angular frequency, ω, and wave number, k. ∇ is the horizontal gradient operator. The parameters R_1 and R_2 determining the higher-order bottom effects are further described in the thesis and are given in Appendix A.

Linear wave theory gives the following relation between the velocity potential at mean water level and the water surface, η, as

$$\varphi = \frac{g}{\omega^2} \eta_t \tag{C2}$$

where η_t is the time derivative of the surface elevation.

The volume flux Q defined by Copeland [1985] is given by

$$Q = \frac{CC_g}{g}\nabla\varphi \tag{C3}$$

Substitution of Eq.(C2) and Eq.(C3) into the model equation Eq.(C1) yields

$$\frac{\partial\eta}{\partial t} + \frac{1}{\frac{C_g}{C} - R_1(\nabla h)^2 - R_2\nabla^2 h}\nabla\cdot Q = 0 \tag{C4}$$

Taking the spatial and temporal derivatives of Eq.(C2), with the use of Eq.(C3), yields

$$\frac{\partial Q}{\partial t} + CC_g\nabla\eta = 0 \tag{C5}$$

Eqs.(C4) and (5) constitute a hyperbolic model, which includes the terms of higher-order bottom effects. Neglecting the higher-order bottom effects, Eqs.(C4) and (C5) reduce to the hyperbolic equations developed by Copeland [1995].

Finite difference approximation

Waves are generated internally inside the model boundaries as described in the thesis. In the modified model as well as the Copeland's model, the value, η^*, to be added to the surface elevation, η, at the wave generation point at each time step is

$$\eta^* = 2\eta\frac{C\Delta t}{\Delta x} \tag{C6}$$

where Δx and Δt are the grid size and time step, respectively.

Sponge layers to minimise wave reflection from the boundaries by dissipating wave energy inside the sponge layers are introduced by modification of Eq.(C5) as

$$\frac{\partial Q}{\partial t} + CC_g\nabla + D_s Q = 0 \tag{C7}$$

D_s is denoted the damping coefficient and given by

$$D_s = \begin{cases} 0, & \textit{outside sponge layer} \\ \omega\left(\dfrac{e^{d/S}-1}{e-1}\right), & \textit{inside sponge layer} \end{cases} \tag{C8}$$

where d is the distance from the starting point of the sponge layer and S is the thickness of the sponge layer.

In a one-dimensional domain, the modified models Eqs.(C4) and (C7) are discretised by a Leap-Frog method in a staggered grid in time and space, which yields

$$\frac{\eta_i^{n+1}-\eta_i^n}{\Delta t}+\frac{1}{\left[\dfrac{C_g}{C}-R_1\left(\dfrac{dh}{dx}\right)^2-R_2\dfrac{d^2h}{dx^2}\right]_i}-\frac{Q_{i+1}^n-Q_i^n}{\Delta x}=0 \tag{C9}$$

and

$$\frac{Q_i^{n+1}-Q_i^n}{\Delta t}+\left[CC_g\right]_{i-½}\frac{\eta_i^{n+1}-\eta_{i-1}^{n+1}}{\Delta x}+\omega\left[D_s\right]_{i-½}\cdot Q_i^n=0 \tag{C10}$$

where the superscript n denotes the time step. The index i denotes the spatial sampling and refers to the value of the i^{th} element where i-½ refers to the average value between element i and element i-1.

All the values of η and Q at the initial time step are set to be zero. For the slow start of wave generation, the left hand side of Eq.(C6) is multiplied by tanh(0.5 t/T), where T is the wave period. At outside boundaries, perfect reflection is assumed, but the reflected wave becomes negligible inside the domain because the sponge layer significantly reduces the incoming wave energy. The time step is chosen so the maximum Courant number $C_r = C\,\Delta t / \Delta x$ is less than 0.2. This ensures a stable solution [Lee et al. 1998].

APPENDIX D: EXPERIMENTAL DATA SHEET

Filename	Slope	Depth on reef-plateau	Inc. wave height	Inc. wave-period	Wave-gauge No. 6	Wave-gauge No. 7	Wave-gauge No. 8	Wave-gauge No. 9	Wave-gauge No. 10	Remark regarding tests
		h_t [m]	H_s [m]	T_p [sec.]	H_{m0} [m]	H_{m0} [m]	H_{m0} [m]	H_{m0} [m]	H_{m0} [m]	
Ureg_1	1:1	0.275	0.19	2.2	0.205	0.165	0.138	0.110	0.099	
Ureg_2	1:1	0.275	0.19	1.8	0.194	0.150	0.128	0.107	0.096	
Ureg_3	1:1	0.275	0.19	1.4	0.160	0.129	0.113	0.102	0.099	tendency to wave breaking at wave paddle
Ureg_4	1:1	0.275	0.16	2.2	0.168	0.143	0.126	0.108	0.097	
Ureg_5	1:1	0.275	0.16	1.8	0.166	0.137	0.121	0.106	0.098	
Ureg_6	1:1	0.275	0.13	2.2	0.134	0.121	0.111	0.101	0.091	mildly breaking waves
Ureg_7	1:1	0.275	0.13	1.8	0.138	0.122	0.110	0.100	0.093	mildly breaking waves
Ureg_8	1:1	0.275	0.13	1.4	0.119	0.107	0.098	0.095	0.092	mildly breaking waves
Ureg_9	1:1	0.275	0.112	2.2	0.108	0.102	0.097	0.091	0.085	mildly breaking waves
Ureg_10	1:1	0.275	0.112	1.8	0.109	0.102	0.095	0.092	0.085	mildly breaking waves
Ureg_11	1:1	0.275	0.19	2.2	0.201	0.163	0.136	0.111	0.100	repetition
Ureg_12	1:1	0.275	0.16	2.2	0.166	0.143	0.126	0.107	0.095	repetition
Ureg_13	1:1	0.275	0.13	2.2	0.140	0.126	0.114	0.101	0.092	repetition
Ureg_14	1:1	0.275	0.112	2.2	0.112	0.105	0.099	0.093	0.087	repetition
Ureg_15	1:1	0.205	0.19	2.2	0.207	0.135	0.105	0.080	0.070	
Ureg_16	1:1	0.205	0.19	1.8	0.192	0.119	0.095	0.079	0.070	
Ureg_17	1:1	0.205	0.19	1.4	0.166	0.104	0.086	0.075	0.074	
Ureg_18	1:1	0.205	0.21	2.2	0.225	0.139	0.108	0.085	0.071	
Ureg_19	1:1	0.205	0.21	1.8	0.210	0.126	0.098	0.079	0.070	
Ureg_20	1:1	0.205	0.21	1.4	0.178	0.107	0.088	0.076	0.074	
Ureg_21	1:1	0.205	0.16	2.2	0.188	0.127	0.103	0.081	0.069	
Ureg_22	1:1	0.205	0.16	1.8	0.164	0.111	0.090	0.077	0.070	
Ureg_23	1:1	0.205	0.16	1.4	0.140	0.097	0.082	0.075	0.072	
Ureg_24	1:1	0.205	0.13	2.2	0.154	0.115	0.094	0.075	0.067	
Ureg_25	1:1	0.205	0.13	1.8	0.142	0.104	0.086	0.075	0.068	
Ureg_26	1:1	0.205	0.13	1.4	0.115	0.088	0.077	0.073	0.069	
Ureg_27	1:1	0.205	0.1	2.2	0.124	0.101	0.086	0.074	0.065	
Ureg_28	1:1	0.205	0.1	1.8	0.115	0.093	0.081	0.072	0.068	
Ureg_29	1:1	0.205	0.1	1.4	0.097	0.079	0.073	0.070	0.066	
Ureg_30	1:1-S	0.205	0.21	2.2	0.254	0.147	0.109	0.091	0.072	slope torn loose due to the waves breaking
Ureg_31	1:1-S	0.205	0.21	1.8	0.220	0.130	0.097	0.087	0.072	
Ureg_32	1:1-S	0.205	0.21	1.4	0.175	0.113	0.084	0.083	0.076	
Ureg_33	1:1-S	0.205	0.19	2.2	0.224	0.140	0.103	0.090	0.071	
Ureg_34	1:1-S	0.205	0.19	1.8	0.200	0.124	0.093	0.086	0.072	
Ureg_35	1:1-S	0.205	0.19	1.4	0.172	0.112	0.085	0.086	0.075	

Filename	Slope	Depth on reef-plateau	Inc. wave height	Inc. wave-period	Wave-gauge No. 6	Wave-gauge No. 7	Wave-gauge No. 8	Wave-gauge No. 9	Wave-gauge No. 10	Remark regarding tests
		h_t	H_s	T_p	H_{m0}	H_{m0}	H_{m0}	H_{m0}	H_{m0}	
		[m]	[m]	[sec.]	[m]	[m]	[m]	[m]	[m]	
Ureg_36	1:1-S	0.205	0.16	2.2	0.199	0.132	0.100	0.090	0.070	
Ureg_37	1:1-S	0.205	0.16	1.8	0.174	0.117	0.088	0.085	0.071	
Ureg_38	1:1-S	0.205	0.16	1.5	0.143	0.102	0.080	0.084	0.075	
Ureg_39	1:1-S	0.205	0.13	2.2	0.147	0.116	0.091	0.084	0.069	
Ureg_40	1:1-S	0.205	0.13	1.8	0.149	0.110	0.084	0.083	0.070	
Ureg_41	1:1-S	0.205	0.1	2.2	0.116	0.100	0.084	0.075	0.068	
Ureg_42	1:1-S	0.205	0.1	1.8	0.113	0.092	0.078	0.073	0.071	
Ureg_43	1:1-S	0.205	0.1	1.4	0.091	0.078	0.071	0.070	0.067	
Ureg_44	1:1-S	0.275	0.19	2.6	0.231	0.180	0.146	0.127	0.101	
Ureg_45	1:1-S	0.275	0.19	2.2	0.218	0.164	0.134	0.122	0.099	
Ureg_46	1:1-S	0.275	0.16	2.6	0.198	0.164	0.141	0.124	0.101	
Ureg_47	1:1-S	0.275	0.13	2.6	0.157	0.140	0.124	0.114	0.096	
Ureg_48	1:1-S	0.275	0.1	2.6	0.134	0.120	0.118	0.111	0.094	This test has not been used due to noise in the signal
Ureg_49	1:1-S	0.275	0.16	2.2	0.174	0.142	0.122	0.114	0.095	
Ureg_50	1:1-S	0.275	0.13	2.2	0.143	0.126	0.114	0.110	0.094	
Ureg_51	1:1-S	0.275	0.112	2.2	0.116	0.107	0.100	0.100	0.087	
Ureg_52	1:1-S	0.275	0.19	1.8	0.195	0.149	0.120	0.105	0.096	
Ureg_53	1:1-S	0.275	0.16	1.8	0.174	0.137	0.115	0.101	0.094	
Ureg_54	1:1-S	0.275	0.13	1.8	0.131	0.115	0.104	0.098	0.094	
Ureg_55	1:1-S	0.275	0.112	1.8	0.101	0.095	0.089	0.087	0.083	
Ureg_56	1:1-S	0.275	0.19	1.4	0.154	0.123	0.105	0.099	0.099	
Ureg_57	1:1-S	0.275	0.13	1.4	0.119	0.103	0.093	0.091	0.091	
Ureg_58	1:1-S	0.275	0.112	1.4	0.090	0.083	0.080	0.080	0.079	
Ureg_59	1:1-S	0.275	0.112	1.4	0.090	0.084	0.080	0.080	0.079	
Ureg_60	1:1-S	0.275	0.19	2.2	0.211	0.161	0.127	0.109	0.097	Uncertainty with the wave period – but used
Ureg_61	1:1-S	0.275	0.19	2.2	0.212	0.162	0.132	0.110	0.098	
Ureg_62	1:1-S	0.275	0.19	1.8	0.189	0.145	0.119	0.104	0.098	
Ureg_63	1:1-S	0.275	0.19	1.4	0.157	0.125	0.109	0.102	0.100	
Ureg_64	1:0.5	0.275	0.19	2.2	0.210	0.166	0.139	0.123	0.101	
Ureg_65	1:0.5	0.275	0.19	1.8	0.191	0.148	0.126	0.118	0.100	
Ureg_66	1:0.5	0.275	0.19	1.4	0.159	0.129	0.116	0.113	0.104	
Ureg_67	1:0.5	0.275	0.16	2.2	0.176	0.144	0.129	0.120	0.100	
Ureg_68	1:0.5	0.275	0.16	1.8	0.173	0.145	0.123	0.107	0.099	
Ureg_69	1:0.5	0.275	0.16	1.4	0.142	0.120	0.107	0.098	0.096	
Ureg_70	1:0.5	0.275	0.13	2.2	0.142	0.123	0.114	0.110	0.095	
Ureg_71	1:0.5	0.275	0.13	1.8	0.139	0.124	0.110	0.102	0.095	
Ureg_72	1:0.5	0.275	0.13	1.4	0.122	0.108	0.099	0.093	0.092	

Filename	Slope	Depth on reef-plateau	Inc. wave height	Inc. wave-period	Wave-gauge No. 6	Wave-gauge No. 7	Wave-gauge No. 8	Wave-gauge No. 9	Wave-gauge No. 10	Remark regarding tests
		h_t	H_s	T_p	H_{m0}	H_{m0}	H_{m0}	H_{m0}	H_{m0}	
		[m]	[m]	[sec.]	[m]	[m]	[m]	[m]	[m]	
Ureg_73	1:0.5	0.275	0.11	2.2	0.112	0.103	0.100	0.101	0.087	
Ureg_74	1:0.5	0.275	0.112	1.8	0.106	0.101	0.093	0.089	0.085	
Ureg_75	1:0.5	0.275	0.112	1.4	0.094	0.090	0.085	0.083	0.082	
Ureg_76	1:0.5	0.205	0.21	2.2	0.254	0.160	0.120	0.091	0.075	
Ureg_77	1:0.5	0.205	0.21	1.8	0.241	0.145	0.109	0.085	0.077	
Ureg_78	1:0.5	0.205	0.21	1.4	0.192	0.122	0.096	0.081	0.077	
Ureg_79	1:0.5	0.205	0.19	2.2	0.245	0.159	0.120	0.090	0.076	
Ureg_80	1:0.5	0.205	0.19	1.8	0.227	0.147	0.108	0.085	0.075	
Ureg_81	1:0.5	0.205	0.19	1.4	0.186	0.122	0.096	0.081	0.077	
Ureg_82	1:0.5	0.205	0.16	2.2	0.206	0.148	0.112	0.086	0.074	
Ureg_83	1:0.5	0.205	0.16	1.8	0.197	0.136	0.102	0.083	0.076	
Ureg_84	1:0.5	0.205	0.16	1.4	0.164	0.116	0.092	0.082	0.078	
Ureg_85	1:0.5	0.205	0.13	2.2	0.164	0.126	0.099	0.081	0.072	
Ureg_86	1:0.5	0.205	0.13	1.8	0.158	0.119	0.095	0.080	0.074	
Ureg_87	1:0.5	0.205	0.13	1.4	0.130	0.101	0.086	0.079	0.075	
Ureg_88	1:0.5	0.205	0.1	2.2	0.131	0.111	0.094	0.080	0.072	
Ureg_89	1:0.5	0.205	0.1	1.8	0.136	0.109	0.088	0.076	0.072	
Ureg_90	1:0.5	0.205	0.1	1.4	0.113	0.092	0.082	0.077	0.074	
Ureg_91	1:2	0.205	0.21	2.2	0.247	0.147	0.117	0.093	0.077	
Ureg_92	1:2	0.205	0.21	1.8	0.230	0.134	0.107	0.088	0.076	
Ureg_93	1:2	0.205	0.21	1.4	0.193	0.116	0.093	0.085	0.080	
Ureg_94	1:2	0.205	0.19	2.2	0.221	0.139	0.111	0.090	0.074	
Ureg_95	1:2	0.205	0.19	1.8	0.208	0.128	0.102	0.089	0.075	
Ureg_96	1:2	0.205	0.19	1.4	0.180	0.113	0.092	0.086	0.078	
Ureg_97	1:2	0.205	0.16	2.2	0.204	0.133	0.107	0.089	0.075	
Ureg_98	1:2	0.205	0.16	1.8	0.198	0.125	0.098	0.088	0.076	
Ureg_99	1:2	0.205	0.16	1.4	0.155	0.107	0.090	0.085	0.077	
Ureg_100	1:2	0.205	0.13	2.2	0.167	0.121	0.098	0.086	0.071	
Ureg_101	1:2	0.205	0.13	1.8	0.161	0.113	0.092	0.084	0.075	
Ureg_102	1:2	0.205	0.13	1.4	0.133	0.100	0.087	0.081	0.074	
Ureg_103	1:2	0.205	0.1	2.2	0.127	0.102	0.088	0.078	0.070	
Ureg_104	1:2	0.205	0.1	1.8	0.121	0.097	0.085	0.078	0.072	
Ureg_105	1:2	0.205	0.1	1.4	0.111	0.092	0.083	0.079	0.074	
Ureg_106	1:2	0.275	0.19	2.4	0.213	0.172	0.142	0.117	0.105	
Ureg_107	1:2	0.275	0.19	1.8	0.191	0.147	0.123	0.107	0.102	
Ureg_108	1:2	0.275	0.16	2.4	0.190	0.157	0.133	0.113	0.104	
Ureg_109	1:2	0.275	0.16	1.4	0.134	0.118	0.106	0.097	0.098	
Ureg_110	1:2	0.275	0.13	2.4	0.148	0.130	0.119	0.103	0.098	

APPENDIX E: NUMERICAL UNIT SOLVING THE WAVE EQUATIONS

Procedure Solve_eta_Radder_Dingemans [DELPHI unit]
(n:integer;Period,dt,time,dx:single;x,h,dh,d2h,R1,R2,D,CG,C,K:vector1);
{the constant terms are already calculated and transferred in the header}
Var
{the procedure "Solve_eta_Radder_Dingemans" solves Radder and Dingemans} {[1985] time-dependent wave equations. Furthermore, higher-order bottom} {terms and wave energy dissipation due to wave breaking and bottom} {friction is included.}

* declaration of parameters omitted here

```
Begin {start of procedure}
 no_timestep:=trunc(time/dt);

 {non-linearity parameter}
 F_c0:=power(9.81,1.25)*power(H_s,0.5)*power(wave_period,2.5)/power(h_2,1.75);

{Parameter used to estimate the max. wave height for reformed wave height on the reef-plateau}
{relation found from experimental tests}
 Breaker_index:=0.438+0.000127*F_c0;

{initialisation of parameters}
  for i:=0 to 4 do
  for ii:=0 to n do
  begin
     t_eta[i]^[ii]^:=0.0;
     t_q[i]^[ii]^  :=0.0;
  end;

  for ii:=0 to n do
  begin
    Q_b[ii]:=0.0;
    sum[ii]:=0.0;
    rms_wave_height[ii]:=0.0;
  end;

  {higher-order bottom terms}
  for ii:=0 to n do
    dummy3[ii]:=sqr(2*pi/period)/gravity*(R1[ii]^
    *sqr(dh[ii]^)+R2[ii]^*d2h[ii]^);
  end;

  {determination of the – CxC_G gradient (temp7)}
  for ii:=0 to n do
  begin
    temp5:=K[ii]^*h[ii]^;
    temp6:=tanh(temp5);
    temp7:=temp5/(temp6+temp5*(1-sqr(temp6)))*
    (1-3*sqr(temp6)+2*temp6/(temp6+temp5*(1-sqr(temp6))));
    temp8[ii]:=C[ii]^*CG[ii]^/h[ii]^*dh[ii]^*temp7/gravity;
  end;

  {start of time step)
 for t:=1 to no_timestep  do
 begin
   for ii:=1 to n-1 do
   begin
```

```
    {prevention of numerical problems in the terms R1 and R2}
    {this only happens when the slope becomes almost vertical}
    if ((dummy3[ii])<0.1) then
   repeat
    inc(help);
    dhdx:=(h[ii-help]^-h[ii+help]^)/(x_[ii+help]^-x_[ii-help]^);
    dh2dx2:= ((h[ii-help]^-h[ii]^)/(x_[ii]^-x_[ii-help]^)-(h[ii]^-h[ii+help]^)/(x_[ii+help]^-x_[ii]^))/
          ((x_[ii+help]^-x_[ii-help]^)/2);
    dummy3[ii]:=((CG[ii]^)/(C[ii]^)-R1[ii]^*sqr(dhdx)-R2[ii]^*dh2dx2);
   until (dummy3[ii])>0.1;
  end;
 {Maximum allowable wave height}
  max_wave:=breaker_index*h[ii]^;
 {calculation of phi_dt}
  G_0:=-gravity*t_eta[1]^[ii]^-2*pi/period*D[ii]^*t_Q[1]^[ii]^;
  G_1:=-gravity*t_eta[2]^[ii]^-2*pi/period*D[ii]^*t_Q[2]^[ii]^;
  G_2:=-gravity*t_eta[3]^[ii]^-2*pi/period*D[ii]^*t_Q[3]^[ii]^;
  G_3:=-gravity*t_eta[4]^[ii]^-2*pi/period*D[ii]^*t_Q[4]^[ii]^;
  temp1:=t_Q[1]^[ii-1]^+t_Q[1]^[ii+1]^;
  temp2:=t_Q[2]^[ii-1]^+t_Q[2]^[ii+1]^;
  temp3:=t_Q[3]^[ii-1]^+t_Q[3]^[ii+1]^;
  temp4:=t_Q[4]^[ii-1]^+t_Q[4]^[ii+1]^;
  {calculation of bottom velocity}
  u_C_0:=u_C*2.5/2.83*rms_wave_height[ii];
  u_C_1:=u_C*2.5/2.83*rms_wave_height[ii];
  u_C_2:=u_C*2.5/2.83*rms_wave_height[ii];
  u_C_3:=u_C*2.5/2.83*rms_wave_height[ii];
  if abs(t_eta[1]^[ii]^)<0.001*H_s then part_Gamma_f_0:=0.0 else part_Gamma_f_0:=
  16*f_r/(3*pi*gravity)*abs(u_C_0*u_C_0*u_C_0)/(sqr(rms_wave_height[ii]));
  if abs(t_eta[2]^[ii]^)<0.001*H_s then part_Gamma_f_1:=0.0 else part_Gamma_f_1:=
  16*f_r/(3*pi*gravity)*abs(u_C_1*u_C_1*u_C_1)/(sqr(rms_wave_height[ii]));
  if abs(t_eta[3]^[ii]^)<0.001*H_s then part_Gamma_f_2:=0.0 else part_Gamma_f_2:=
  16*f_r/(3*pi*gravity)*abs(u_C_2*u_C_2*u_C_2)/(sqr(rms_wave_height[ii]));
  if abs(t_eta[4]^[ii]^)<0.001*H_s then part_Gamma_f_3:=0.0 else part_Gamma_f_3:=
  16*f_r/(3*pi*gravity)*abs(u_C_3*u_C_3*u_C_3)/(sqr(rms_wave_height[ii]));
  {wave breaking applied from start of reef to last gauge in lab}
  if (ii<741) or (ii>898)) then
  begin
    part_Gamma_b_0:=0.0;
    part_Gamma_b_1:=0.0;
    part_Gamma_b_2:=0.0;
    part_Gamma_b_3:=0.0;
  end else
  begin {calculation of wave breaking dissipation}
    if rms_wave_height[ii]<0.01 then
    begin
      part_Gamma_b_0:=0.0;
      part_Gamma_b_1:=0.0;
      part_Gamma_b_2:=0.0;
      part_Gamma_b_3:=0.0;
  end else
  begin
    if rms_wave_height[ii]>0.55*max_wave then; {the ratio 0.55 is found from experimental tests}
    begin
      ratio_W:=rms_wave_height[ii];  {modification–more correct dissipation}
    end else
    begin
      ratio_W:=power(3,max_wave)/sqr(rms_wave_height[ii]);
```

```
    end;
    part_Gamma_b_0:=Q_b[ii]*alpha*2/period*sqrt(gravity*h[ii]^)/(2*pi/(period*K[ii]^))*
                    power(3,max_wave)/sqr(rms_wave_height[ii])/h[ii]^;
    part_Gamma_b_1:=Q_b[ii]*alpha*2/period*sqrt(gravity*h[ii]^)/(2*pi/(period*K[ii]^))*
                    power(3,max_wave)/sqr(rms_wave_height[ii])/h[ii]^;
    part_Gamma_b_2:=Q_b[ii]*alpha*2/period*sqrt(gravity*h[ii]^)/(2*pi/(period*K[ii]^))*
                    power(3,max_wave)/sqr(rms_wave_height[ii])/h[ii]^;
    part_Gamma_b_3:=Q_b[ii]*alpha*2/period*sqrt(gravity*h[ii]^)/(2*pi/(period*K[ii]^))*
                    power(3,max_wave)/sqr(rms_wave_height[ii])/h[ii]^;
  end;
end; {end calculation of wave breaking dissipation}
Gamma_0:=part_Gamma_f_0+part_Gamma_b_0;
Gamma_1:=part_Gamma_f_1+part_Gamma_b_1;
Gamma_2:=part_Gamma_f_2+part_Gamma_b_2;
Gamma_3:=part_Gamma_f_3+part_Gamma_b_3;
{calculation of eta_dt}
F_0:=-temp8[ii]*(t_Q[1]^[ii-1]^-t_Q[1]^[ii+1]^)/(2*dx)-C[ii]^*CG[ii]^/gravity*(temp1-
      2*t_Q[1]^[ii]^)/sqr(dx)+(sqr(2*pi/period)-sqr(K[ii]^)*C[ii]^*CG[ii]^)/gravity*t_Q[1]^[ii]^
     +dummy3[ii]*t_Q[1]^[ii]^-Gamma_0*t_eta[1]^[ii]^;
F_1:=-temp8[ii]*(t_Q[2]^[ii-1]^-t_Q[2]^[ii+1]^)/(2*dx)-C[ii]^*CG[ii]^/gravity*(temp2-
      2*t_Q[2]^[ii]^)/sqr(dx)+(sqr(2*pi/period)-sqr(K[ii]^)*C[ii]^*CG[ii]^)/gravity*t_Q[2]^[ii]^
     +dummy3[ii]*t_Q[2]^[ii]^-Gamma_1*t_eta[2]^[ii]^;
F_2:=-temp8[ii]*(t_Q[3]^[ii-1]^-t_Q[3]^[ii+1]^)/(2*dx)-C[ii]^*CG[ii]^/gravity*(temp3-
      2*t_Q[3]^[ii]^)/sqr(dx)+(sqr(2*pi/period)-sqr(K[ii]^)*C[ii]^*CG[ii]^)/gravity*t_Q[3]^[ii]^
     +dummy3[ii]*t_Q[3]^[ii]^-Gamma_2*t_eta[3]^[ii]^;
F_3:=-temp8[ii]*(t_Q[4]^[ii-1]^-t_Q[4]^[ii+1]^)/(2*dx)-C[ii]^*CG[ii]^/gravity*(temp4-
      2*t_Q[4]^[ii]^)/sqr(dx)+(sqr(2*pi/period)-sqr(K[ii]^)*C[ii]^*CG[ii]^)/gravity*t_Q[4]^[ii]^
     +dummy3[ii]*t_Q[4]^[ii]^-Gamma_3*t_eta[4]^[ii]^;

{Adam-Bashforth predictor}
t_eta[0]^[ii]^:=t_eta[1]^[ii]^+dt/24*(55*F_0-59*F_1+37*F_2-9*F_3);
t_Q[0]^[ii]^  :=t_Q[1]^[ii]^+  dt/24*(55*G_0-59*G_1+37*G_2-9*G_3);

*The Moulton step, i.e. the corrector step is similar as the step
described above (from calculation of phi_dt and therefore not shown

{calculation of root-mean-square wave height}
sum[ii]:=sum[ii]+(t_eta[0]^[ii]^)*(t_eta[0]^[ii]^);
rms_wave_height[ii]:=2.83*sqrt(sum[ii]/(t));

{calculation of fraction of waves breaking Q_b}
b:=power(2,rms_wave_height[ii]/max_wave));
if ((ii>741) and (ii<899) and (b>0.001)) then
begin
  if (rms_wave_height[ii]>0.55*max_wave) then Q_b[ii]:=1.0
  else
  begin
    Q_b[ii]:=0.5;
    repeat
      old_Q_b:=Q_b[ii];
      Q_b[ii]:=exp(-(1-Q_b[ii])/(forhold));
      eps:=abs(Q_b[ii]-old_Q_b);
    until eps<0.01;
  end;
end;  {end calculation of fraction of waves breaking Q_b}

 {wave generation if the scheme reach the point of the wave generator}
 if wave_generation[ii] then
```

```
  begin
    {procedure calculating spectral parameters from a JONSWAP spectrum}
    Div_of_2D_spectra_JONSWAP(no_waves,H_s,period,H,T_,phi);
    gen_eta:=0.0;
    for mj:=1 to no_waves do
    begin
      Cor_waveheight:=H_[mj]*T_[mj]/period*sqrt(1+C[ii]^/CG[ii]^*(sqr(period/T_[mj])-));
      gen_eta:=gen_eta+cor_waveheight/2*cos(2*pi*1/T_[mj]*t*dt+phi[mj]);
    end;
    t_eta[0]^[ii]^:=t_eta[0]^[ii]^+tanh(0.5*t*t_width/period)*gen_eta*2*CG[ii]^*t_width/x_width;
  end;
end{timestep}
```

Parameters declared as constants in the numerical model for simulating wave energy dissipation

Geometry	
Depth of water before start of reef-slope (h)	0.655 m
Depth of water on reef-plateau (h_t)	0.275 m
Number of nodes	1600
Number of the last node of the up-wave section of damping elements	385
Number of the first node of the down-wave damping elements	1215
Number of the node where waves will be generated	435
First node forming the slope	742
Reef-slope (tan β_s)	1
Length of one element (Δx)	0.04 m
Wave parameters	
Type of spectrum to be generated	JONSWAP
Peakness factor of the spectrum (γ_p)	3.3
Significant incident wave height (H_{m0})	0.16 m
Peak period of incident wave spectrum (T_p)	2.2 sec
Low cut-off frequency (f_{min})	0.074 Hz
High cut-off frequency (f_{max})	0.174 Hz
Time parameters	
Length of simulation	500 x T_p
Time step (Δt)	0.004 sec
Energy dissipation parameters	
Factor governing the intensity of energy dissipation due to wave breaking (α_0)	1
Factor governing the intensity of energy dissipation due to bottom friction (f_r)	0.1
Breaker index (γ) is depending on the non-linearity parameter as $H_{max} / h = 0.438+1.28x10^{-4} F_{c0}$	

Tabel E1: *Typical input file in numerical simulation.*

APPENDIX F: UNCERTAINTY RELATED TO FORMULAE

Uncertainty due to the formulae presented in the thesis is shown in Figures F1 and F2. From these curves the 90% confidence limit is estimated.

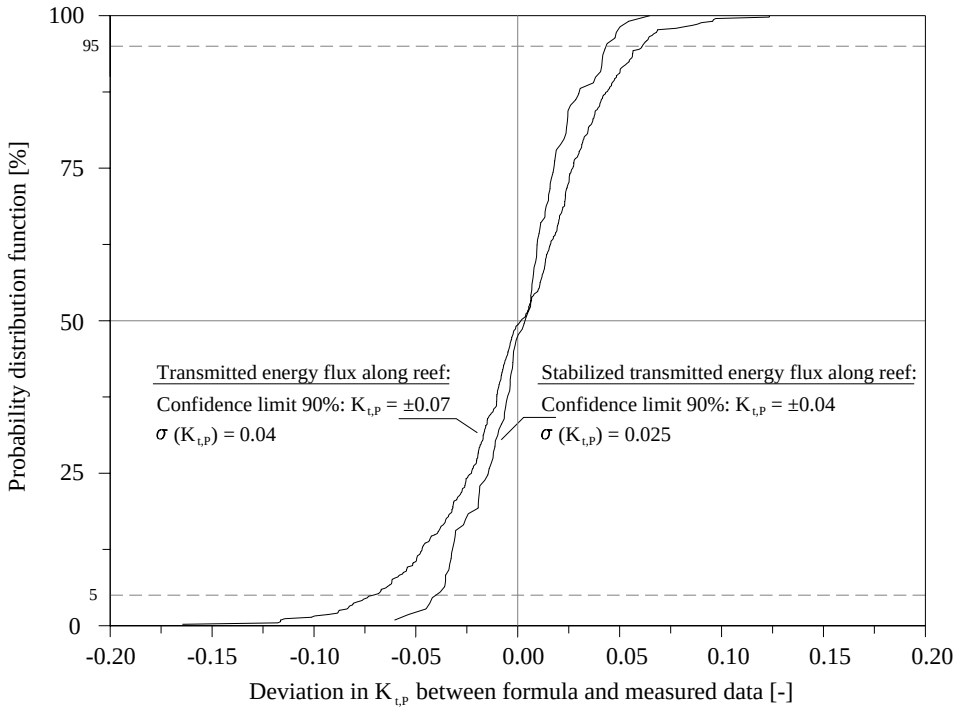

Figure F1: *Distribution curves regarding the uncertainty related to the formula predicting the wave energy flux*

Figure F1 shows the distribution of the errors between the measured wave energy fluxes along the reef-plateau. Two graphs are depicted. The graph showing the larger deviation refers to the formula predicting the transmitted wave energy flux along the reef. Measurements are sampled at four locations from the waves initiate wave breaking until the waves are reformed. The graph showing less deviation refers to the formula predicting the total transmitted wave energy flux.

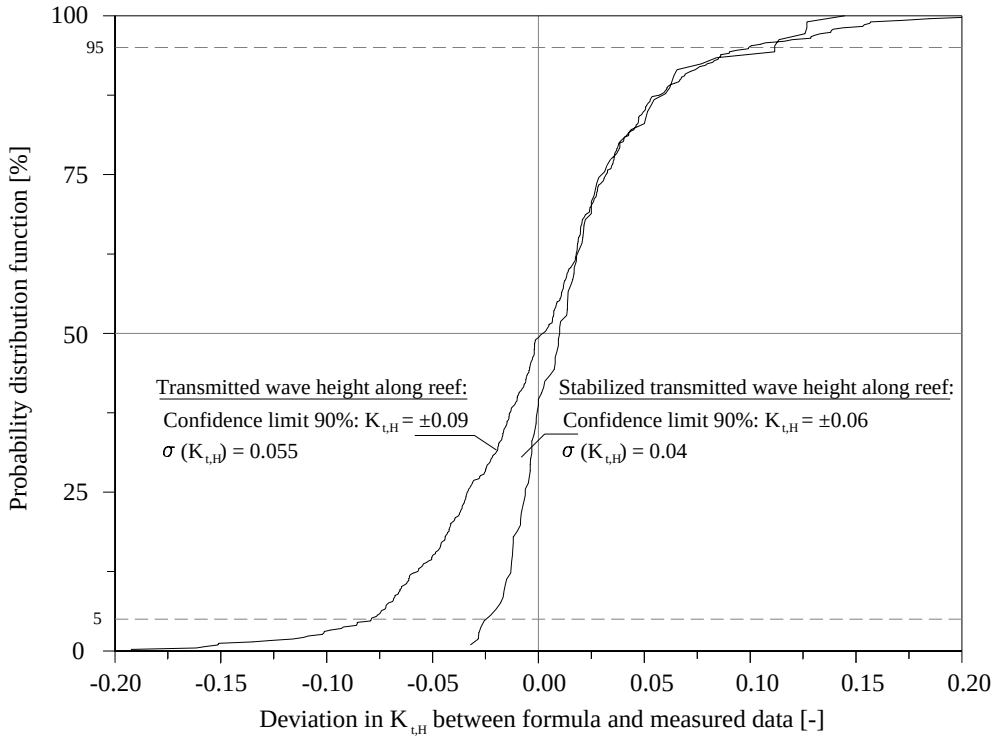

Figure F2: *Distribution curves regarding the uncertainty related to the formula predicting the wave energy density.*

Figure F2 shows the distribution of the errors between the predicted and measured values of the wave energy density. Two graphs are depicted. The graph showing the larger deviation refers to the formula predicting the transmitted wave energy density along the reef. Measurements are taken at four locations from where wave breaking is initiated until the waves are reformed. The graph showing less deviation refers to the formula predicting the total transmitted wave energy density. This last graph shows large deviations between the predicted wave energy densities and those actually measured, where the predicted energy densities are higher. The wave trains with mild wave breaking are represented here. These waves represent a threshold of wave breaking and yield results not comparable with other tests regarding the fitted formula.

APPENDIX G: WAVES AND THEIR STATISTICS

Often used terms associated with this thesis are defined in present appendix. In general waves are characterised with common used notations as the significant wave height, peak spectral wave period etc. Actually, the definition of the significant wave height can be many and it makes a difference whether it is the spectral significant wave height derived from the wave energy spectrum or the significant wave height derived from a zero-crossing analysis, i.e. the statistical significant wave height.

Waves are generally recorded for short periods of say 20 minutes duration. This yields often an adequate number of waves to produce some statistics based upon the water surface profile and the waves. In the experimental tests performed during the time of measurements regarding irregular wave generation was 15–30 minutes, depending on the peak period of the wave event. A total 650 waves were generated.

The surface profile is relatively easy to assess, as it is only necessary to divide the elevation space into a suitable number of intervals and then obtain statistics such as the mean elevation, standard deviation (σ^2), skewness and kurtosis. These variables are useful in relating the time series to properties derived from a spectral analysis. In general, the scientists, researchers or engineers are interested in the wave heights in an irregular wave train. When the statistical approach is used in the thesis the zero-downcrossing method has been used as recommended by IAHR/PIANC [1986]. See Figure G1 for the definition of the individual wave height and the associated wave period found by zero-downcrossing.

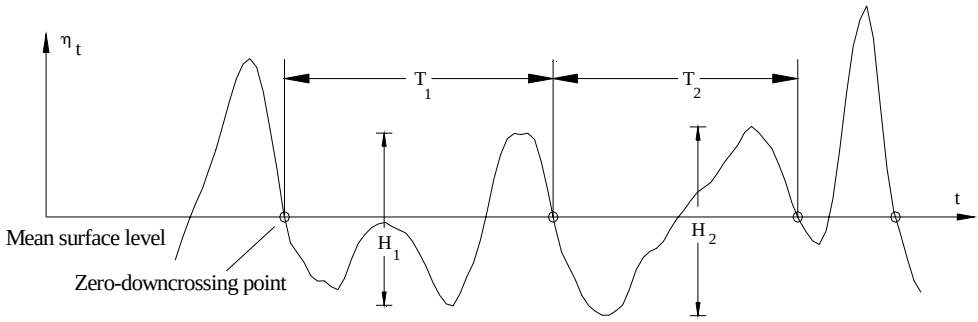

Figure G1: *Waves defined by zero-downcrossing.*

Having defined the waves in a record it is then possible to calculate statistics of the wave heights. These are known as short-term statistics, since they are only for one wave event or wave record. If all the wave heights are ordered it is usual to compute the significant wave height H_s. This is defined as the average height of the highest one-third waves, and is sometimes known as $H_{1/3}$ and is important historically

because it appears to be approximately the wave height, which is recorded by a trained observer, when asked to estimate the wave height. Other characteristic wave heights are of interest, including the average of the one-tenth highest waves $H_{1/10}$ the mean wave height H_{mean}, the root-mean-square wave height H_{rms} and the maximum wave height, $H_{max.}$

Several important publications by researchers, but especially Longuet-Higgins [1952], have established relationships between the water surface statistics, the wave height statistics and the spectral properties. The water surface is usually assumed to follow a Gaussian or Normal distribution. For a narrow band spectrum with a spectral width parameter of zero, Longuet-Higgins has shown that the wave peaks η in a record will follow a Rayleigh distribution described by

$$p(\eta_{\max}) = \eta_{\max} / \sigma^2 \exp(-\eta_{\max}^2 / 2\sigma^2) \tag{G1}$$

where σ^2 is the standard deviation of the water surface.

In the case of a narrow band spectrum the wave heights are twice the wave crests so that the Rayleigh probability density function of wave heights may be defined thus

$$p(H) = \frac{1}{4}\frac{H}{\sigma^2}\exp\left(-\frac{H^2}{8\sigma^2}\right) \tag{G2}$$

The mean value of η_{max} is given by

$$\eta_{\max} = \int_{-\infty}^{\infty} \eta_{\max} P(\eta_{\max}) d\eta_{\max} = \sqrt{\frac{\pi}{2}\sigma} \tag{G3}$$

so that the Rayleigh probability density function of wave heights in terms of the mean wave height $\overline{H}$ becomes

$$p\left(\frac{H}{\overline{H}}\right) = \frac{\pi}{2}\left(\frac{H}{\overline{H}}\right)\exp\left(-\frac{\pi}{4}\left(\frac{H}{\overline{H}}\right)^2\right) \tag{G4}$$

The Rayleigh distribution function in terms of the mean wave height $\overline{H}$ becomes

$$P\left(\frac{H}{\overline{H}}\right) = 1 - \exp\left(-\frac{\pi}{4}\left(\frac{H}{\overline{H}}\right)^2\right) \tag{G5}$$

From Eq.(G4) relationships between characteristic wave heights can be listed as

$$\begin{aligned} \overline{H} &= 2.507\,\sigma \\ H_{rms} &= 1.13\overline{H} = 2.828\,\sigma \\ H_{1/3} &= 1.60\overline{H} = 4.004\sigma \\ H_{1/10} &= 2.03\overline{H} = 5.088\,\sigma \end{aligned} \tag{G6}$$

According to Eq.(G5) exceedence levels of the wave heights can be found as

$$\begin{aligned} H_{50\%} &= 0.94\overline{H} = 2.355\,\sigma \\ H_{10\%} &= 1.71\overline{H} = 4.292\,\sigma \\ H_{1\%} &= 2.42\overline{H} = 6.070\sigma \\ H_{0.1\%} &= 2.97\overline{H} = 7.434\,\sigma \\ H_{0.01\%} &= 3.42\overline{H} = 8.584\,\sigma \end{aligned} \tag{G7}$$

where $H_{10\%}$ is the wave height only exceeded by 10% of the waves.

All these relationships are only valid for a wave record with a spectral width of zero or close to zero. In practice most wave height distributions differ a little from the Rayleigh distribution but the difference is usually ignored. Only in relatively deep water, the Rayleigh distribution is a good approximation to the distribution of individual wave heights. When wave breaking takes place due to limited water depths, the individual wave height distribution will differ from the Rayleigh distribution.

APPENDIX H: FORMULAE REVISED AFTER DALLY ET AL. (1985)

This appendix is written after the Ph.D. thesis was presented and the Ph.D. degree awarded in February 2003. After suggestion from the Assessment Committee formulae in the thesis are fitted to expressions having a more physical meaning. It is particular the expressions Eqs. (87) and (89) in the thesis, which seem artificial. The terms describe the reduction of wave energy flux and wave height along the reef, respectively.

Michael Brorsen, Stanislaw R. Massel and Terry S. Hedges represented the Assessment Committee.

WAVE HEIGHT TRANSMISSION COEFFICIENT

A sounder solution can be developed using the concept of gradient of the energy flux on the reef plateau. Massel and Brinkman (2001) used this approach based on a model proposed by Dally et al. (1985). The model predicts the transformation of energy flux along the reef plateau. Applying this model to the experimental layout, the following equation for wave height on the reef plateau can be obtained as

$$\frac{H_t(x)}{h_t} = \left\{ \left[\left(\frac{H_t}{h_t} \right)_i^2 - \gamma^2 \right] \exp\left[-k_a \frac{(x - x_i)}{h_t} \right] + \gamma^2 \right\}^{1/2} \tag{H1}$$

where $H_t(x)$ is the transmitted wave height along the reef plateau. Lower index i indicates the value of non-dimensional wave height $\left(H \,/ h_t\right)$ at the i^{th} gauge. Location of the gauge is denoted x_i and k_a is the attenuation coefficient. Wave heights at i^{th} gauge are measured in the experimental tests. Both wave gauge No. 6 and wave gauge No. 7 are later used as reference points. The location of wave gauge No. 6 is at the reef edge and wave gauge No. 7 is located 0.9 m after the reef edge.

By rearranging Eq.(H1) and using wave gauge No. 6 as a reference point the wave height transmission coefficient $K_{t,H}(x)$ becomes

$$K_{t,H}(x) = \frac{\sqrt{\left[\left(\frac{H_t}{h_t} \right)_6^2 - \gamma^2 \right] \exp\left[-k_a \frac{(x - x_6)}{h_t} \right] + \gamma^2} \cdot h_t}{H_s} \tag{H2}$$

Rearranging again, the height transmission coefficient $K_{t,H}(x)$ becomes

$$K_{t,H}(x)=\sqrt{\left(\frac{\gamma h_t}{H_s}\right)^2+\left(\frac{h_t}{H_s}\right)^2\left\{\left[\left(\frac{H_t}{h_t}\right)_6^2-\gamma^2\right]\exp\left[-k_a\frac{(x-x_6)}{h_t}\right]\right\}} \tag{H3}$$

At $x = x_6$ the wave height transmission coefficient becomes

$$K_{t,H}(x_6)=\frac{H_6}{H_s} \tag{H4}$$

and for $x\to\infty$ we obtain

$$K_{t,H}(x\to\infty)=\frac{\gamma h_t}{H_s} \tag{H5}$$

Eq.(H5) is the expression obtained for the reformed wave height in the thesis. This indicates that formula Eq.(H3) is sound.

In Eq.(H3) the term $\left(\frac{h_t}{H_s}\right)^2\cdot\left\{\left[\left(\frac{H_t}{h_t}\right)_6^2-\gamma^2\right]\exp\left[-k_a\cdot\frac{(x-x_6)}{h_t}\right]\right\}$ plays the role of

the tanh [ ] term used in Eqs. (87) and (89).

WAVE ENERGY FLUX TRANSMISSION COEFFICIENT

Similarly, the wave energy flux transmission becomes

$$K_{t,P}(x)=\frac{P_t}{P_i}=\frac{H_t^2\cdot C_{g,t}}{H_s^2\cdot C_{g,i}}=\frac{\left\{\left[\left(\frac{H_t}{h_t}\right)_i^2-\gamma^2\right]\exp\left[-k_a\frac{(x-x_i)}{h_t}\right]+\gamma^2\right\}\cdot h_t^2\cdot C_{g,t}}{H_s^2\cdot C_{g,i}} \tag{H6}$$

It is noted that the square root is not applied in Eq.(H6) as was done in the thesis.

In Eq.(H6), the group velocities, $C_{g,t}$ and $C_{g,i}$, are be based on the actual water depth. At the reef plateau it can be discussed if the shallow water approximation of the group velocity shall be used, but significantly improved correlation between the measured and predicted data is obtained using the group velocity based on the actual water depth at the reef plateau.

WAVE HEIGHT DISTRIBUTION AT THE REEF PLATEAU

Wave heights measured in the laboratory are all given as spectral wave heights. An analysis of the relationship between the parameters H_{m0}, H_s and H_{max} on the reef plateau is performed in the thesis where various ratios are depicted against the non-linearity parameter F_{c0}.

It is shown that for high values of F_{c0}, the ratio between H_{m0} and H_s is reduced from 1.0 to approximately 0.85 as can be seen in Figure 29. That is, H_{m0} is slightly underestimated for high values of F_{c0} compared to the significant wave height, H_s. It is also observed that the highest waves no longer follow the Rayleigh distribution. This results in a relation between the significant wave height and the maximum wave height of 1.37.

WAVE HEIGHT TRANSMISSION COEFFICIENT FORMULA

In Figure H1 plots are made with reference points at wave gauge No. 6 (top graph) and wave gauge No. 7 (bottom graph), respectively. The plots show the deviation between measured data in the experiments and the predicted data based on the expression for transmission of the wave height as given in Eq.(H3). The length along the reef plateau is given by the parameter X, with starting point at the reference point, i.e. if the starting point is defined at wave gauge No. 6 then $X = 0$ at x_6.

It is observed that using wave gauge No. 7 as a reference point reduces the available experimental measurements to 330 data. This is because the measurements at wave gauge No. 7 are not plotted. Measurements at wave gauge No. 7 are by definition equal to the expression given in Eq.(H4) and, if plotted, the data is situated on the "line of agreement".

There are plotted data that seem to follow on another trend than the rest of the depicted data. This is most obvious in the bottom graph shown in Figure H1. The predicted wave heights are higher than the measured wave heights. These data are all experiments involving the smaller incident significant wave height combined with the deepest water depth at the reef plateau. In these wave trains, the waves are only "mildly" breaking, meaning that many of the waves pass the reef slope without breaking. These conditions are considered as a threshold for the formulae developed in the thesis.

The correlation between measured data and the predicted data according to formula Eq.(H3) is relatively good. A least square method is used to obtain a calibration of γ and k_a. A calibration of the breaker index results in $\gamma = 0.35$. This value is close to the result obtained in Chapter 10 being $\gamma = 0.36$. The attenuation coefficient becomes $k_a = 0.20$. The coefficients do not change regardless of which gauge is used, but the

standard deviation is higher using the reference point at the reef edge, i.e. wave gauge No. 6. The larger deviation is expected because many waves initiate breaking right on the reef edge.

To summarise, it is shown that the attenuation of the waves on the reef plateau after the waves break on the reef edge can be calculated according to the formula given in Eq.(H7)

$$K_{t,H}(X) = \sqrt{\left(\frac{0.35h_t}{H_s}\right)^2 + \left(\frac{h_t}{H_s}\right)^2 \left\{\left[\left(\frac{H_{t,X=0}}{h_t}\right)^2 - 0.35^2\right] \exp\left[-0.2\frac{X}{h_t}\right]\right\}} \qquad \text{(H7)}$$

Where $H_{t,X=0}$ is the transmitted wave height on the reef plateau at the reference point and X is the distance from the location of the reference wave height. The standard deviation of the wave transmission coefficient is $\sigma(K_{t,H}) = 0.035$ with a 90% confidence interval, $K_{t,H} = \pm 0.057$.

Eq.(H7) does not depend on the incident wave height, H_s, and can therefore be written

$$H_t(X) = \sqrt{(0.35h_t)^2 + h_t^2 \left\{\left[\left(\frac{H_{t,X=0}}{h_t}\right)^2 - 0.35^2\right] \exp\left[-0.2\frac{X}{h_t}\right]\right\}} \qquad \text{(H8)}$$

To ensure wave breaking over the reef slope, the requirement using formulae Eq.(H7) and Eq.(H8) is

$$H_s/h_t \geq 0.4 \qquad \text{(H9)}$$

which is the smallest ratio used in the experiments. Furthermore, the transmitted wave height on the reef plateau, $H_{t,X=0}$ cannot be smaller than the reformed wave height on the reef plateau resulting in the requirement

$$H_{t,X=0}/h_t \geq \lambda \quad \Rightarrow \quad H_{t,X=0}/h_t \geq 0.35 \qquad \text{(H10)}$$

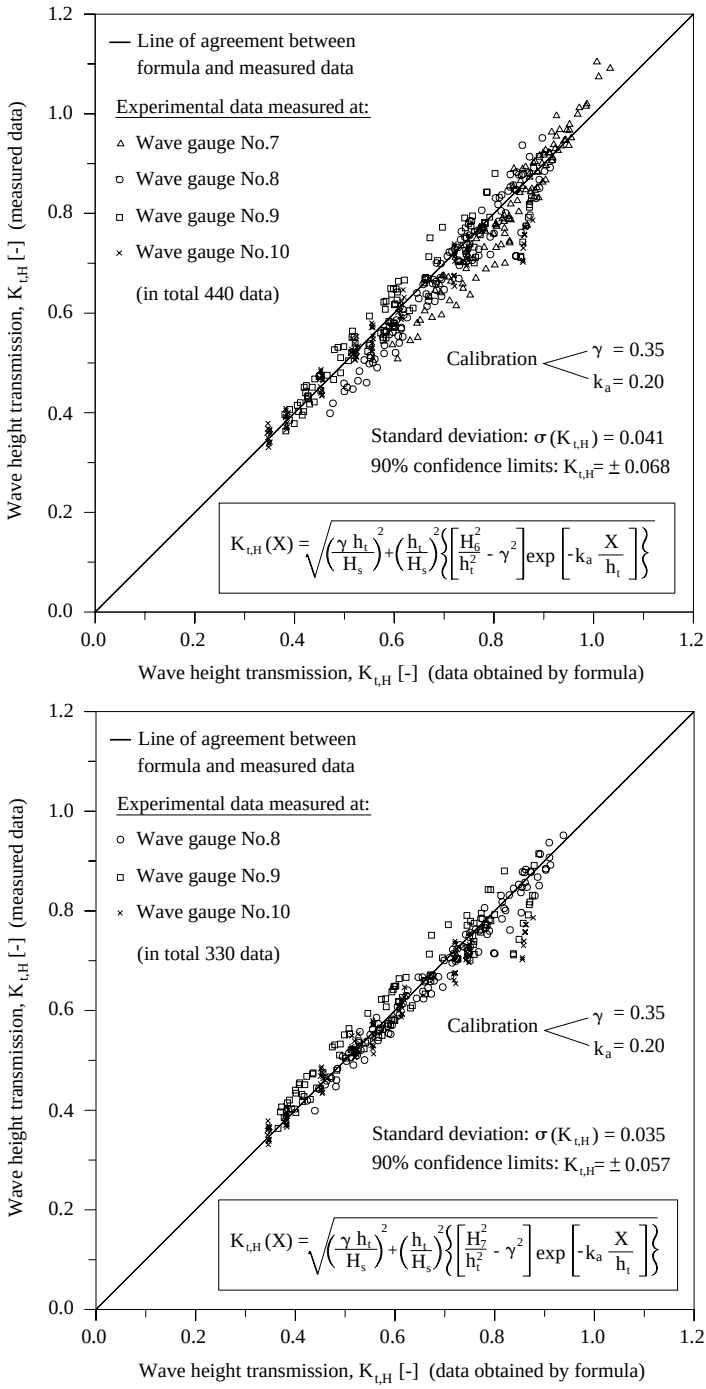

Figure H1: *Wave height transmission with reference point at gauges No. 6 & 7.*

Eqs.(H7) and (H8) provides a tool for prediction of the wave height transformation along the reef. Often the wave heights are not known on the reef or an artificial reef is to be designed. It is therefore important to be able to relate the incident waves to the transmitted waves at the reef plateau. In the following, such an attempt is made based on the expression given in Eq.(H3).

Instead of the reference wave height on the reef plateau, the incident significant wave height is used, see Eq.(H11). It is expected that there is a close relationship between the incident wave height and the wave height measured at the reef edge, i.e. at wave gauge No. 6.

$$K_{t,H}(X) = \sqrt{\left(\frac{\gamma h_t}{H_s}\right)^2 + \left(\frac{h_t}{H_s}\right)^2 \left\{\left[\left(\frac{H_s}{h_t}\right)^2 - \gamma^2\right] \exp\left[-k_a \frac{X}{h_t}\right]\right\}} \qquad \text{(H11)}$$

The distance X has its starting point at the reef edge.

In Figure H2 plots are made based on the significant wave height (top graph). The scatter is more significant, but a trend in the data is obvious. The calibration of γ and k_a yields similar results compared to the previous calibrations using a reference wave height on the reef plateau. Eq.(H12) is the formula predicting the wave height on the reef plateau based on the incident significant wave height.

$$K_{t,H}(X) = \sqrt{\left(\frac{0.35 h_t}{H_s}\right)^2 + \left(\frac{h_t}{H_s}\right)^2 \left\{\left[\left(\frac{H_s}{h_t}\right)^2 - 0.35^2\right] \exp\left[-0.2 \frac{X}{h_t}\right]\right\}} \qquad \text{(H12)}$$

It is experienced in the thesis that the wave period is a parameter, which influences the process of wave breaking. The wave period is not represented in Eq.(H12), which is a limitation when trying to relate the none-breaking incident waves with the transmitted waves on the reef plateau. It is believed that the amount of waves, in the wave train, breaking over the steep slope is correlated to the steepness of the waves. The wave steepness is the ratio between the wave height and the wavelength. The wavelength is governed by the wave period. The wave steepness is non-dimensional and can be used directly in a formula based on Eq.(H12). Several attempts are performed to include the wave steepness. Connecting the wave steepness directly to the wave attenuation parameter seems to hold the best physical arguments. Waves break differently depending on the wave steepness, and the wave energy dissipation is severest during the first wavelength. The wave attenuation factor controls the wave height attenuation, especially along the first wavelength. After a certain distance, the value of the wave attenuation factor has little influence.

In figure H2 (bottom graph) an attempt is made to in include the wave steepness. The wave steepness is given by Eq.(H13). The wavelength L_p is calculated using the incident spectral peak period and the finite water depth seaward the reef.

$$S_i = \frac{H_s}{L_P}, \qquad L_P = \frac{g}{2\pi} T_P{}^2 \tanh\left(\frac{2\pi h}{L_P}\right) \tag{H13}$$

The correlation between predicted and measured data is improved by including the wave steepness. The values of γ and k_a are chosen as the previously calibrated values. The factor multiplied by the wave steepness parameter yields m = 22. Eq.(H14) is an improved formula predicting the transmitted wave height on the reef plateau based on the incident significant wave height.

$$K_{t,H}(X) = \sqrt{\left(\frac{\lambda h_t}{H_s}\right)^2 + \left(\frac{h_t}{H_s}\right)^2 \left\{\left[\left(\frac{H_s}{h_t}\right)^2 - \lambda^2\right] \exp\left[-m S_i k_a \frac{X}{h_t}\right]\right\}} \tag{H14}$$

Inserting the calibrated parameters Eq.(H14) can be written

$$K_{t,H}(X) = \sqrt{\left(\frac{0.35 h_t}{H_s}\right)^2 + \left(\frac{h_t}{H_s}\right)^2 \left\{\left[\left(\frac{H_s}{h_t}\right)^2 - 0.35^2\right] \exp\left[-4.4 S_i \frac{X}{h_t}\right]\right\}} \tag{H15}$$

The standard deviation of the wave transmission coefficient is $\sigma(K_{t,H}) = 0.053$ with a 90% confidence interval, $K_{t,H} = \pm 0.084$.

A requirement using formula Eq.(H15) is $H_s / h_t \geq 0.4$ to ensure wave breaking over the reef plateau.

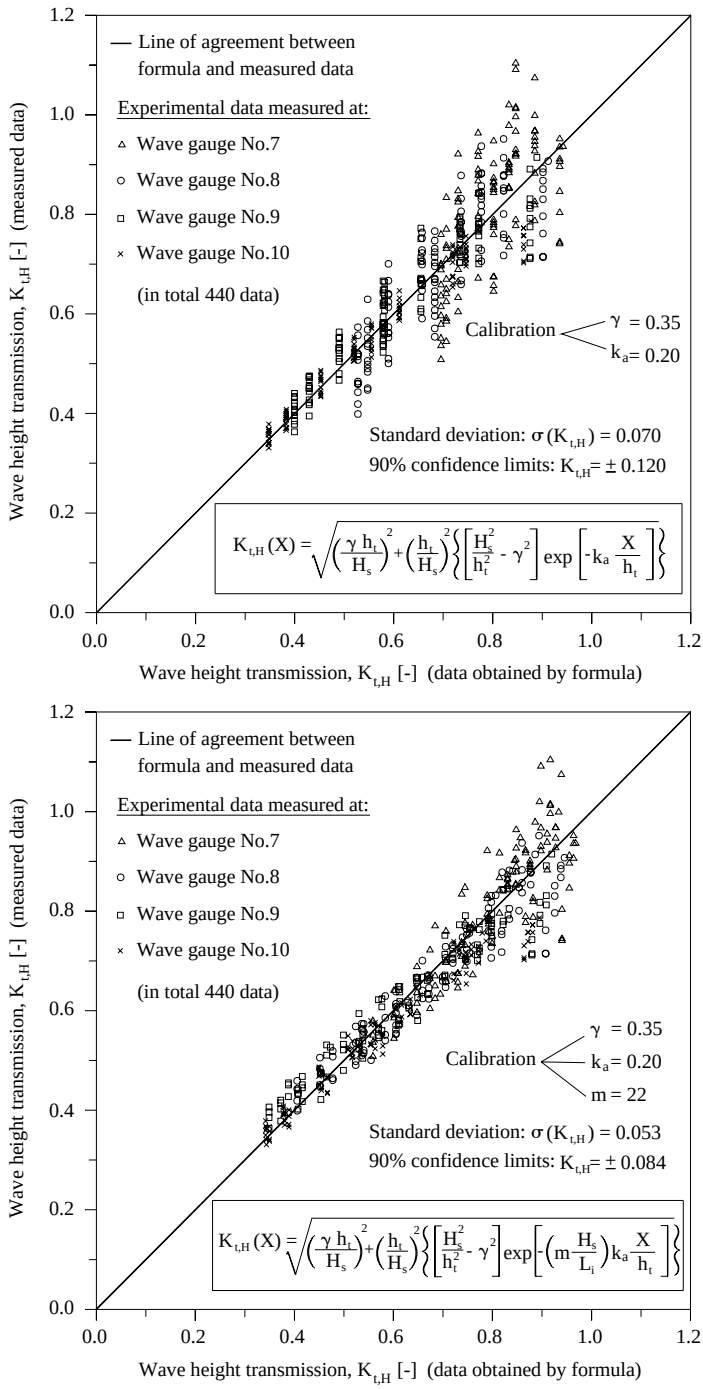

Figure H2: *Wave height transmission related to the incident wave height.*

FORMULAE RELATED TO TRANSMISSION OF THE WAVE ENERGY FLUX

In Figure H3 plots are made with reference points at wave gauge No. 6 (top graph) and wave gauge No. 7 (bottom graph), respectively. The plots show the deviation between measured data in the experiments and the predicted data based on the expression for transmission of wave energy flux as given in Eq.(H6).

The "measured" wave energy flux is estimated from the wave energy spectrum obtained from a Fourier analysis of the surface elevation. It is noted that depicted data in bottom graph in Figure H3 is not limited to 330 compared to Figure H1. This is because the predicted wave energy flux is based directly on the measured wave height, where as the "measured" wave energy flux is estimated from the wave energy spectrum.

In Figure H3 it is observed that the transmitted wave energy flux are influenced by most scatter at the first gauges. The correlation is already fairly good for measurements obtained from wave gauge No. 8.

A calibration of the breaker index results in $\gamma = 0.35$, which is similar to the breaker index calibrated in Eq.(H7). This value is the same as the one found previously regarding transmission of wave height. This is to be expected. The attenuation coefficient becomes slightly lower, $k_a = 0.19$. The coefficients do not change regarding the gauge used.

To summarise, it is shown that the wave energy flux at the reef plateau can be calculated according to the formula given in Eq.(H16)

$$K_{t,P}(X) = \frac{\left\{\left[\left(\frac{H_{t,X=0}}{h_t}\right)^2 - 0.35^2\right]\exp\left[-0.19\frac{X}{h_t}\right] + 0.35^2\right\}\cdot h_t^2 \cdot C_{g,t}}{H_s^2 \cdot C_{g,i}} \qquad \text{(H16)}$$

The standard deviation of the wave energy flux transmission coefficient is $\sigma(K_{t,H}) = 0.047$ with a 90% confidence interval, $K_{t,H} = \pm 0.064$.

Eq.(H16) does not depend on the incident wave height H_s and can be written

$$P_t(X) = \left\{\left[\left(\frac{H_{t,X=0}}{h_t}\right)^2 - 0.35^2\right]\exp\left[-0.19\frac{X}{h_t}\right] + 0.35^2\right\}\cdot h_t^2 \cdot C_{g,t} \qquad \text{(H17)}$$

To ensure wave breaking over the reef slope, the requirement using formulae Eq.(H16) and Eq.(H17) is

$$H_s / h_t \geq 0.4 \tag{H18}$$

Furthermore, the transmitted wave height on the reef plateau, $H_{t,X=0}$, cannot be smaller than the reformed wave height on the reef plateau resulting in the requirement

$$H_{t,X=0} / h_t \geq \lambda \quad \Rightarrow \quad H_{t,X=0} / h_t \geq 0.35 \tag{H19}$$

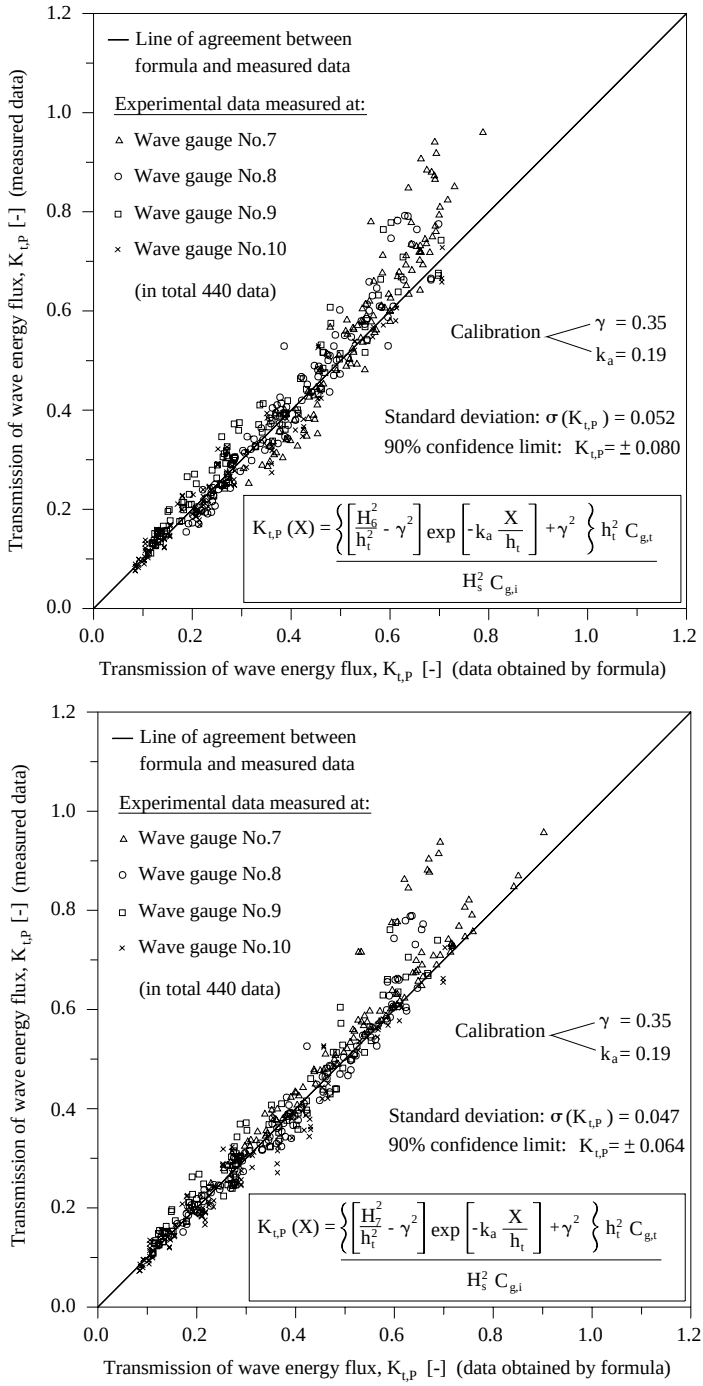

Figure H3: *Wave energy flux transmission with reference point at gauges No. 6 & 7.*

It is attempted to relate the incident waves seaward the reef to the transmitted wave energy flux on the reef. In Figure H4 plots are presented. The top graph shows the significant wave height being replaced by the transmitted wave height at a reference point. The scatter is more significant compared to the results depicted in Figure H3 but a trend between the data is obvious. The calibration of γ and k_a yields similar results compared to the previous calibrations using a reference wave height at the reef plateau. Eq.(H20) is the formula predicting the wave energy transmission coefficient on the reef plateau based on the incident significant wave height.

$$K_{t,P}(X) = \frac{\left\{\left[\left(\frac{H_s}{h_t}\right)^2 - 0.35^2\right]\exp\left[-0.19\frac{X}{h_t}\right] + 0.35^2\right\}\cdot h_t^2 \cdot C_{g,t}}{H_s^2 \cdot C_{g,i}} \qquad \text{(H20)}$$

In Figure H4 (bottom graph), an attempt is made to include the wave steepness. The same approach used for the wave height transmission coefficient is used.

The correlation between predicted and measured data is improved by including the wave steepness. The values of γ and k_a are chosen as the previously calibrated values. The factor multiplied by the wave steepness parameter yields m = 22, similar to the value calibrated in Eq.(H14). Formula Eq.(H21) is an improved expression predicting the transmitted wave height at the reef plateau based on the incident significant wave height.

$$K_{t,P}(X) = \frac{\left\{\left[\left(\frac{H_s}{h_t}\right)^2 - \lambda^2\right]\exp\left[-m\,S_i\,k_a\frac{X}{h_t}\right] + \lambda^2\right\}\cdot h_t^2 \cdot C_{g,t}}{H_s^2 \cdot C_{g,i}} \qquad \text{(H21)}$$

Inserting the calibrated parameters

$$K_{t,P}(X) = \frac{\left\{\left[\left(\frac{H_s}{h_t}\right)^2 - 0.35^2\right]\exp\left[-4.18\,S_i\frac{X}{h_t}\right] + 0.35^2\right\}\cdot h_t^2 \cdot C_{g,t}}{H_s^2 \cdot C_{g,i}} \qquad \text{(H22)}$$

The standard deviation of the wave transmission coefficient is $\sigma(K_{t,H}) = 0.062$ with a 90% confidence interval, $K_{t,H} = \pm 0.106$. A requirement using formula Eq.(H22) is $H_s/h_t \geq 0.4$ to ensure the wave breaking over the reef slope.

Important conclusions are summarized in the following.

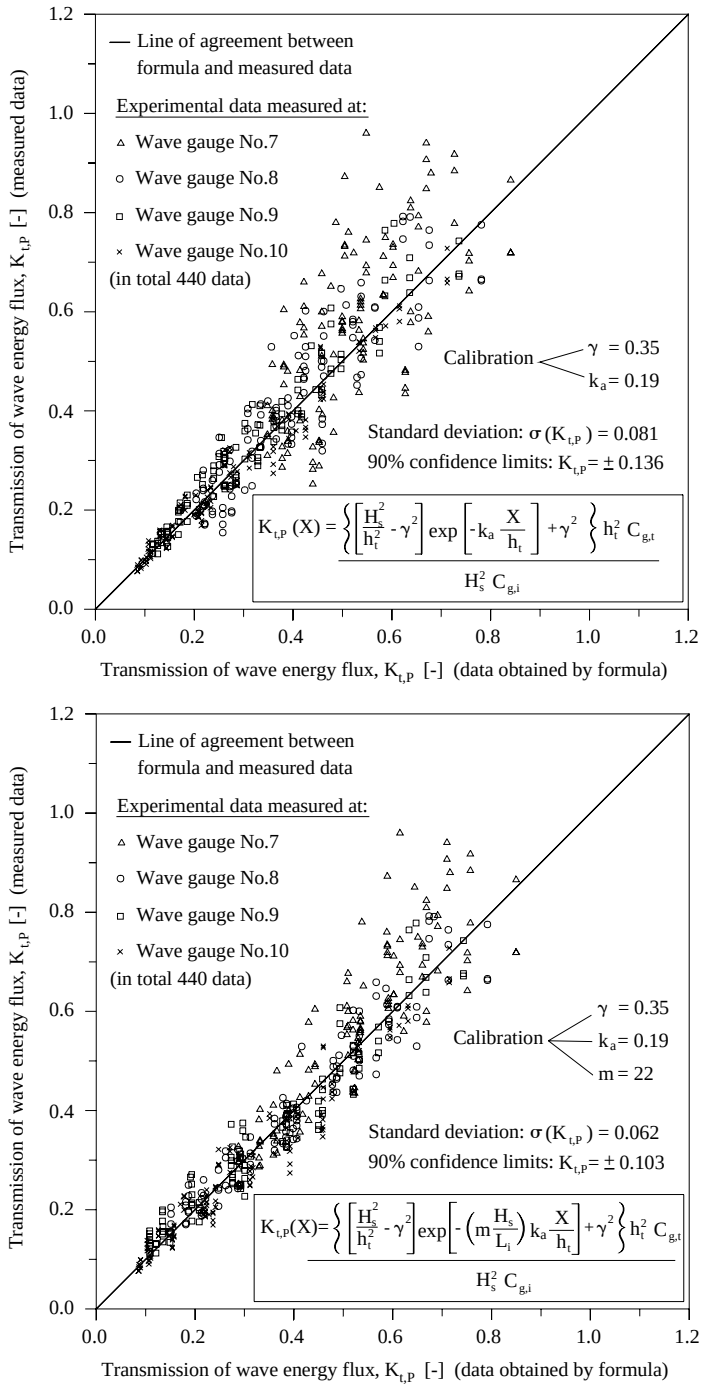

Figure H4: *Wave energy flux related to the incident wave height.*

Transmission of wave heights along a reef plateau:

$$H_t(X) = \sqrt{(0.35h_t)^2 + h_t^2 \left\{ \left[\left(\frac{H_{t,X=0}}{h_t} \right)^2 - 0.35^2 \right] \exp\left[-0.2 \frac{X}{h_t} \right] \right\}}$$

Limits of validity are $H_{t,X=0}/h_t > 0.35$ and $H_s/h_t > 0.4$.

Wave height transmission coefficient along a reef plateau including the incident wave height:

$$K_{t,H}(X) = \sqrt{\left(\frac{0.35h_t}{H_s} \right)^2 + \left(\frac{h_t}{H_s} \right)^2 \left\{ \left[\left(\frac{H_s}{h_t} \right)^2 - 0.35^2 \right] \exp\left[-4.4 S_i \frac{X}{h_t} \right] \right\}}$$

The standard deviation of the wave transmission coefficient is $\sigma(K_{t,H}) = 0.053$ with a 90% confidence interval, $K_{t,H} = \pm 0.084$. Limit of validity is $H_s/h_t > 0.35$.

Transmission of wave energy flux along a reef plateau:

$$P_t(X) = \left\{ \left[\left(\frac{H_{t,X=0}}{h_t} \right)^2 - 0.35^2 \right] \exp\left[-0.19 \frac{X}{h_t} \right] + 0.35^2 \right\} \cdot h_t^2 \cdot C_{g,t}$$

Limits of validity are $H_{t,X=0}/h_t > 0.35$ and $H_s/h_t > 0.4$.

Wave energy flux transmission coefficient along a reef plateau including the incident wave height:

$$K_{t,P}(X) = \frac{\left\{ \left[\left(\frac{H_s}{h_t} \right)^2 - 0.35^2 \right] \exp\left[-4.18 S_i \frac{X}{h_t} \right] + 0.35^2 \right\} \cdot h_t^2 \cdot C_{g,t}}{H_s^2 \cdot C_{g,i}}$$

The standard deviation of the wave transmission coefficient is $\sigma(K_{t,H}) = 0.062$ with a 90% confidence interval, $K_{t,H} = \pm 0.106$. Limit of validity is $H_s/h_t > 0.35$.

Breaking of Waves over a Steep Bottom Slope

Morten Sand Jensen

The thesis is accepted for the degree of Doctor of Philosophy at the Faculty of Engineering and Science, Aalborg University, Denmark. Defence took place February 21, 2003.

The thesis deals with the wave breaking process of waves propagating over a steep submerged bottom slope. The amount of energy dissipated in the wave breaking process is focused upon.

An extensive number of experimental tests (>400) using regular and irregular waves breaking over a simulated reef in the hydraulic laboratory are performed.

Based on the experimental tests several formulae are developed. Formulae are capable of predicting the transmitted wave height and wave energy flux, respectively.

Furthermore, a numerical wave model based on the extended Mild-Slope equation has been developed. The model is capable of generating progressive irregular waves. Wave breaking has been included using a modification of the Battjes and Janssen [1978] periodic bore approach.

The results from this study will be applicable in the design of coastal structures as submerged breakwaters or artificial reefs.

Hydraulics & Coastal Engineering Laboratory
Department of Civil Engineering
AALBORG UNIVERSITY
ISSN 0909-4296
Series Paper No. 22